RMIT UNIVERSITY

AERO2263 AEROSPACE STRUCTURES STUDIO

Lecturer : **Associate Professor Akbar Khatibi**

Assignment : **Final Report: Design improvement of a trainer aircraft wing towards green aviation**

Team : **Team 14**

Group Members :

1. Olivia Janice Curtis	**-**	**S3660213**
2. Jay Anthony Dickson	**-**	**S3719855**
3. Faris Adlan Roslan	**-**	**S3833075**
4. Mary Denkha	**-**	**S3650640**
5. Khac Son Trinh	**-**	**S3845907**

Due on the 20th of October 2023 at 11:59 PM

EXECUTIVE SUMMARY

This report proposes the redesign of a PC9 aircraft wing to enhance strength and reduce weight. Utilizing fibre-reinforced polymers, a prevalent choice in aerospace, the project entails static and dynamic analysis of the existing metallic wing, validated finite element modelling, advanced composite material selection, and internal wing box structure optimization while retaining the current aerofoil. The primary objective is to decrease the weight of the PC9 wing, boosting its performance under maximum load conditions compared to the present metal design. Ultimately, this initiative aligns with sustainable aviation goals by leveraging advanced composites, refining design methodologies, and integrating cutting-edge configurations and systems.

Main Findings:

Under typical operating circumstances, the primary spar of the PC-9 wing structure is unlikely to break, according to static and dynamic studies. Notches in the spar, on the other hand, can considerably increase stress concentrations and cause plastic deformation. Cracks originating from flange holes must be handled with care, although the centre crack in the web is less essential. The wing stiffness is greatest at the point of application and lowest near the wingtip. The major strains, stresses, and shear stress vary across the wing, showing non-uniform deformation and stress distribution. The bottom spar cap has the largest Von Mises stress, indicating that the load is not distributed uniformly throughout the wing components. Because of its position and decreased exposure to pressures and moments, the rib has the lowest Von Mises stress.

The Finite Element Analysis (FEA) model for the PC-9 wing demonstrated remarkable accuracy and reliability, with Von Mises stresses and wingtip displacement values falling within a 10 percent tolerance range when compared to experimental results. This successful validation ensures the FEA model's credibility, providing a strong foundation for assessing the structural integrity of the PC-9 wing under various load conditions and for evaluating the potential benefits of a composite material alternative.

When modelled, the composite excels under similar loading conditions, consistently surpassing or closely matching the performance of the original structure while achieving a remarkable weight reduction of nearly 25%

Under typical operating conditions, the PC-9 wing structure has overall structural integrity. Notches and cracks, on the other hand, might weaken the structure and make it more prone to fatigue failure. The necessity for careful load distribution and monitoring of important locations, notably the bottom spar cap and flange holes, is highlighted by non-uniform deformation and stress distribution.

The strategic significance of model simplifications for efficient yet accurate analysis, as well as the successful validation of our FEA model against experimental data. The structural integrity of the PC-9 wing is guaranteed and exceeds aerospace requirements. This lays the path for realistic weight and strength comparisons between aluminium and composite materials.

AUTHORS

	**Olivia Janice Curtis** ***Bachelor of Aerospace Engineering 4th Year*** - Olivia is currently in her final year of Aerospace Engineering (Honours) at RMIT.
	**Faris Adlan Roslan** ***Bachelor of Aerospace Engineering 4th Year*** - Graduated from Kuala Lumpur University in 2019 in Avionics Aircraft Maintenance. He is currently in his final year of aerospace engineering at RMIT University.
	**Jay Anthony Dickson** ***Bachelor of Aerospace Engineering*** - Progressing through my degree at RMIT. - Fan of ducks. Quack.
	**Mary Denkha** ***Bachelor of Aerospace Engineering 4th Year*** - Graduated from RMIT university in 2021 with associate degree in engineering technology. Currently Mary is in her final year.
	**Khac Son Trinh** ***Bachelor of Aerospace Engineering*** - Overall awesome human.

TABLE OF CONTENTS

TABLE OF FIGURES

TABLE OF TABLES

GLOSSARY

- AOSG - Aerospace Operational Support Group
- CFD - computational fluid dynamics
- CFRP - carbon fibre reinforced polymer
- CO2 - carbon dioxide
- EPFM - elastic-plastic fracture mechanics
- FAA - Federal Aviation Administration
- FEA - finite element analysis
- FEM - finite element method/model
- FOS - factor of safety
- FSFT - full-scale fatigue tests
- GA - general aviation
- GFRP - glass fibre reinforced polymer
- ICAO - International Civil Aviation Organization
- L/D - lift-to-drag ratio
- LEFM - linear elastic fracture mechanics
- MOS - margin of safety
- MTOW - maximum take-off weight
- NACA - National Advisory Committee for Aeronautics
- OLM - operational loads monitoring
- RAAF - Royal Australian Air Force
- RMIT - Royal Melbourne Institute of Technology
- SIF - stress intensity factor

NOTATIONS AND SUBSCRIPTS

- $(MoS)_P$ - margin of safety plastic collapse
- $(MoS)_F$ - margin of safety brittle fracture
- $N_{Interval}$ - number of intervals
- P_0 - load to cause fully plastic yielding
- X_K - safety factor brittle facture
- X_N - inspection intervals
- X_N - number of services
- X_P - safety factor plastic collapse
- a_c - final crack size facture toughness
- a_i - detectable crack length
- a_p - final crack size plastic collapse
- μ_g - airplane mass ratio
- a - the crack size
- a (fracture, Case I) - crack length + radius of curvature
- a (fracture, Case II) - crack length
- a (fracture, Case III) - half the crack length
- a (input data) - slope of airplane normal force coefficient curve
- A (safe life) - fitting constant
- A f-ratio - area flange ratio
- a_c - final crack size
- a_p - final crack size on plastic collapse
- AW Ratio - area web ratio
- b (fracture) - width of flange
- b (input data) - wingspan
- b - fatigue strength exponent
- c (fracture) - radius of curvature
- c (safe life) - fatigue ductility exponent
- C - mean chord
- C (damage tolerance) - Intercept
- D - drag
- D/W (notched) - diameter of the hole over main spar flange width
- Delta_K - change in stress intensity factor
- F (unnotched) - total load
- F_both wings - lift force produced by both wings
- F_d (fracture) - F from curve
- F_d - geometric factor
- F_Main Spar Root - applied load on main spar
- F_single wing - lift force on single wing
- g - gravity acceleration
- K - stress intensity factor
- K_IC - fracture toughness value
- Kt - stress concentration factor
- l - crack length
- L - lift

- m (damage tolerance) - slope
- n (input data) - gust load factor
- n (Ramberg-Osgood) - strain hardening constant
- n (safe life) - loads per wing
- N_i - number of cycles
- N_t - transition fatigue life
- Nf - number of cycles
- *p* - air density
- Py1 - principal force of y1
- Py2 - principal force of y2
- Pz1 - principal force of z1
- Pz2 - principal force of z2
- q - dynamic pressure
- qs_max - max shear flow
- R - stress ratio
- rp - plane stress
- S (unnotched) - distance from bottom of top flange
- S (unnotched) - distance from bottom of top flange
- S (unnotched) - wing area
- S_f - fatigue limit
- Sv - internal shear force
- Sv_w - internal shear force at web
- t (fracture) - flange thickness
- T_f - thickness of the flange
- T_w - thickness of the web
- Ƭw_max - max shear stress
- U_{de} - derived gust velocities
- V - airspeed
- Va - manoeuvring speed
- Vc - cruise speed
- W/S - wing loading
- ȳ - Y centroid
- ε max - maximum strain
- ε_a - strain amplitude
- ε_e - elastic strain
- ε_p - plastic strain
- ε'f - fatigue ductility coefficient
- εy - residual strain
- θ - polar coordinates
- σ_0 - yield strength
- σ_amplitude - stress amplitude
- σ_ar - equivalent stress amplitude at zero mean stress
- σ_bending - bending stress
- σ_c (unnotched) - allowable stress
- σ_f - fatigue stress
- σ_m - mean stress
- σ_max - maximum stress
- σ_min - minimum stress

- σ1 - normal stress in top flange
- σ2 - normal stress in bottom flange
- σ'f - fatigue strength coefficient
- σy - residual stress
- σz - normal stress in top flange
- E - young’s modulus
- H - strength coefficient
- S - nominal stress
- π - pi
- σ - applied stress
- ϵ - strain

CHAPTER 1: INTRODUCTION

1.1 Problem Statement

This report addresses the environmental impact of the aviation industry and proposes enhancing an existing aircraft's wing design to promote eco-friendly aviation. The aviation sector contributed approximately 2% of the total CO2 emissions in 2018. Efforts to reduce this carbon footprint are a priority for aircraft manufacturers, airlines, and regulators, aiming for carbon neutrality by 2050.

Composite materials offer a promising alternative to traditional metals, demonstrating superior strength and flexibility while maintaining shape integrity. This project focuses on utilizing composites for redesigning the wing structure of the Pilatus PC-9 aircraft, aiming to improve efficiency and reduce weight. The static analysis includes various assessments on the main wing spar, providing baseline characteristics for comparison in later stages. Dynamic analysis evaluates stress, stress concentrations, cracks, and fatigue effects over the expected operational lifespan of the PC-9, categorized into Safe-Life, Fail-Safe, and Damage Tolerant analyses.

1.2 Methodology

The methodology for this project involves a comprehensive analysis of the current metal wing structure of the Pilatus PC-9 aircraft and proposes a new wing design using composite materials. The analysis is categorized into static and dynamic evaluations.

1.2.1 Static Analysis

Static analysis involves assessing the main wing spar at the location of Rib 5 under cruise conditions, as it represents a significant portion of the aircraft's operational lifespan. The analysis comprises the following components.

1. Unnotched Analysis:
    - Simplifies the spar structure into a cantilever beam with an I-shape cross section, assuming no holes on the structure.
2. Notched Analysis:
    - Considers stress concentrations caused by holes created for fasteners and objectives on the main spar's webs and flanges.
3. Fracture Analysis:
    - Accounts for stress concentrations, cracks, and potential plastic or elastic failures, analysing phenomena like crack development on holes or the I-beam itself.

1.2.2 Dynamic Analysis

Dynamic analysis evaluates the effects of stress, stress concentrations, cracks, and fatigue over the expected operational lifespan of the PC-9, divided into the following categories where it determines the expected lifespan of the aircraft, analysing stress and fatigue factors to ensure safe operation until retirement:

1. Safe-Life Analysis:
    - Determines the expected lifespan of the aircraft, analysing stress and fatigue factors to ensure safe operation until retirement.

2. Fail-Safe Analysis:
    - Focuses on evaluating potential failures and ensuring the aircraft can still operate safely and maintain structural integrity in the event of certain failures.
3. Damage Tolerant Analysis:
    - Assesses the ability of the proposed composite wing structure to tolerate damage, such as cracks, and continue safe operation without catastrophic failure.

The results from the static and dynamic analyses will serve as a basis for comparing the current metal wing structure with the proposed composite wing structure in terms of weight, efficiency, and overall performance, aligning with the project's objectives of enhancing eco-friendliness in aviation.

In this report, the problem statement has been identified as what is the impact of the aviation industry to the world's environment and how to make improvements on an existing aircraft's wing to converge towards a green and eco-friendly aviation. According to reports from Aviation Benefits, air transportation has generated roughly 895 million tonnes of carbon dioxide or CO2 in 2018 when compared to the CO2 generated by humans which is around 42 billion tonnes of CO2 [1]. That equates to approximately 2 percent. It is estimated that passenger numbers to increase to an average of 5 percent each year but the addition of the COVID-19 pandemic, the percentage have plummeted and since 2020 and is seen to increase steadily by 2022.

From above statistics, reducing CO2 emission, or carbon footprint, has been primary objective of aircraft manufacturers, as well as airlines and regulations. Emissions in air transportations are produced not only during flights, but also in manufacturing stages and supply chains. ICAO and other regulators have agreed commitments in transforming the aviation sector in to carbon-neutral by 2050 [2], and multiple plans and solutions have been proposed, these include improvements in material selection and manufacturing processes, alongside with optimizations in aircraft designs [3], [4]. Composite materials have been proposed as an ideal alternative material to traditional metals and have been implemented in a wide range of aircraft class, from GA [5] to large commercial aircrafts [6]. Despite being a controversial subject in terms of the manufacturing process due to a significant contribution of Polymer as Matrix material [7], which raise concerns regarding its sustainability and recyclability [8], advantages of composite over conventional metals within aircraft performances are undeniable [9].

Composites are stronger than Aluminium, more flexible and can bend more significantly, yet still maintain its shape and avoid deformations [10]. Therefore, this project will utilize composite as the material for the proposal of a new wing structure for the Pilatus PC-9 aircrafts. In the Progress Report, Static and Dynamic Analysis of metal structures and current wing design will be calculated as the baseline characteristics, which will be compared in later stages to determine the improvements in terms of weight and efficiency.

Static Analysis consists of Unnotched, Notched and Fracture Analysis on the main wing spar of the PC-9, at the location of the Rib 5, under Cruise conditions. Cruise conditions are selected as they account for the majority of an aircraft's lifespan and significantly contribute to the Static and Dynamic Analysis criteria. The main wing spar at Rib 5 is the connection between the fuselage and the wing structures, which is expected to experience highest load and moment magnitude, therefore highest stress and strain. Unnotched Analysis considering the spar without holes on the structure, which simplifies it into a cantilever beam with I-shape cross section.

Holes on the main spar's webs and flanges are created for fasteners installation, as well as objectives, however this will cause stress concentration during loading and unloading conditions, which will be additionally considered in the Notched Analysis. Due to additional stress, stress magnitude might exceed the material's Yield Strength, Ultimate Tensile Strength, and Young's Modulus, which led to plastic and possibly elastic failure, displayed through crack developing on holes or on the I-beam itself. Those phenomena will be considered within the Fracture Analysis.

On the other hand, Dynamic Analysis considering the effects of those stress, stress concentrations, cracks developments and fatigue under the expected operation lifespan of the PC-9 and will be divided into 3 sections: Safe-Life, Fail-Safe and Damage Tolerant.

1.3 Aims and Objectives

The project's goal is to rebuild a PC9 aircraft's wing utilising cutting-edge composite materials and a cutting-edge wing box structure. The project's main goals are to lighten the aircraft overall and improve its performance.

The project has several phases to accomplish these goals, including static and dynamic analysis of the existing metallic wing, finite element analysis using a model that has been validated through experimentation, selection of advanced composite materials, and optimisation of the internal structure of the wing box while retaining the existing aerofoil.

The design limitations of the metallic wing under different loads, such as aerodynamic, gust, wind, and turbulence, as well as aeroelastic and structural loads, will be determined by the static analysis of the wing. The behaviour of the composite wing under various loading circumstances will be simulated by the finite element analysis using a model that has been experimentally validated. It will be necessary to use innovative composite materials that are both light and strong enough to match the design specifications. Creating a structure that is both light and robust enough to handle the stresses encountered during flight is the final step in optimising the interior design of the wing box.

The project's aim is to lighten the weight of the composite PC9 wing and enhance it in comparison to the existing metallic structure's performance under maximum loading circumstances. By attaining these goals, the project will help advance the development of more economical and ecologically friendly aviation, which is a core objective of contemporary aircraft design.

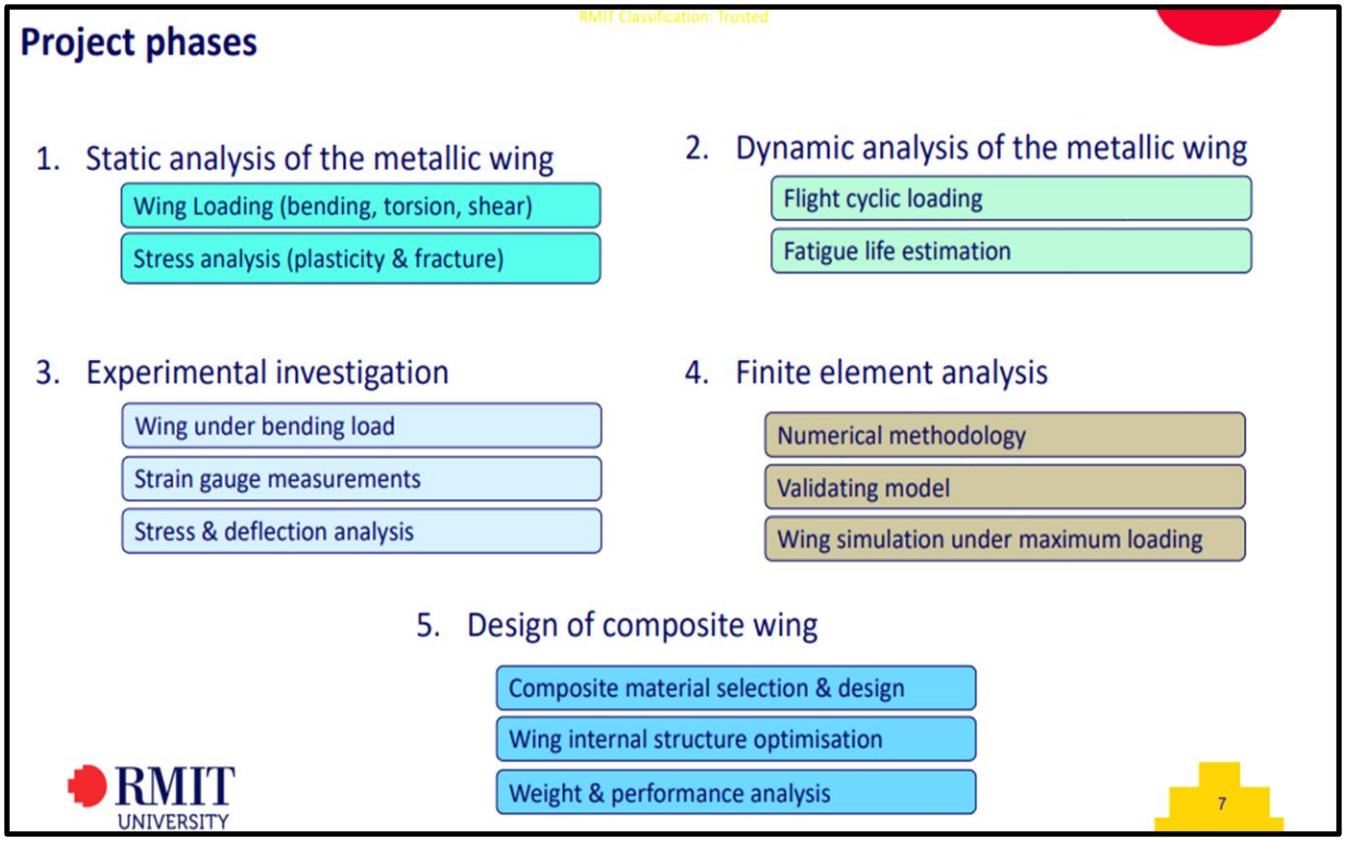

Figure 1 The project phases of the PC9 Wing project (Source: RMIT Canvas)

1.4 Scope and Limitations

The project's goal is to remodel a PC9 aircraft's wing utilising cutting-edge composite materials and a cutting-edge wing box structure to decrease the aircraft's total weight and improve performance.

The project is divided into many parts, including static and dynamic study of the existing metallic wing, finite element analysis using a model that has undergone experimental validation, selection of cutting-edge composite materials, and optimisation of the interior structure of the wing box while retaining the existing aerofoil.

The design limitations of the metallic wing under different loads, such as aerodynamic, gust, wind, and turbulence, as well as aeroelastic and structural loads, will be determined by the static analysis of the wing. The behaviour of the composite wing under various loading circumstances will be simulated by the finite element analysis using a model that has been experimentally validated.

It will be necessary to use innovative composite materials that are both light and strong enough to match the design specifications. Creating a structure that is both light and robust enough to handle the stresses encountered during flight is the final step in optimising the interior design of the wing box.

The project has several restrictions. One restriction is the 12-week deadline for the project's completion. This could restrict the scope of the testing and analysis that can be carried out and necessitate making some assumptions during the design phase. The availability of resources, such as tools and materials, is another restriction that may affect how thoroughly the design can be tested and validated. Additionally, the project only addresses the PC9 aircraft's wing and ignores other parts of the aircraft that could affect how well it performs.

Finally, the project may not immediately apply to other aircraft designs as it is restricted to the particular design needs of the PC9 aircraft. Despite these drawbacks, the project has the potential to advance the development of more economical and ecologically friendly aviation, which is a major objective of contemporary aircraft design. The project may assist to lower fuel consumption and emissions, increase air travel safety and efficiency, and cut emissions by lightening the weight of the composite PC9 wing and enhancing its performance under maximum loading circumstances in comparison to the present metallic construction.

1.5 Methods of Approach

The strategy employs a few techniques, such as optimising the internal structure of the wing box while retaining the existing aerofoil, finite element analysis using an experimentally verified model, selecting advanced composite materials, and static and dynamic analysis of the existing metallic wing. The static analysis of a metallic wing entails simulating its behaviour under various loads, including as aerodynamic, gust, wind, and turbulence, as well as aeroelastic and structural loads, using mathematical models.

This study will assist establish the wing's design parameters and point out potential improvement areas. The behaviour of the composite wing under various loading circumstances is simulated by the finite element analysis using a model that has been empirically validated. The interior construction of the wing box will be optimised using the results of this research to make it as robust and lightweight as possible to handle the stresses encountered during flight. Finding materials that are both light and strong enough to suit design criteria is a key step in the selection of innovative composite materials. This will include considering variables like the fibre type, stacking order, and geometrical dimensions of the composite constructions.

Finally, developing a structure that is both light and robust enough to handle the stresses encountered during flight is necessary for optimising the interior design of the wing box. To do this, mathematical simulations of the behaviour of the wing under various loading circumstances will be used to pinpoint areas for improvement. Overall, the project methodically redesigns the wing of the PC9 aircraft utilising cutting-edge composite materials and a novel wing box structure employing a mix of mathematical modelling, simulation, and experimental validation.

1.6 Literature Review

Static Structural Analysis of Fighter Aircraft's Wing Spars outlines a meticulous methodology for performing Static Structural Analysis on the wing spars of Fighter Aircraft using Finite Element Analysis (FEA). The authors delve into the key flight loads experienced by aircraft wings, such as lift, weight, and drag, and emphasize the role of wing spars in providing structural support. The FEA procedure is outlined step by step, encompassing the creation of a 3D spar model, application of varied flight loads, and stress calculation. Material properties of the spar, including Young's modulus and Poisson's ratio, and the spectrum of materials like titanium and aluminium alloys are discussed in relation to the analysis. Several significant findings emerge from this analysis. [11]

Critical stress locations in the wing spar vary according to load types and magnitudes. The material properties of the spar significantly influence the wing's safety threshold. The paper suggests using the results for fatigue life estimation of spars and proposes employing the actual load spectrum for cumulative damage assessment using Miner’s rule. Ultimately, this technique can be universally applied across aircraft types, making it an invaluable asset for aerospace researchers and engineers. In essence, this literature review offers a comprehensive guide to Static Structural Analysis of Fighter Aircraft's Wing Spars. The detailed methodology, applicable to diverse aircraft, underscores the significance of identifying stress concentrations in wing spars and ensuring that material properties are adequate to endure these stresses. [11]

The "Standard Specification for Design and Performance of a Light Sport Airplane" lays out airworthiness prerequisites for powered fixed-wing light sport aircraft design. It particularly details wing and wing carry-through structure requirements. Key among these is the ability to endure specific loads. Calculation methods for these loads and corresponding wing design are delineated. This involves withstanding 100% of Condition "A" load on one plane side and 70% on the other, where Condition A signifies the highest positive limit manoeuvring load factor at design speed.

Furthermore, the wing and structures should handle the loads resulting from 75% of positive manoeuvring wing loading on both sides of symmetry, along with maximal wing torsion from aileron movement. The specification additionally outlines how to evaluate aileron displacement's impact on wing torsion. It adapts the basic air foil moment coefficient within the aileron span section, using this modified coefficient for calculating wing torsion from aileron movement at specified speeds (Vc or Va). In essence, the specification mandates wing designs to sustain designated loads and accommodate the influence of aileron displacement on wing torsion. It supplies exhaustive guidelines for load calculations and corresponding wing design considerations. [12]

This research paper conducts a Finite Element Analysis (FEA) of aircraft wing structures crafted from Carbon Fibre Reinforced Polymer (CFRP), Glass Fibre Reinforced Polymer (GFRP), and aluminium alloy. The study aims to compare their performance concerning deformation and stress during varying loading situations. The paper commences with an introduction to composite materials, highlighting their advantages over traditional options. It emphasizes the significance of lightweight, robust materials for aircraft wings. [12]

Previous research on composite use in wing design is discussed, underscoring the necessity for further investigation. The subsequent section outlines materials and methods. The design of the wing structure, including dimensions and air foil shape, is detailed. FEA software for simulating wing behaviour under different loads is explained. Results are presented next. Deformation and stress of CFRP, GFRP, and aluminium alloy wing structures are compared under bending, torsion, and shear loads. CFRP exhibits the least deformation and stress, followed by GFRP. [12]

Aluminium alloy records the highest, suggesting its inadequacy for wing construction compared to composites. The paper concludes with implications for wing design. CFRP and GFRP are recommended due to their strength-to-weight ratios and low deformation/stress. Further research is urged to refine composite wing structures, address fatigue and damage tolerance, and optimize design. In essence, this paper offers a comprehensive exploration of composite materials in aircraft wing structures.

Through FEA, it unveils the superior performance of CFRP and GFRP over aluminium alloy. This study holds vital implications for the efficient and safe design of lightweight, robust aircraft wings. [13]

Ground and Operational Vibration Assessment of the RAAF PC-9/A Airframe paper focuses on the structural dynamic and vibration analysis of the Pilatus PC-9/A aircraft, primarily used for pilot training by the Royal Australian Air Force (RAAF). While the aircraft's structural integrity is supported by full-scale fatigue tests (FSFT), the study aimed to supplement these tests by using an operational loads monitoring (OLM) aircraft. The OLM aircraft was equipped with strain gauges and accelerometers to measure strains, accelerations, elevator and rudder deflections, and other flight parameters. This allowed for the assessment of dynamic loads during various operational conditions. The aircraft was tested both in an empty and fully fuel configuration, with deflated tires and preloaded control surfaces. The measurement system was developed and installed by the RAAF Aerospace Operational Support Group (AOSG). [14]

The study aimed to evaluate the aircraft's structural dynamics, including buffet flight testing, vibration analysis, and dynamic load derivation. The collected data facilitated the assessment of empennage buffeting fatigue. The results of both ground and flight tests were presented and discussed, including the dynamic response of the airframe, strain and accelerometer responses to dynamic forces, and the correlation with a dynamic finite element model (FEM) of the aircraft. In essence, the paper offers a comprehensive overview of the assessment of ground and operational vibrations for the RAAF PC-9/A airframe. By using an OLM aircraft with specialized instrumentation, the study provided deeper insights into the dynamic loading experienced by the aircraft's aft fuselage and empennage during various manoeuvres and operational conditions. This additional evaluation is crucial for enhancing the understanding of the aircraft's structural behaviour and ensuring its continued safe and effective operation. [14]

The paper "Green Aircraft Technology Imperatives for Environmental Sustainability" presents a comprehensive examination of aviation's ecological impact and the ongoing endeavours to uphold the Earth's environmental stability. It begins by delineating two primary channels through which aviation affects the climate: greenhouse gas emissions and the formation of contrails and cirrus clouds. The authors then delve into the scientific and technological guidelines aimed at comprehending these phenomena and their environmental implications. The paper proceeds to explore a diverse array of technologies and strategies designed to mitigate the environmental footprint of commercial aviation. These encompass advancements in engine and wing design, the adoption of alternative fuels, and alterations to air traffic management systems. [15]

Throughout the paper, the authors underscore the paramount significance of collaboration among industry, government bodies, and academia in the development and implementation of sustainable aviation technologies. They also accentuate the continuous necessity for research and development in this sphere to enable the aviation sector to grow and flourish while curbing its impact on the environment. In summary, "Green Aircraft Technology Imperatives for Environmental Sustainability" offers a valuable synopsis of the ongoing research and development in sustainable aviation technologies. The paper is extensively researched and provides a well-balanced perspective on the challenges and prospects facing the aviation industry as it endeavours to mitigate its environmental repercussions. [15]

Mounika Ragamshetty and colleagues investigated the design and analysis of an aeroplane wing in depth in their paper Design and Finite Element Analysis of Aircraft Wing. The purpose was to figure out how much stress and deformation the wing could take in different configurations. Stress analysis is essential in the design of a replacement wing because it predicts material failure and optimises wing strength without increasing weight. The wing's deformation, stress, strain, and natural frequency were all examined using ANSYS software. The double lattice approach proved extremely useful for analysing the aerodynamics of a swept-back wing. The use of fluidic oscillators at the natural flow separation line for separation control was also beneficial. A greater sweep angle raised the critical Mach number, resulting in faster cruising speed. Aluminium alloy and titanium alloy were compared using static structural analysis. Titanium alloy has shown to be the best material for subsonic flight wings. The research gives useful information for developing and analysing aircraft wings, which might lead to improved aircraft performance [16]

Das and Roy investigated the use of composite materials in aviation wing design in their paper Finite element analysis of aircraft wing using carbon fibre reinforced polymer and glass fibre reinforced polymer, especially CFRP and GFRP. Their FEA using ANSYS software revealed that CFRP and GFRP wings outperformed aluminium alloy wings in stiffness and strength. A natural frequency of 22.5 Hz was discovered using modal analysis, which is within the ideal range for aeroplane wings.

The research emphasises the potential advantages of employing CFRP and GFRP in aircraft wing construction, such as increased strength, stiffness, and dynamic qualities. However, obstacles like as production complexity and expense persist.

Main findings:

- CFRP and GFRP offer superior stiffness and strength for aircraft wings compared to aluminium alloy.
- Modal analysis showed a natural frequency within the desired range for aircraft wings.
- Challenges include manufacturing complexity and cost.

The increasing prevalence of fibre-reinforced polymer matrix composites (FRPMC) in aircraft structures necessitates accurate failure prediction tools. The authors address this challenge by developing a three-dimensional finite element model to assess the interlaminar fracture toughness of fibre-reinforced woven composites. The study delves into the experimental and numerical determination of mode II fracture toughness in FRPMC. The authors emphasize the importance of fracture toughness, particularly mode II fracture toughness, in predicting the fatigue life of aircraft structures due to the high shear stresses experienced by these materials.

Experimental testing using double cantilever beam (DCB) tests and numerical simulations with a three-dimensional finite element model based on the DCB test findings demonstrate the model's ability to accurately predict mode II fracture toughness in fibre-reinforced woven composites. The findings align with existing literature and validate the reliability of the testing methodology.

The model considers the anisotropic nature of these materials and can predict their interlaminar fracture toughness. Numerical simulation results show good agreement with experimental data, suggesting that the model can optimize the design of composite structures and can be applied to other types of composites beyond fibre-reinforced woven composites. In conclusion, the study provides a comprehensive overview of experimental and numerical methods used to determine the mode II fracture toughness of fibre-reinforced polymer matrix composites. The three-dimensional finite element model offers a valuable tool for predicting interlaminar fracture toughness and has significant implications for designing composite structures.

Because of the requirement for expanded cargo capacity, increased fuel economy, and improved performance, the aerospace sector has been a pioneer in developing sophisticated production procedures for lightweight materials. The article "Manufacturing Technology of Lightweight Materials in Aerospace" goes into the current condition and future direction of this field's manufacturing technology.

The high cost of lightweight materials is a significant barrier for aircraft makers. The paper emphasises the need of low-cost manufacturing systems capable of producing high-quality lightweight materials. Additive manufacturing, automation, and robots are examples of advanced manufacturing technologies that can help cut costs and enhance efficiency. Another problem is ensuring the safety and dependability of lightweight materials. The necessity of quality management and testing in ensuring that lightweight materials fulfil the strict criteria for aeronautical applications is discussed in the article. These materials' design and performance can also be improved using advanced simulation and modelling approaches.

The paper emphasises the importance of intellectualisation in the production of lightweight materials. Artificial intelligence, machine learning, and big data analytics are examples of digital technologies that may improve the efficiency and accuracy of industrial operations. Integrating these technologies can help shorten the time and cost of product creation.

The article provides instances of effective lightweight material application in aircraft production, such as the usage of composite materials in the Boeing 787 Dreamliner and Airbus A350 XWB, and titanium alloys in the Lockheed Martin F-35 Lightning II. These examples show the possible benefits of lightweight materials, such as higher fuel efficiency, cargo capacity, and performance. Finally, the article "Manufacturing Technology of Lightweight Materials in Aerospace" presents a complete summary of the current condition and future direction of aircraft manufacturing technology. Lightweight materials have the potential to revolutionise the industry, and embracing innovative manufacturing methods and digitalisation can assist firms in overcoming hurdles.

The publication "Ultimate Load Analysis of Simple Structures" by M. J. Hillier presents a method for evaluating the ultimate static load bearing capacity of ductile thin shells. The need of understanding the final load bearing capacity, rather than just predicting the yield point load, is emphasised throughout the study. While limit analysis approaches can estimate yield point loads, they do not consider the material's strain-hardening ability, which is critical for properly forecasting ultimate load bearing capacity, according to Hillier.

Hillier offers an integrated approach for determining the ultimate load bearing capacity of thin shells subjected to primarily tensile stresses to solve this restriction. The approach assumes that the material is incompressible, isotropic, rigid-plastic, and strain-hardening. Hillier develops a set of fundamental equations for the issue, which are then solved using a numerical method. The study finishes with examples of the approach being applied to cylindrical and spherical shells.

Hillier compares his approach's results to those obtained using limit analysis techniques in each example, indicating that his method delivers a more accurate estimate of the ultimate load bearing capability. Overall, Hillier's article contributes to structural engineering by offering a method for properly forecasting the ultimate load bearing capacity of ductile thin shells. The method is theoretically valid and has been proved to produce more accurate findings than conventional limit analysis techniques.

- The study describes a method for estimating the ultimate load bearing capacity of ductile thin shells.
- By considering the material's strain-hardening capacity, the method overcomes the constraints of limit analysis techniques.
- Examples show how the method outperforms limit analysis techniques in terms of accuracy.

1.7 PC9 Aircraft

The Pilatus PC-9 aircraft is a Swiss origin single-engine, low-wing tandem-seated turboprop training aircraft produced in 1984 and still in operation until now. It is the choice of aircraft for this project because of existing live aircraft situated at RMIT Bundoora hangar.

The technical specifications of the aircraft are available in the appendix section of the report. The Pilatus PC-9 has a range of 1643 km and travels at subsonic speeds. It is manufactured both in Switzerland by Pilatus and in Australia by Hawker de Havilland [16]. The project’s analysis will be focused on the wing’s main spar as shown in **Figure 3**.

Figure 2 The Pilatus PC-9 aircraft (Source: Air Power Australia [17]

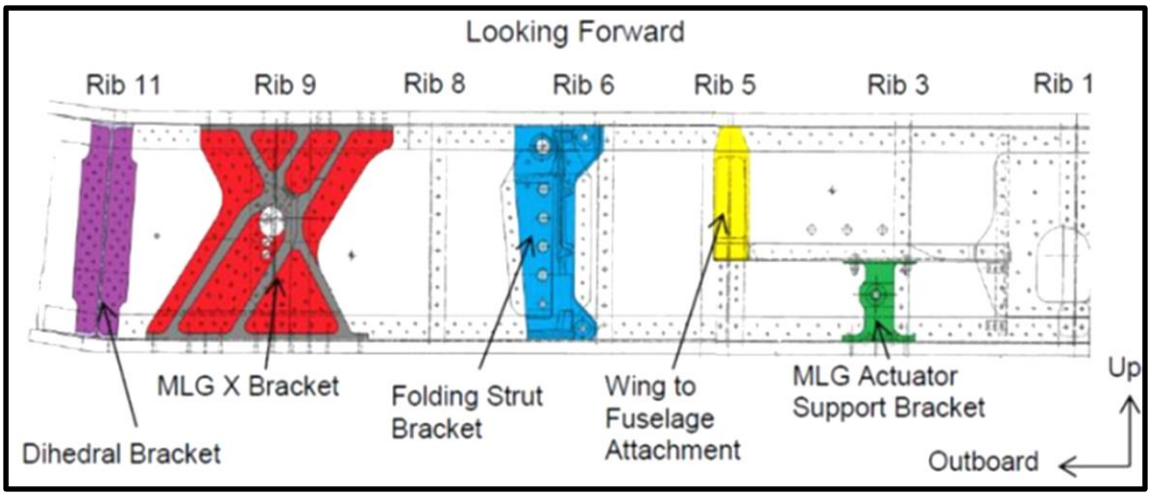

Figure 3: The Pilatus PC-9 aircraft wing's main spar (Source: RMIT Canvas)

1.8 Outline of Content

This paper investigates the Pilatus PC-9 main wing spar that is made of the material aluminium 2124. Two analyses which comprised of static analyses and dynamic analyses were conducted in this progress report. A 'cruise' was assumed for our loading conditions while examining the effects of it on the main spar which was modelled as a beam with the dimensions and other specifications were supplied in the project brief.

The static analysis explores the notched analysis, unnotched analysis, and fracture analysis to determine stress concentrations at the uniaxial holes crack, single edge cracks, and a web crack in the middle of the flange. The analysis conducted shows the wing's main spar entered plasticity by the evidence of residual stresses.

The dynamic analysis explores the fatigue life through safe-life and fail-safe approach, and the damage tolerant method which includes the inspection intervals.

1.9 Project Timeline

	Date & Day	13-Sep-23	17-Sep-23	21-Sep-23	25-Sep-23	29-Sep-23	3-Oct-23	7-Oct-23	11-Oct-23	15-Oct-23	20-Oct-23
		Wed	Thu	Fri	Sat	Sun	Mon	Tue	Wed	Thu	Fri
	Item										
1	Introduction	*Faris, Jay & Mary*									
2	Static & Dynamic Revise	*Olivia, Mary & Son*									
3	Experimental Investigation	*Faris, Olivia & Son*									
4	FEA	*Faris, Jay, Olivia & Son*									
5	Composite Design	*Jay & Mary*									
6	Report Formatting and Referencing	*Everyone*									

Figure 4 Project timeline (Source: Faris Roslan)

Figure 4 presents the project timeline of the final report.

CHAPTER 2: STATIC & DYNAMIC ANALYSIS

2.1 Static Analysis

In Assignment 1 "Progress Report" the static analysis focuses on evaluating the structural integrity and performance of a PC-9 Wing Main Spar at Rib 5, where three scenarios are examined: Unnotched Analysis, Notched Analysis, and Fracture Analysis.

In the unnotched analysis, an idealised, defect-free main spar with a I-shaped cross section is considered. To simplify the analysis, the effects of stringers and ribs are neglected. In this analysis, stress and strain values are likely overestimations, which serves to identify potential failure modes. Furthermore, different loading conditions, with either the flange or web bearing stress are explored.

The notched analysis investigates the structural behaviour of a notched main spar, where circular notched holes in the flange and web are considered, in turn, affecting stress distribution. In this analysis, both loading and unloading conditions are examined to assess their impact on the performance of the main spar.

Lastly, the fracture analysis explores the likelihood and consequences of fractures in the main spar, which often results from material defects and wear. Three cases are considered: cracks from a circular hole in the flanges, single edge cracks on the flanges, and a centre crack on the web.

2.2 Static Analysis: Unnotched Analysis

The unnotched analysis involved calculating principal stresses in the main spar, with an additional calculation of Von Mises stress for a more conservative assessment of the maximum stress the material can endure without yielding. Two primary force paths were considered for stress analysis:

1. **Forces Applied at the Top of the Beam:** This simulates load distribution when forces are applied away from the centroid, such as at the top of the wing.
2. **Forces Applied at the Centreline:** This represents the scenario where forces are applied directly through the centroid of the spar.

In this analysis, two approaches were used for calculations, denoted as "Case A" and "Case B", they were considered sequentially in the analysis:

1. **Case A:** The main spar's web is responsible for shear forces, while the flanges bear the stress, this leads to compression at the top and bottom flange.
2. **Case B:** The main spar's web supports both shear and bending stresses from aerodynamic loads and aircraft weight, while the flanges handle axial loads (tension and compression forces). The flanges play a role in distributing these forces from the wing's skin to the spar web.

Ultimately, Case B was utilised where the web is fully effective in resisting shear and bending forces, the analysis involves calculating the combination of stresses resulting from lift and moment in the z-direction. This is achieved by calculating the total moment in the x-direction, multiplying it by the y-centroid of the web, and then dividing it by the second moment of inertia in the yy direction of the web. It is assumed that the web carries an equal amount of stress at each end, and the taper ratio remains consistent along the span.

The stress in the z-direction is resolved into stress in the y-direction, as well as the total stress (σ_1 and σ_2), these stress values are multiplied by the area of the web to calculate principal forces. However, during this loading condition, shear stress and shear flow are not considered uniform along the web height. Instead, they exhibit an elliptical distribution due to the presence of bending moments.

In this analysis, the maximum bending stress is observed at the top and bottom of the I-beam, while the maximum shear stress is found in the middle of the I-beam. These stresses are combined to calculate the effective stress, known as Von Mises Stress, at three locations: the top, middle, and bottom of the main spar at rib 5.

Given that a Factor of Safety (FoS) of 1.5 has been applied to the lift load and moment, the calculated stresses remain unchanged when determining the Margin of Safety (MoS). The highest Von Mises Stress is found at the top of the I-beam, measuring 237.598MPa. However, this value is still below the allowable stress (σ_c), resulting in a MoS greater than 0 in comparison to the material yield strength of 441Mpa. Consequently, there is no failure anticipated due to the stress levels.

2.2.1 Unnotched Analysis Results

Table 1 Forces on tapered beam of unnotched analysis

Forces on Tapered Beam		
	Value	**Units**
$\boldsymbol{P_{y1} = P_{y2}}$	2444.675	N
$\boldsymbol{P_{z1} = P_{z2}}$	163304.284	N
$\boldsymbol{P1 = P2}$	163322.581	N
Normal Stresses		
$\boldsymbol{\sigma_1 = \sigma_2}$	158.416	MPa
$\boldsymbol{S_{y,w}}$	17477.45	N
$\boldsymbol{q_s}$	-102.237	N/mm

Table 2 Principal stress A at top of I beam of unnotched analysis

Principle Stress A – Top of I Beam		
	Value	**Units**
$\boldsymbol{\sigma_z}$	158.416	MPa
$\boldsymbol{\sigma_1}$	208.538	MPa
$\boldsymbol{\sigma_2}$	-50.122	MPa
τ_{max}	129.33	MPa
Von Mises Stress and Margin of Safety – Top of I Beam		
Von Mises σ	237.598	MPa
MoS	0.85	-

Table 3 Principal stress C at middle of I beam of unnotched analysis

Principle Stress C – Middle of I Beam		
$\boldsymbol{\sigma_z}$	0	MPa
$\boldsymbol{\sigma_1}$	102.237	MPa
$\boldsymbol{\sigma_2}$	-102.237	MPa
τ_{max}	102.237	MPa
Von Mises Stress and Margin of Safety – Middle of I Beam		
Von Mises σ	177.08	MPa
MoS	1.49	-

Table 4 Safety factor of unnotched analysis

Safety Factor		
Allowable Stress $\boldsymbol{\sigma_c}$	294	MPa

2.3 Static Analysis: Notched Analysis

The notched analysis retains the assumptions and approximations from the unnotched analysis, with a focus on understanding how notches impact stress distribution. To achieve this, stress concentration factors (K_t) were calculated. To better model real material behaviour, the Ramberg-Osgood relationship is utilised. This equation is commonly used for describing real materials and forms the basis for our calculations.

In this analysis, we simplified the problem by considering only half a flange. We observed plasticity occurring in both the flange and the web notches. To analyse this, Neuber's rule was used, to calculate the local maximum and residual stresses and strain around the notches. An 8% elongation value was used as a reference to determine the H and n values, as shown in **Figure 5** and **Figure 6** below.

Approximating Stress Strain Curve	
Source: Engineers Edge	
Date:	
Project:	Tool Development
Engineering Material:	Aluminium 2124-T851
Yield Strength (lbs/in^2, N/mm^2) S_{Ys} =	441.000
Ultimate Strength (lbs/in^2, N/mm^2) S_{Us} =	483.000
Elastic modulus (lbs/in^2/ N/mm^2) E =	73100
Elongation (%) =	8.0

Figure 5 Approximating stress strain curve

Calculations Misc.	
Strain Hardening Constant n =	0.0247
Yield Strain (in/in^2, mm/mm^2) ε_{yield} =	0.0080
Plastic strain at failure (in/in, mm/mm) ε_f =	0.0800
Ultimate Strain (in/in^2, mm/mm^2) ε_{ult} =	0.0866
Strength coeffcient (lbs/in^2, N/mm^2) H =	497
Plastic Strain (in/in^2, mm/mm^2) ε_p =	0.0020

Figure 6 Calculations of stress strain curve

2.3.1 Notched Analysis Results

Table 5 The notched flange loading and unloading, notched web loading and unloading

Notched Flange Analysis - Loading		
	Value	**Units**
Hole diameter (D)	6.35	mm
H	497	MPa
n	0.0247	-
D/W	0.193	-
K_t	2.55	-
S	392.55	MPa
K_t**S**	1001.02	MPa
σ ε	13.71	MPa
Local σ_{max}	445.86	MPa
Local ε_{max}	0.03074	mm/mm
Notched Flange Analysis - Unloading		
△S	392.55	MPa
K_t**△S**	1001.02	
$2 \times \sigma_o$	882	MPa
△σ△ε	13.71	MPa
△σ	854.35	MPa
△ε	0.01604	mm/mm
Residual Stress and Strain		
σ_y	-408.49	MPa
ε_y	0.0147	mm/mm

Notched Web Analysis - Loading		
	Value	**Units**
Hole diameter (D)	6.35	mm
H	497	MPa
n	0.0247	-
D/W	0.0295	-
K_t	4	-
S	340.45	MPa
K_t**S**	1361.79	MPa
σ ε	25.37	MPa
Local σ_{max}	444.79	MPa
Local ε_{max}	0.057	mm/mm
Notched Web Analysis - Unloading		
△S	340.45	MPa
K_t**△S**	1361.79	MPa
$2 \times \sigma_o$	882	MPa
△σ△ε	25.37	MPa
△σ	883.11	MPa
△ε	0.0287	mm/mm
Residual Stress and Strain		
σ_y	-438.32	MPa
ε_y	0.0283	mm/mm

2.4 *Static Analysis: Fracture Analysis*

The fracture analysis involved the examination of 1.5mm cracks located in three different positions on the main spar at rib 5, as shown in **Figure** 8. These cracks were categorised into three types: cracks emanating

from flange holes, single edge cracks on side of top and bottom flanges, and a centre crack in the web. These will be referred to as Case I, Case II, and Case III respectively.

The analysis of each crack location required distinct methods and involved different assumptions to simplify the analysis process, alongside this, it utilised the fracture toughness of the material, represented as K_{IC}. The measurement of fracture toughness involves conducting specialised tests on a material, such as the Single Edge Notch Bend (SENB) or Compact Tension (CT) tests [24,25]. These tests subject the material specimen to controlled loading conditions and create a crack or notch in the material. By measuring the critical stress intensity factor (K_{IC}) under these controlled conditions, the material's fracture toughness is determined.

The objective was to provide conservative estimates of the K-solutions (stress intensity factors), MoS against brittle fracture and plastic collapse, and to investigate the applicability of Linear Elastic Fracture Mechanics (LEFM) [25] using the process in **Figure 7**.

For Case I and Case II, a Mode I analysis was conducted. Mode I fracture occurs when the in the material is subjected to loading that causes the crack to open or extend in a direction perpendicular to the crack plane. The primary fracture behaviour involves tensile stress acting normal to the crack surfaces. It is often described as 'opening mode' because the crack faces move directly apart. For Case III, a Mode II fracture occurs when the crack surfaces slide past each other in a parallel or shear motion. The applied load in this mode is parallel to the direction of crack growth. This mode is characterised by in-plane shear stress acting parallel to crack surfaces.

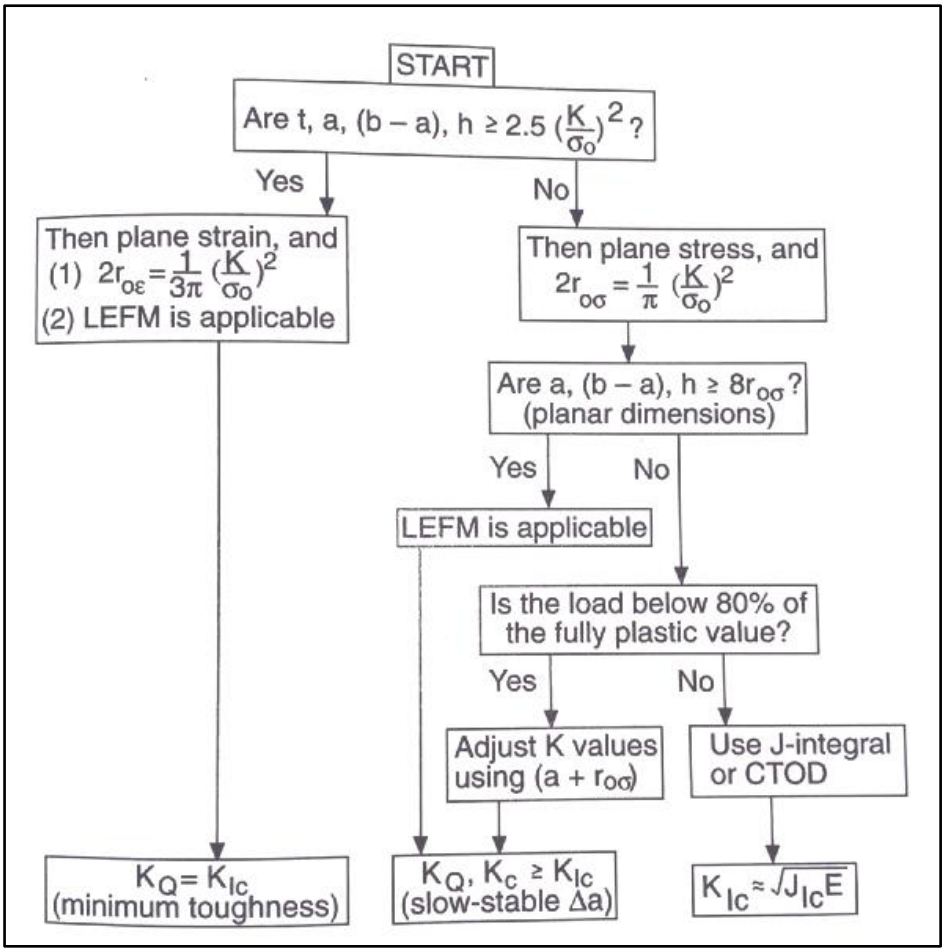

Figure 7 The applicability of LEFM process (Source: Mechanic Behaviour of Materials [25])

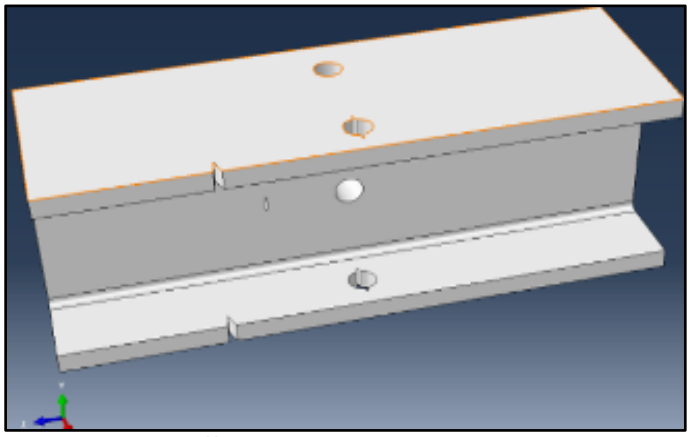

Figure 8 Three different cracks on rib 5 (Source: RMIT Canvas)

2.4.1 Fracture Analysis Results

Table 6 Cracks emanating from flange holes

Cracks Emanating from Flange Holes		
	Value	**Units**
$\mathbf{K_{IC}}$	26	MPa × $m^{1/2}$
l	1.5	mm
c	3.175	mm
a	4.675	mm
t	15.65	mm
b	16.467	mm
d	0.3208	-
$\mathbf{F_d}$	1.861	-
$S_{maximum\ notch\ local\ stress}$	392.55	MPa
$S_{plastic\ collapse}$	315.8	MPa
$S_{brittle\ fracture}$	203.5	MPa
$\mathbf{K_I}$	50.15	MPa × $m^{1/2}$
a_c	5.58	mm
a_p	8.86	mm
Safety Factor against Brittle Fracture X_k	0.518	-
Safety Factor against Plastic Collapse X_p	0.804	-
Margin of Safety (MoS)		
$(MoS)_{Brittle\ fracture}$	-0.481	-
$(MoS)_{Plastic\ Collapse}$	-0.195	-
LEFM Applicability		
Criteria		**Applicability (Y/N)**
Plain Strain Condition $\mathbf{t, a, (b\text{-}a), h \geq 2.5\left(\frac{K}{\sigma_o}\right)^2}$		N
Plain Stress Condition $\mathbf{a, (b-a), h \geq 8r_{o\sigma}}$		N
Nominal Stress (S) < $0.8\sigma_o$		N

Table 7 Single edge cracks on side of top and bottom flanges

Single Edge Cracks on Side of Top and Bottom Flanges

	Value	Units
$\mathbf{K_{IC}}$	26	MPa × $m^{1/2}$
a	1.5	mm
b	32.93	mm
t	15.65	mm
F	1.12	
$\mathbf{S_g}$	316.87	MPa
$\mathbf{K_I}$	28.03	MPa × $m^{1/2}$
$\mathbf{P_0}$	216951	N
P	163322	N
a_c	1.70	mm
a_p	9.27	mm
Safety Factor against Brittle Fracture X_k	0.927	-
Safety Factor against Plastic Collapse X_p	1.328	-

Margin of Safety (MoS)

$(MoS)_{Brittle\ fracture}$	-0.07	-
$(MoS)_{Plastic\ Collapse}$	0.328	-

LEFM Applicability

Criteria	Applicability (Y/N)
Plain Strain Condition	N
t, a, (b-a), h $\geq 2.5\left(\frac{K}{\sigma_o}\right)^2$	
Plain Stress Condition	N
a, **(b − a)**, **h** $\geq 8r_{o\sigma}$	
Nominal Stress (S) < 0.8σ_o	Y

Table 8 Centre crack in the web

Centre Crack in the Web

	Value	Units
$\mathbf{K_{IC}}$	26	MPa × $m^{1/2}$
τ_{max}	102.237	MPa
a	0.75	mm
b	107.46	mm
t	2.3	mm
F	1	
$\mathbf{K_{II}}$	4.96	MPa × $m^{1/2}$
$\mathbf{P_0}$	216478	N
P	25269.46	N
a_c	20.58	mm
a_p	82.55	mm
Safety Factor against Brittle Fracture X_k	5.23	-
Safety Factor against Plastic Collapse X_p	8.56	-

Margin of Safety (MoS)

$(MoS)_{Brittle\ fracture}$	4.23	-

$(MoS)_{Plastic\ Collapse}$	7.56	-

LEFM Applicability

Criteria	Applicability (Y/N)
Plain Strain Condition $\mathbf{t, a, (b\text{-}a), h \geq 2.5\left(\frac{K}{\sigma_o}\right)^2}$	N
Plain Stress Condition $\mathbf{a, (b-a), h \geq 8r_{o\sigma}}$	N
Nominal Stress (S) < 0.8σ_o	Y

2.5 Dynamic Analysis

In this section, the focus is on dynamic analysis, specifically assessing the long-term effects of cyclical stresses and strains on PC-9 aircrafts main spar. The analysis is aimed at understanding how these factors relate to three different design methodologies: fail-safe, safe-life, and damage tolerant design.

The analysis concentrates on three specific types of cracks that are likely to occur in the main spar: uniaxial cracks emanating from notches on the flanges, single edge cracks on the top and bottom flange, and a centre crack in the web. A crack is considered detectable if it measures longer than 1.5mm.

The three design methodologies are explained as follows:

1. **Fail-Safe Design:** This approach ensures that if a component fails, it does so in a way that is visible during routine inspections and minimally damaging to the aircraft's overall structural integrity. It allows for isolated failures without catastrophic outcomes.
2. **Safe-Life Design:** This methodology involves pre-emptively replacing components based on estimated lifespans to minimise the chances of failure during operation. It includes determining the expected fatigue life of each component and creating a replacement schedule.
3. **Damage Tolerant Design:** This approach focuses on understanding how an aircraft structure can continue to function even when damaged. It involves studying crack propagation and assessing how loading conditions change as damage progresses.

The key deliverables of this analysis include determining the fatigue life of the PC9 wing main spar under each of the three design methodologies and developing a maintenance schedule. This involves calculating the expected loading conditions for typical flights and analysing their effects on the main spar over time.

Furthermore, the analysis demonstrates the importance of breaking does the various loading conditions experienced by the beam to accurately assess material fatigue in aerospace components. It involves identifying forces, calculating cycle counts for each condition, and determining mean stress and stress amplitude. The Smith-Watson-Topper (SWT) rule is utilised to provide a more realistic Equivalent Stress Amplitude by considering both mean stress and stress amplitude in the calculations.

Table 9 Dynamic analysis input data

Dynamic Analysis Input Data

	Value	Units
σ'f	706	MPa
ε'f	0.15	mm/mm
A	670.23	-
b	-0.075	-
c	-053	-
σf	201.68	MPa
σ_{max}	453.27	MPa

σ_{min}	-413.72	MPa
σ_m	19.77	MPa
σ_{ar}	443	MPa
A	670.23	-
C	2.95121E-15	
m	8.45	-

Table 10 PC-9 typical load spectrum for one flight

PC-9 Typical Load Spectrum (One Flight)

Loading Condition	**Loading Range (g)**	**Cycles**
I	0.5 → 1.0	1200
II	1.0 → 1.75	560
III	1.75 → 2.5	70
IV	2.5 → 3.5	25
V	3.5 → 5.0	30
VI	5.0 → 6.0	5
VII	6.0 → 7.0	25
VIII	1.0 → 4.5	6
IX	0 → 5.0	8
X	-(3.5) → 1.5	25

2.6 *Dynamic Analysis: Safe-Life and Fail-Safe*

The S-N curve is a useful tool for assessing a material's ability to withstand cyclic loading with zero mean stress. For non-ferrous alloys like aluminium, the typical fatigue limit occurs at around 108 cycles with a stress amplitude of approximately 200MPa. However, when dealing with stress concentration at holes, as revealed through Notched Analysis, the stress amplitude becomes higher, as well as non-zero mean stress. This situation is particularly significant when dealing with shorter cyclic loading periods.

A comparative examination between unnotched and notched components reveals that maximum stress concentration occurs at the holes on the flange, with a value of 445.86MPa. This stress level serves as the structural threshold for various flight phases, where constant loading amplitudes of each phase are analysed. Under the maximum loading conditions of 445.86MPa, coupled with a residual stress of 408.49 MPa, the hole on the flanges of the main spar at rib 5 is expected to withstand approximately 247 cycles before potential failure. However, in practical operation, this component is likely to last considerably longer since these stress amplitudes rarely happen.

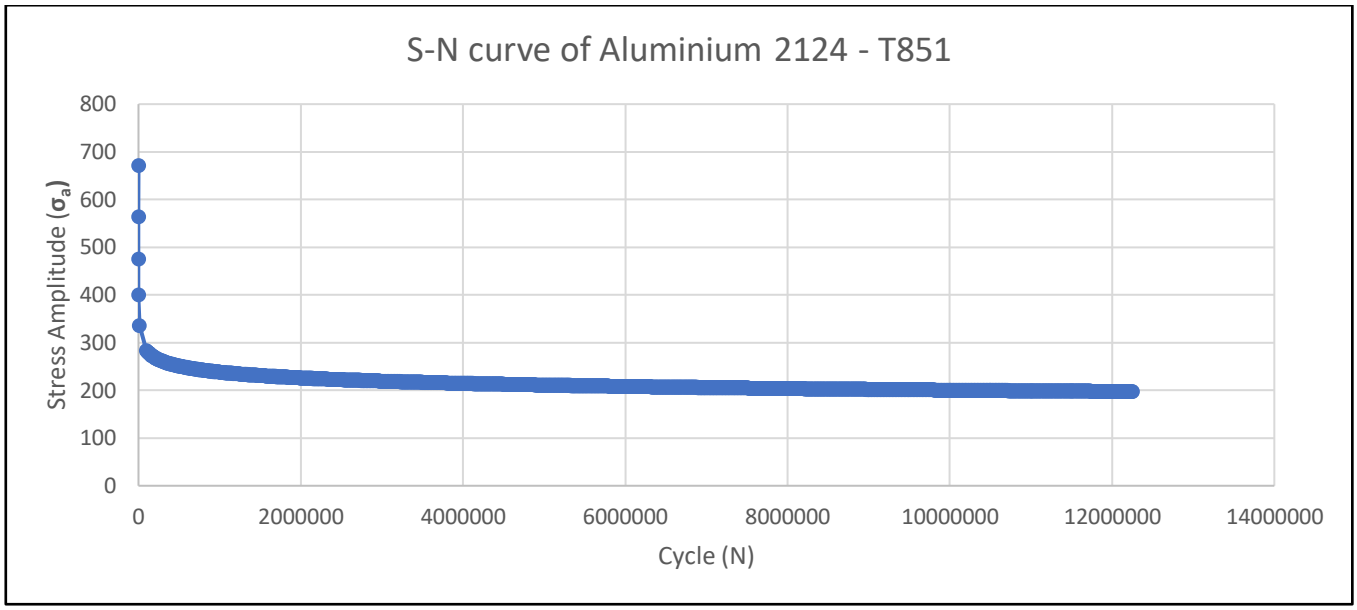

Figure 9 S-N curve of aluminium 2124 – T851

To determine the lifespan under operational conditions, a loading spectrum representative of the PC-9 aircraft is employed and displayed in **Table 11**, allowing for the calculation of repetitions until failure.

The maximum stress corresponds to 7g load during flight, necessitating the analysis of loading ranges derived from these equivalents, resulting in minimum (σ_{min}), and maximum (σ_{max}) stress values. As these stress levels are not symmetrical from the zero-mean stress, the equivalent stress amplitude at $\sigma_m = 0$, $\sigma_{ar,}$ is calculated.

The analysis revealed a significantly higher number of repetitions, approximately 199998.1979, compared to the earlier estimate of 247 cycles. This indicates that the PC-9 aircraft can endure approximately 200,000 flights under the given loading spectrum without experiencing failure.

Table 11 Loading spectrum calculations of repetitions until failure

Loading Conditions	Loading Range (g)	Cycles (**N_i**)	σ_min	σ_max	σ_amplitude	σ_m	σ_ar	**N_f**	**N_i /N_f**
I	0.5-1	1200	32.38	64.75	16.19	48.57	32.38	3.5E+17	3.4E-15
II	1-1.75	560	64.75	113.32	24.28	89.04	52.46	5.7E+14	9.9E-13
III	1.75-2.5	70	113.32	161.89	24.28	137.60	62.70	5.2E+13	1.3E-12
IV	2.5-3.5	25	161.89	226.64	32.38	194.26	85.66	8.2E+11	3.1E-11
V	3.5-5	30	226.64	323.77	48.57	275.21	125.40	5.1E+09	5.9E-09
VI	5-6	5	323.77	388.52	32.38	356.15	112.16	2.2E+10	2.2E-10
VII	6-7	25	388.52	453.28	32.38	420.90	121.14	8.0E+09	3.1E-09
IIX	1-4.5	6	64.75	291.39	113.32	178.07	181.72	3.6E+07	1.7E-07
IX	0-5	8	0.00	323.77	161.89	161.89	228.94	1.7E+06	4.8E-06
X	(-3.5)-1.5	25	-226.64	97.13	161.89	-64.75	125.40	5.1E+09	4.9E-09

The final value of repetitions is 199998.1979. Through the analysis, the type of failure that occurs first, or has the lower strain value, takes precedence at each cycle count. In this evaluation, we focus on two failure types: Plastic (Ductile) and Elastic Strain. Elastic Strain dominates at approximately 200 cycles, after which Plastic Strain becomes the dominant failure mode.

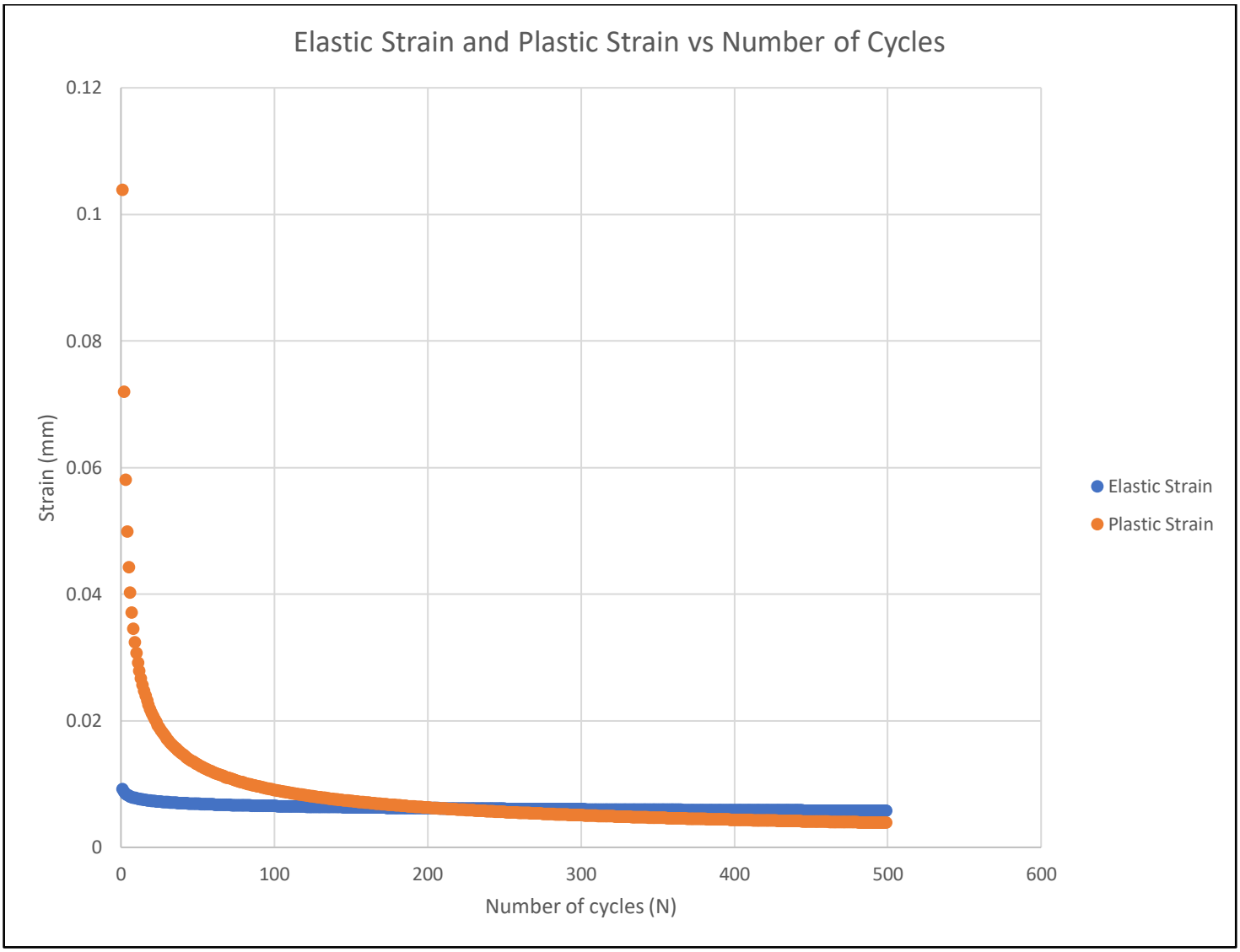

Figure 10 Elastic strain & plastic strain vs number of cycles graph

2.7 *Dynamic Analysis: Damage Tolerant*

Derived from the comparison of Elastic and Plastic Strain, it is evident that the Elastic failure criteria only dominate within the first 207 cycles of operation. This period is relatively insignificant when viewed in the context of the total number of cycles and spectrums. Notably, the critical crack length for Plastic Failure is lower than that for Elastic Failure, making it the governing factor for crack growth.

In damage tolerance, structural defects like cracks are expected to exist in specific areas of a component, and these defects act as stress concentration points. To prevent catastrophic structural failure, its essential to inspect and identify these cracks in advance.

The first step in this process is determining the critical crack length that would lead to structural failure. These critical lengths are established through prior fracture analyses, considering both elastic and plastic failure modes. The smaller of these two lengths is selected as the critical crack length. With this information, the next step of these calculations involved solving the crack growth equation numerically for each unique loading condition. The reason for using a numerical approach is that both the Stress Intensity Factor (ΔK) and Geometry Correction Factor (F) are not constant; they change as the crack length evolves.

After completing the numerical assessment, a prediction was made of how many cycles it will take for the crack length to exceed the fatigue limit. This prediction is crucial for planning inspection intervals, where the cycles to failure (Nf) is divided by the expected service life of the component. A ratio below one suggests that the components may fail before its intended service life, indicating the need for more frequent inspections.

Table 12 Detectable crack length for all cases

Detectable Crack length for All Cases		
Detectable crack length a_i	1.5	mm
Final Crack Lengths for the Flange Holes		
Final crack length a_c in brittle fracture	5.58	mm
Final crack length a_p in plastic collapse	8.86	mm
Final Crack Lengths for the Single Edge Cracks on Top and Bottom Flange		
Final crack length a_c in brittle fracture	1.70	mm
Final crack length a_p in plastic collapse	9.27	mm
Final Crack Lengths for the Centre Crack in the Web		
Final crack length a_c in brittle fracture	20.58	mm
Final crack length a_p in plastic collapse	82.55	mm

2.7.1 Damage Tolerance Results

Table 13 Final crack length for the flange holes

Final Crack Lengths for the Flange Holes		
Detectable crack length a_i	1.5	mm
Final crack length a_c in brittle fracture	5.58	mm

Table 14 Crack growth of 200000 repetitions calculation with the final crack length for the flange holes

Loading Condition	Number of Cycles	Crack Growth (200000 repetitions) (mm)	Failure (Y/N)
I	1.20E+03	0.002684	No
II	5.59E+02	0.036996	No
III	6.47E+01	0.004636	No
IV	2.50E+01	0.018276	No
V	3.00E+01	0.643676	No
VI	5.46E+00	0.004	No
VII	7.64E+01	0.016	No
IIX	6.00E+00	218.68	Yes
IX		Assume Failure	
X		Assume Failure	

Table 15 Detectable and final crack lengths for single edge crack on top and bottom flange

Detectable and Final Crack Lengths for Single Edge Crack on Top and Bottom Flange		
Detectable crack length a_i	1.5	mm
Final crack length a_c in brittle fracture	1.70	mm

Table 16 Crack growth of 200000 repetitions calculation with the detectable crack length for single edge crack on top and bottom flange

Loading Condition	Number of Cycles	Crack Growth (200000 repetitions) (mm)	Failure (Y/N
I	1.21E+03	0.088	No
II	5.6E+02	1.25	No
III	7.11E+01	0.159	No

IV	2.5E1+01	0.619	No
V	2.5E+01	18.35	Yes
VI	4.99E+00	0.12	No
VII	2.51E+01	0.619	No
IIX	6.0E+00	5416.152	Yes
IX		Assume Failure	
X		Assume Failure	

Table 17 Detectable and final crack lengths for centre crack in the web

Detectable and Final Crack Lengths for Centre Crack in the Web		
Detectable crack length a_i	1.5	mm
Final crack length a_c in brittle fracture	20.58	mm

Table 18 Crack growth of 200000 repetitions calculation with the detectable and final crack length for centre crack in the web

Loading Condition	Number of Cycles	Crack Growth (200000 repetitions) (mm)	Failure (Y/N
I	1.21E+03	0.04	No
II	5.71E+02	0.52	No
III	8.16E+01	0.04	No
IV	2.59E+01	0.24	No
V	3.00E+01	9.56	No
VI	7.39E+00	0.04	No
VII	2.59E+01	0.24	No
IIX	6.01E+00	879.92	Yes
IX		Assume Failure	
X		Assume Failure	

2.7.2 Inspection Intervals

Cracks are frequently discovered in certain types of large, welded hardware, including structures like bridges, ships, and aircraft components like the main spar of the PC-9, the presence of cracks necessitates an analysis using fracture mechanics. In this analysis, it is assumed that the wing's main spar at rib contains cracks with a minimum detectable length of 1.5mm, and a critical crack length a_c. When brittle fracture occurs after N_f loading cycles, the safety factor on life X_N is determined. If the safety factor on life if less than 1, periodic inspections are required every $N_{Interval}$ cycles.

2.7.3 Inspection Intervals Results

Table 19 Inspection intervals of cracks emanating from the circular hole in the flange

Inspection Intervals of Cracks Emanating from the Circular Hole in the Flange		
	Value	**Units**
N_f	7.14E+05	Cycles
X_N	0.002	-
$N_{Interval}$	4.76E+05	Cycles

Table 20 Inspection intervals of single edge crack on top and bottom flange

Inspection Intervals of Single Edge Crack on the Top and Bottom Flange

	Value	Units
N_f	3.13E+07	Cycles
X_N	0.08	-
$N_{Interval}$	2.09E+07	Cycles

Table 21Inspection intervals of centre crack in the web

Inspection Intervals of Centre Crack in the Web

	Value	Units
N_f	9.0306+09	Cycles
X_N	23.11	-
$N_{Interval}$	-	-

2.8 Discussion: Static analysis and dynamic analysis

Static analysis is critical for evaluating the structural integrity and load distribution of the PC-9 wing under various operational situations, which aids in efficient design and material consumption. It aids in the determination of stresses, strains, and deformations, guaranteeing that the wing can endure aerodynamic forces and other environmental conditions.

Dynamic analysis, on the other hand, is critical for understanding how the wing responds to time-varying loads, anticipating flying behaviour, and developing aero elastically stable wings that resist flutter. We can optimise the PC-9 wing for safety, stability, and performance in a variety of flying circumstances by integrating static and dynamic analysis.

2.8.1 Static analysis

Unnotched: The unnotched analysis of the main spar revealed that the maximum stress occurs at the top of the I-beam, but it remains below the allowable stress limit, indicating that the main spar is unlikely to fail due to stress under normal operating conditions. The stress distribution varies depending on the force path, with forces applied at the top of the beam resulting in maximum bending stress at the top and bottom of the I-beam, while forces applied at the centreline lead to maximum shear stress in the middle of the I-beam.

Case B, which considers the combined effects of shear and bending stresses, provides a more accurate stress calculation compared to Case A. The slight discrepancy between the calculated Sy and the total shear load is likely due to rounding errors or minor differences in assumptions and is not expected to significantly impact the overall results. While the unnotched analysis suggests the main spar is unlikely to fail under normal stress conditions, further analysis may be required to fully assess its structural integrity, considering factors like fatigue and other potential failure modes.

Notched: The notched analysis revealed that the presence of notches in both the flange and web of the main spar significantly increases stress concentrations, with stress concentration factors (Kt) of 2.55 and 4, respectively. These elevated stress levels exceed the yield strength of the material, indicating that plastic deformation is likely to occur around the notches.

While residual stresses in both the flange and web were found to be compressive, which can improve fatigue life, the overall conclusion is that notches can weaken the main spar and increase its susceptibility to fatigue failure.

Fracture: The fracture analysis revealed that cracks in different locations on the main spar pose varying levels of risk. Cracks emanating from flange holes (Case I) were found to be most concerning, with a high likelihood of brittle fracture and a safety factor of 0.518.

Single edge cracks on the flanges (Case II) presented a lower risk, with a safety factor of 0.927, while the centre crack in the web (Case III) posed the least concern, with a safety factor of 5.23. These findings suggest that cracks emanating from flange holes require the most attention, while the centre crack in the web is less critical. Further analysis may be needed to fully assess the impact of cracks on the structural integrity of the main spar and determine appropriate mitigation strategies.

2.8.2 Dynamic analysis

The dynamic analysis provided valuable insights into the long-term effects of cyclical stresses and strains on the PC-9 aircraft's main spar under three design methodologies: fail-safe, safe-life, and damage-tolerant design. The analysis considered three types of cracks and determined the fatigue life of the main spar under each design approach. This information can be used to develop maintenance schedules, replacement strategies, and damage management approaches to ensure the continued safe operation of the aircraft.

The parameter R, representing the stress ratio, significantly impacts fatigue life, with higher R values leading to longer fatigue lives and lower R values resulting in shorter fatigue lives. Therefore, it is essential to consider the appropriate R value when conducting fatigue analysis for accurate predictions.

Safe-Life and Fail-Safe: The S-N curve, a valuable tool for evaluating material fatigue resistance, indicates that non-ferrous alloys like aluminium typically reach their fatigue limit at around 10^8 cycles with a stress amplitude of approximately 200 MPa. However, stress concentrations at holes introduce higher stress amplitudes and non-zero mean stress, particularly relevant for shorter cyclic loading periods. Comparing unnotched and notched components highlights a maximum stress concentration of 445.86 MPa at the flange holes.

Under maximum loading conditions, the hole on the flanges of the main spar at rib 5 is expected to withstand approximately 247 cycles before potential failure. To determine the lifespan under operational conditions, a loading spectrum representative of the PC-9 aircraft is employed.

The analysis revealed that the PC-9 aircraft can endure approximately 200,000 flights under the given loading spectrum without experiencing failure. Throughout the analysis, the type of failure that occurs first, or has the lower strain value, takes precedence at each cycle count. Elastic Strain dominates initially, after which Plastic Strain becomes the dominant failure mode.

Damage Tolerance: The analysis reveals that elastic failure criteria are only dominant during the initial 207 cycles, a relatively insignificant period compared to the total operational cycles. As plastic failure has a lower critical crack length, it becomes the governing factor for crack growth. Damage tolerance emphasizes identifying and inspecting structural defects like cracks, which act as stress concentration points.

The critical crack length leading to structural failure is determined through fracture analyses, considering both elastic and plastic failure modes, with the smaller length being selected. The crack growth equation is solved numerically for each unique loading condition due to the varying Stress Intensity Factor (ΔK) and Geometry Correction Factor (F) with crack length. This numerical assessment predicts the number of cycles required for the crack length to exceed the fatigue limit, crucial for planning inspection intervals. The cycles to failure (Nf) divided by the expected service life indicates inspection frequency.

The damage tolerance results show that for most loading conditions, crack growth remains within acceptable limits, and failure is not predicted within 200,000 repetitions. However, for loading conditions VIII, IX, and X, the crack growth exceeds the critical length, leading to potential failure. These conditions require particular attention and may necessitate more frequent inspections or design modifications.

Inspection Intervals: For the inspection intervals, the cracks emanating from the circular holes in the flange can endure approximately 7.14E+05 cycles before reaching a critical crack length, leading to brittle collapse. Since the safety factor on life is 0.002, periodic inspections should be conducted every 4.76E+05 cycles,

equivalent to 243 flights, it can complete 365 flights before failure. For the single edge cracks on the top and bottom flange, it will grow to a critical length after 3.13E+07 cycles.

The safety factor on life is 0.08, indicating the need for inspections every 2.09E+07 cycles. This allows for 16025 flights before failure, requiring an inspection every 10683 flights. As for the centre crack in the web, the critical crack length is reached after 9.0306+09 cycles, as the safety factor on life exceeds 1, no periodic inspections are necessary for this crack.

CHAPTER 3: EXPERIMENTAL INVESTIGATION

3.1 Introduction

The experimental investigation within this project is a pivotal phase involving an in-depth analysis of the PC-9 wing's performance through practical experimentation on a specific cut-out section of the wing. The central aim of this investigation is to meticulously gather empirical data essential for validating the finite element model developed. The wing has been precisely cut at rib three on the right side, allowing for ample area to simulate the fuselage. The experimental setup involves the strategic placement of five strain gauges within the wing, designed to measure strain induced by external loading.

Moreover, the experiment encompasses the measurement of applied load magnitude and the corresponding deflection of the wing at both the point of application and the wingtip. Each participating team will be granted a dedicated one-hour practical session to conduct a thorough inspection and experimentally assess the wing's performance. The results garnered from these experiments by each team will play a crucial role in validating the finite element model and, by extension, enhancing its accuracy and reliability. The role of experimental investigation in aircraft design cannot be overstated, as it stands as a linchpin for acquiring precise data that validates and enhances the credibility of numerical models and simulations, ultimately advancing the trajectory of aerospace engineering.

Based on **Figure 11**, the PC-9 wing used in the experimental investigation is the left wing where a wooden chock set to the wing curvature where support beams are connected to two fixed hydraulic actuators to apply pressure which provides bending and is placed on the wing’s aerodynamic centre.

This chapter of the report discusses the experimental methods, experimental analysis, experimental results, and experimental discussion.

Figure 11 The PC-9 Wing at RMIT Bundoora

3.2 Experimental Method

The experimental investigation was led by two laboratory technicians which first present a briefing about the investigation before carrying out the experiment. Before conducting the actual experiment, an official risk

assessment form from RMIT "***Risk Assessment Activity HSW PR09 TM01***" in **Figure 12** must be filled in. The complete risk assessment form can be found in the appendices chapter of the report. The process flow of the experiment is shown in **Figure 13**.

The aim of the experiment is for the finite element validation which will introduce bending to an actual PC9 wing that will be done through two electromechanical mini actuators which can be seen in **Figure 11** from two load cells connected to the underside of the mini actuators. From that, strain readings will be taken from different locations, one LVDT sensor or linear variable differential transformer and a tape measure.

The actuators will be moved up in 10mm increments which then the transducers will give a reading, this will continue to a maximum of 95mm displacement. The strain data collected by the five strain gauage rosettes will be used in the experimental analysis part of the report. The locations of the five strain gauge rosettes are located on the aft between rib 5 and rib 6 on the top spar cap, web of the main spar, bottom spar cap, on the skin between rib 5 and rib 6 and on rib 11's neutral axis. The load applied from the actuators is located between rib 17 and rib 18. At the wing tip of the PC9, a relative measurement from the ground is taken using a measuring tape.

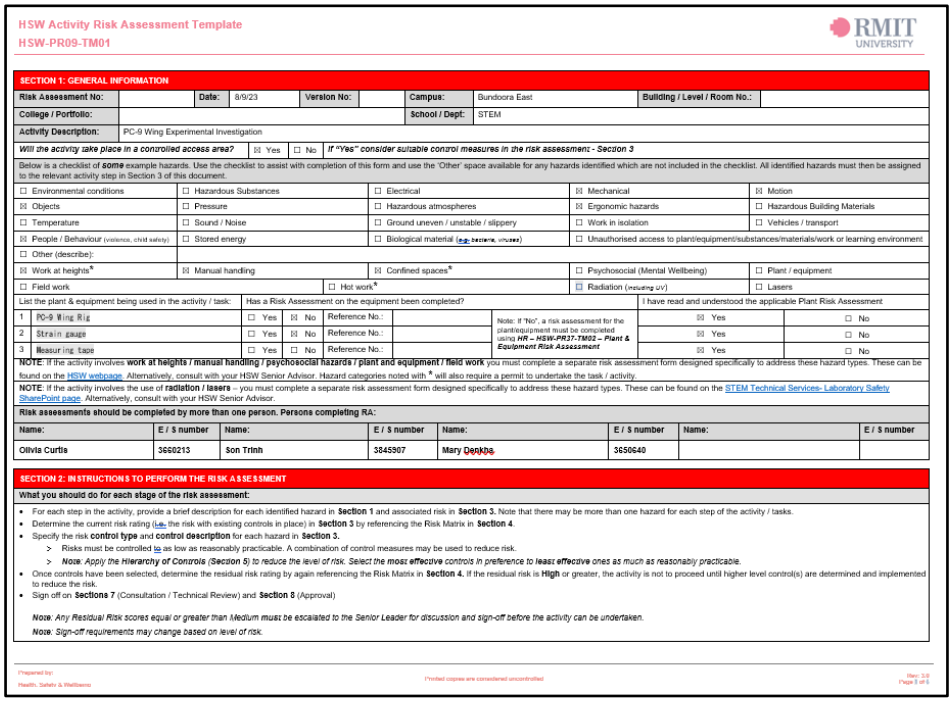

HSW Activity Risk Assessment Template
HSW-PR09-TM01

RMIT UNIVERSITY

SECTION 1: GENERAL INFORMATION

Risk Assessment No:		**Date:** 8/9/23	**Version No:**	**Campus:** Bundoora East	**Building / Level / Room No.:**
College / Portfolio:				**School / Dept:** STEM	
Activity Description:	PC-9 Wing Experimental Investigation				

Will the activity take place in a controlled access area? ☒ Yes ☐ No *If "Yes" consider suitable control measures in the risk assessment - Section 3*

Below is a checklist of *some* example hazards. Use the checklist to assist with completion of this form and use the 'Other' space available for any hazards identified which are not included in the checklist. All identified hazards must then be assigned to the relevant activity step in Section 3 of this document.

☐ Environmental conditions	☐ Hazardous Substances	☐ Electrical	☒ Mechanical	☒ Motion
☒ Objects	☐ Pressure	☐ Hazardous atmospheres	☒ Ergonomic hazards	☐ Hazardous Building Materials
☐ Temperature	☐ Sound / Noise	☐ Ground uneven / unstable / slippery	☐ Work in isolation	☐ Vehicles / transport
☒ People / Behaviour (violence, child safety)	☐ Stored energy	☐ Biological material (e.g. bacteria, viruses)	☐ Unauthorised access to plant/equipment/substances/materials/work or learning environment	
☐ Other (describe):				
☒ Work at heights*	☒ Manual handling	☒ Confined spaces*	☐ Psychosocial (Mental Wellbeing)	☐ Plant / equipment
☐ Field work		☐ Hot work*	☒ Radiation (including UV)	☐ Lasers

List the plant & equipment being used in the activity / task:		Has a Risk Assessment on the equipment been completed?				I have read and understood the applicable Plant Risk Assessment	
1	PC-9 Wing Rig	☐ Yes	☒ No	Reference No.:	Note: If "No", a risk assessment for the plant/equipment must be completed using *HR – HSW-PR37-TM02 – Plant & Equipment Risk Assessment*	☒ Yes	☐ No
2	Strain gauge	☐ Yes	☒ No	Reference No.:		☒ Yes	☐ No
3	Measuring tape	☐ Yes	☐ No	Reference No.:		☒ Yes	☐ No

NOTE: If the activity involves **work at heights / manual handling / psychosocial hazards / plant and equipment / field work** you must complete a separate risk assessment form designed specifically to address these hazard types. These can be found on the HSW webpage. Alternatively, consult with your HSW Senior Advisor. Hazard categories noted with * will also require a permit to undertake the task / activity.

NOTE: If the activity involves the use of **radiation / lasers** – you must complete a separate risk assessment form designed specifically to address these hazard types. These can be found on the STEM Technical Services- Laboratory Safety SharePoint page. Alternatively, consult with your HSW Senior Advisor.

Risk assessments should be completed by more than one person. Persons completing RA:

Name:	E / S number	Name:	E / S number	Name:	E / S number	Name:	E / S number
Olivia Curtis	3660213	Son Trinh	3845907	Mary Doukas	3650640		

SECTION 2: INSTRUCTIONS TO PERFORM THE RISK ASSESSMENT

What you should do for each stage of the risk assessment:

- For each step in the activity, provide a brief description for each identified hazard in **Section 1** and associated risk in **Section 3**. Note that there may be more than one hazard for each step of the activity / tasks.
- Determine the current risk rating (i.e. the risk with existing controls in place) in **Section 3** by referencing the Risk Matrix in **Section 4**.
- Specify the risk **control type** and **control description** for each hazard in **Section 3.**
  - Risks must be controlled to as low as reasonably practicable. A combination of control measures may be used to reduce risk.
  - *Note: Apply the Hierarchy of Controls (Section 5) to reduce the level of risk. Select the most effective controls in preference to least effective ones as much as reasonably practicable.*
- Once controls have been selected, determine the residual risk rating by again referencing the Risk Matrix in **Section 4.** If the residual risk is **High** or greater, the activity is not to proceed until higher level control(s) are determined and implemented to reduce the risk.
- Sign off on **Sections 7** (Consultation / Technical Review) and **Section 8** (Approval)

Note: Any Residual Risk scores equal or greater than Medium must be escalated to the Senior Leader for discussion and sign-off before the activity can be undertaken.

Note: Sign-off requirements may change based on level of risk.

Figure 12 Risk Assessment Activity HSW PR09 TM01 (Source: RMIT Canvas

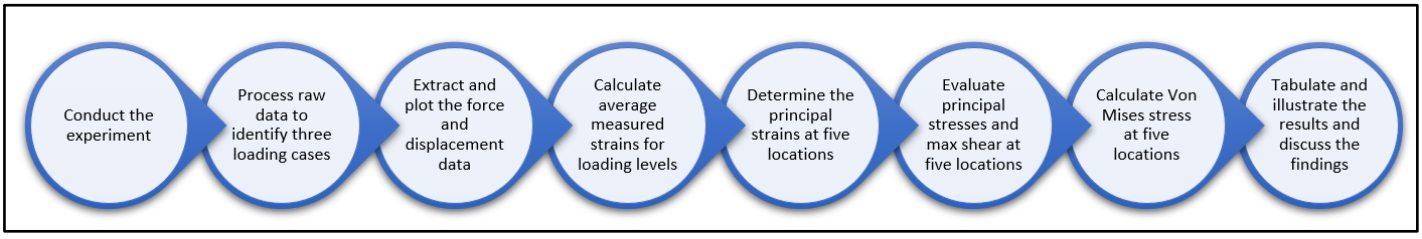

Figure 13 Process for experimental investigation

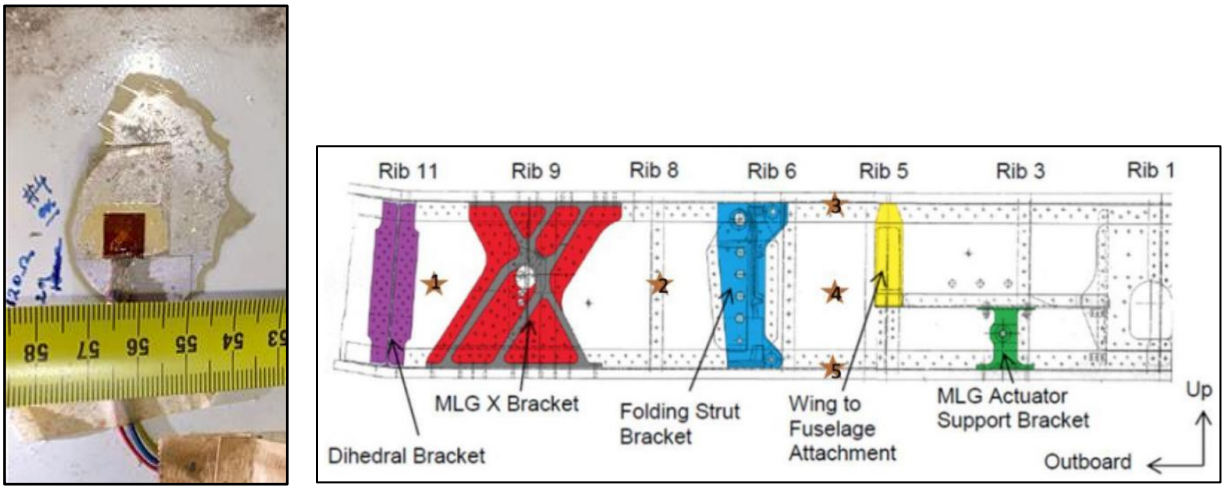

Figure 14 Rossette strain gauge and the location of five of them on the PC-9 wing (Source: RMIT Canvas)

Table 22 The distance of the rosette strain gauges from the main spar, bottom skin and distance from rib 11

No.	Location	Distance from Main Spar (mm)	Distance from Bottom Skin (mm)	Distance from Rib 11 (mm)
1	Top Spar Cap	35	700	690
2	Bottom Spar Cap	35	20	690
3	Spar Web	0	300	690
4	Rib	110	350	0
5	Skin	330	0	395

The steps taken for the experimental investigation is as follows:

1. Apply 10 mm increments displacement
2. Measure the wing tip displacement
3. Repeat steps 1 and 2 until the maximum displacement intended

3.3 Experimental Analysis

An experimental analysis can be completed by using the raw experimental data collected by the five rectangular strain gauge rosettes during the PC-9 wing experiment. The strain gauge rosettes were placed at five locations on the PC-9 wing, allowing us to analyse the strain experienced at these locations during each loading level: top spar cap, bottom spar cap, spar web, rib, and skin.

The strain gauge rosette measures the strain data from external loading in the *a*, *b*, and *c* direction at each location over the duration of the course of the loading, further to this, the displacement, loading, and time data is also recorded. By graphing the time (s) vs displacement (mm) from the raw experimental data, the increasing external force (N) denoted as “Level 1, 2, and 3” applied to the wing during the experiment can be identified.

From this, the displacement at the point of application from each loading level is recognised and compared to the wingtip displacement which was physically measured at each loading level during the experiment. Alongside this, the average strain values for each loading level are displayed in Appendix K1, K2, and K3.

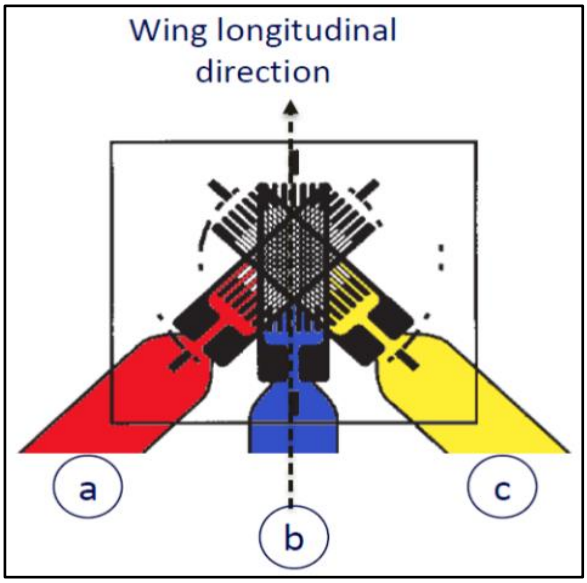

$$\varepsilon_a = \varepsilon_x$$

$$\varepsilon_c = \varepsilon_y$$

$$\gamma_{xy} = 2\varepsilon_b - \varepsilon_a - \varepsilon_c$$

Figure 15 Strain Gauge Rosette Measurement Directions & the three levels loading of the rosette strain gauges with its associated equations

By utilising the equations below, the principal strains, principal stresses, maximum shear stress and strain, and Von Mises stress can be calculated for each location and loading level. These results will be used to validate the FEA model.

Table 23 The equations for principal strains and stresses, maximum shear strain and stresses, and Von Mises stresses

Principle Strains	$\varepsilon_{1,2} = \frac{\varepsilon_x + \varepsilon_y}{2} \pm \sqrt{\left(\frac{\varepsilon_x - \varepsilon_y}{2}\right)^2 + \left(\frac{\gamma_{xy}}{2}\right)^2}$
Maximum Shear Strain	$\gamma_{max} = 2\sqrt{\left(\frac{\varepsilon_x - \varepsilon_y}{2}\right)^2 + \left(\frac{\gamma_{xy}}{2}\right)^2}$
Principle Stresses	$\sigma_1 = \frac{E}{1-v^2}(\varepsilon_1 + v\varepsilon_2)$ $\sigma_2 = \frac{E}{1-v^2}(\varepsilon_2 + v\varepsilon_1)$
Maximum Shear Stress	$\tau_{max} = abs\left(\frac{\sigma_1 - \sigma_2}{2}\right)$
Von Mises Stress	$\sigma_{eq} = \sqrt{{\sigma_1}^2 - \sigma_1\sigma_2 + {\sigma_2}^2}$

3.4 Results

The results collected from the experimental investigation are displayed below, where from the raw experimental data the time (s) vs Displacement (mm) was first plotted. By plotting these values, the graph displays how the PC-9 wing section responds to loads applied by the actuators, by taking the average displacement value at the 'flat' part of the plotted data as shown in **Error! Reference source not found.**, loading levels 1, 2, and 3 can be identified in the raw data. By analysing the graph, it shows that as the load is increased, the displacement at the point of application also increases, this implies that the wing is undergoing deflection due to the applied load.

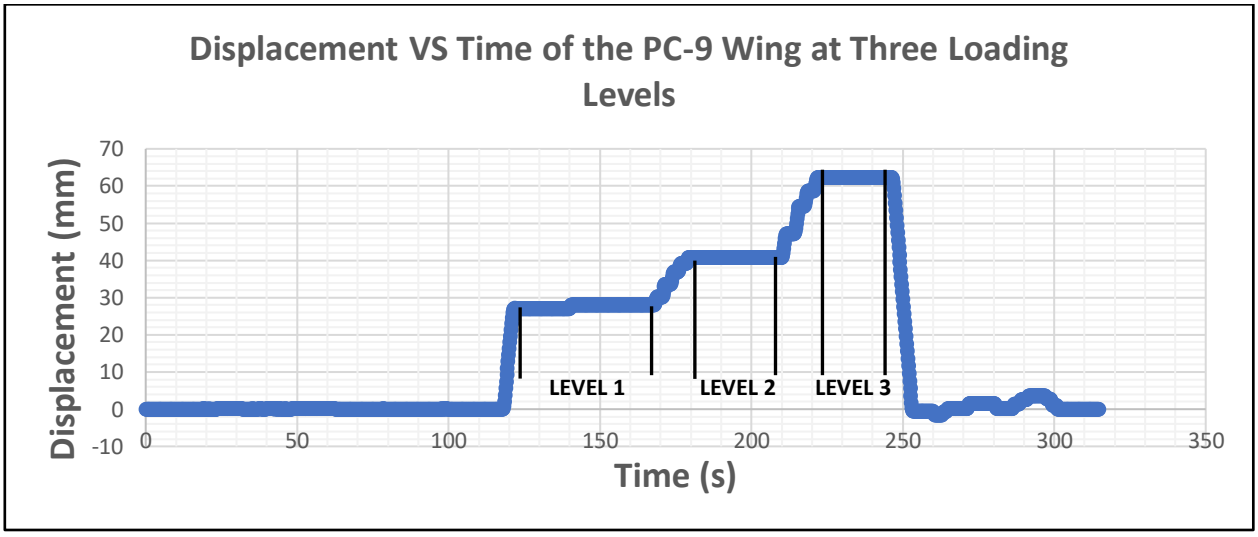

Figure 16 **Loading Sequence in Displacement VS Time Graph**

In **Error! Reference source not found.**, the force vs displacement graph shows a comparison between the displacement values recorded by the experiment at the point of application, and the wingtip displacement recorded manually during the experiment at each loading level. The gradient ($y = \boldsymbol{m}x$) has been defined next to each line, this represents the stiffness in N/mm of the wing at each location.

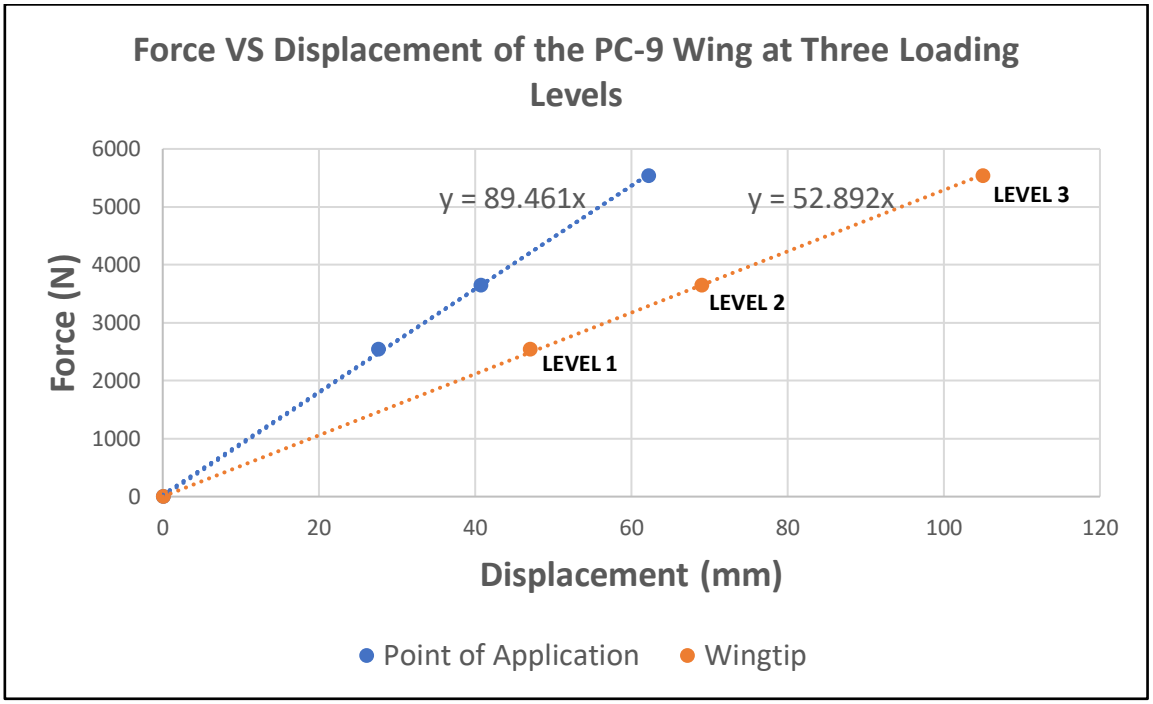

Figure 17 Graph of Load VS Displacement

Table 24 The displacement values at the three loading levels

Loading Level	Average Load (N)	Displacement at Point of Application (mm)	Wingtip Displacement (mm)
1	2533.775961	27.60198962	47
2	3649.37284	40.73796732	69
3	5532.280164	62.19587689	105

In **Table 25**, **Table 26**, and **Table 27** below, the principle strains ($\varepsilon_{1,2}$), principle stresses ($\sigma_{1,2}$), maximum shear stress (τ_{max}), maximum shear strain (γ_{max}), and Von Mises stress ($\boldsymbol{\sigma}$eq) is shown for each loading levels at five locations on the PC-9 Wing: top spar cap, bottom spar cap, spar web, rib, and skin.

Table 25 Level 1 loading values

LEVEL 1: 2533.775961N

	Top Spar Cap	Bottom Spar Cap	Spar Web	Rib	Skin
$\boldsymbol{\varepsilon}$ x (mm/mm)	-1.16E-04	9.23E-05	-1.16E-04	8.35E-06	-3.59E-05
$\boldsymbol{\varepsilon}$ b (mm/mm)	-1.85E-04	2.16E-04	-3.05E-05	-7.59E-06	-9.13E-05
$\boldsymbol{\varepsilon}$ y (mm/mm)	-2.20E-05	5.32E-05	1.10E-04	-2.03E-05	-3.65E-05
$\boldsymbol{\gamma}$ xy (rad)	-2.31E-04	2.86E-04	-5.45E-05	-3.23E-06	-1.10E-04
$\boldsymbol{\varepsilon}$ 1(mm/mm)	5.59E-05	2.17E-04	1.13E-04	8.45E-06	1.88E-05
$\boldsymbol{\varepsilon}$2(mm/mm)	-1.94E-04	-7.18E-05	-1.19E-04	-2.04E-05	-9.13E-05
$\boldsymbol{\gamma}$ max (rad)	2.50E-04	2.89E-04	2.32E-04	2.88E-05	1.10E-04
$\boldsymbol{\sigma}$1(MPa)	-0.6589	15.8818	6.0339	0.1407	-0.9258
$\boldsymbol{\sigma}$2 (MPa)	-14.3824	-0.0061	-6.7392	-1.4444	-6.9767
$\boldsymbol{\tau}$ max (MPa)	6.8617	7.9440	6.3865	0.7925	3.0255
Von Mises $\boldsymbol{\sigma}$eq (MPa)	14.0645	15.8849	11.0674	1.5196	6.5630

Table 26 Level 2 loading values

LEVEL 2: 3649.37284N

	Top Spar Cap	Bottom Spar Cap	Spar Web	Rib	Skin
$\boldsymbol{\varepsilon}$ x (mm/mm)	-1.77E-04	1.39E-04	-1.64E-04	2.47E-05	-2.80E-05
$\boldsymbol{\varepsilon}$ b (mm/mm)	-2.54E-04	3.26E-04	-2.53E-05	2.72E-06	-1.10E-04
$\boldsymbol{\varepsilon}$ y (mm/mm)	8.96E-07	9.80E-05	1.82E-04	-1.40E-05	-3.60E-05
$\boldsymbol{\gamma}$ xy (rad)	-3.31E-04	4.14E-04	-6.90E-05	-5.30E-06	-1.55E-04
$\boldsymbol{\varepsilon}$ 1(mm/mm)	9.99E-05	3.27E-04	1.86E-04	2.49E-05	4.57E-05
$\boldsymbol{\varepsilon}$2(mm/mm)	-2.76E-04	-8.94E-05	-1.67E-04	-1.41E-05	-1.10E-04
$\boldsymbol{\gamma}$ max (rad)	3.76E-04	4.16E-04	3.53E-04	3.90E-05	1.55E-04
$\boldsymbol{\sigma}$1(MPa)	0.7176	24.3883	10.6991	1.6590	0.7776
$\boldsymbol{\sigma}$2 (MPa)	-19.9611	1.5154	-8.6923	-0.4865	-7.7583
$\boldsymbol{\tau}$ max (MPa)	10.3393	11.4364	9.6957	1.0727	4.2679
Von mises $\boldsymbol{\sigma}$eq (MPa)	20.3294	23.6670	16.8233	1.9483	8.1748

Table 27 Level 3 loading values

LEVEL 3: 5532.280164N

	Top Spar Cap	Bottom Spar Cap	Spar Web	Rib	Skin
ε x (mm/mm)	-3.25E-04	1.87E-04	-2.77E-04	2.13E-05	-5.67E-05
ε b (mm/mm)	-4.12E-04	4.78E-04	-4.69E-05	-9.45E-06	-1.83E-04
ε y (mm/mm)	2.24E-05	1.42E-04	2.75E-04	-3.16E-05	-7.30E-05
γ xy (rad)	-5.21E-04	6.27E-04	-9.24E-05	-8.63E-06	-2.36E-04
ε 1(mm/mm)	1.62E-04	4.79E-04	2.79E-04	2.17E-05	5.36E-05
ε2(mm/mm)	-4.64E-04	-1.50E-04	-2.81E-04	-3.20E-05	-1.83E-04
γ max (rad)	6.26E-04	6.29E-04	5.60E-04	5.36E-05	2.37E-04
σ1(MPa)	0.7017	35.2256	15.3085	0.9131	-0.5652
σ2 (MPa)	-33.7056	0.6731	-15.4549	-2.0348	-13.5906
τ max (MPa)	17.2037	17.2763	15.3817	1.4740	6.5127
Von mises σeq (MPa)	34.0619	34.8939	26.6420	2.6139	13.3170

3.4 Discussion

The PC-9 wing experiment provided valuable insight into the structural behaviour of various wing components when subjected to applied loads. The findings of this experimental play a crucial role in not only validating the FEA model, but also by offering real-world, practical observations of an aircraft wing.

By plotting the force vs displacement graph of the experimentally recorded displacement data at the point of application, and the physically measured wingtip displacement, it was found that at the point of application, the stiffness is greater, with a value of 89.461N/mm. At the wingtip, there is a lower stiffness value at 52.892N/mm. This indicates that different sections of the PC-9 wing have distinct mechanical properties when subjected to the same external load, the point of application deforms less when subjected to a force, meaning it has a greater ability to resist deformation and maintain its shape.

Whereas the wingtip experiences greater deformation under this same force, however, sections with lower stiffness are often designed to allow for some degree of deformation to distribute loads more evenly along the span of the wing.

In **Table 25**, **Table 26**, and **Table 27**, the principle strains ($\varepsilon_{1,2}$), principle stresses ($\sigma_{1,2}$), maximum shear stress (τ_{max}), maximum shear strain (γ_{max}), and Von Mises stress ($\boldsymbol{\sigma}$eq) is shown for each loading levels at five locations on the PC-9 wing: top spar cap, bottom spar cap, spar web, rib, and skin. The principal strains, $\varepsilon_{1,2}$, represent the maximum and minimum strains in differing directions.

From the results, the strains vary across the different locations of the wing, this indicates that each location experiences varying levels of deformation in response to the applied load. The principal stresses, $\sigma_{1,2}$, describe the maximum and minimum normal stresses, which is also varying across each location on the PC-9 wing. When a normal stress value is negative, it means that the material is experiencing compression in that direction, when it is positive, it indicates that it is experiencing tension.

Maximum shear stress, τ_{max}, represents the highest shear stress experienced at each of the five locations under each loading level. It varies across each location, indicating different shearing effects on the each of the components on the wing. From the results, it appears that the maximum shear stress increases for each component as the loading level increases, the highest shear stress is experienced on the top and bottom of the spar caps. The maximum shear strain, γ_{max}, varies at each location, indicating differences in the shearing deformation which increase with the loading level, the highest shear strain occurs at the bottom of the spar cap.

The Von mises stress at each location is used to validate the FEA model, the Von Mises stress is a measure of the combined effect of normal and shear stresses and is often used to predict yielding or failure of materials.

In each case, the Von mises stress is significantly lower than the yield strength of the material (441MPa), this suggests that each of these structural components can safely withstand the applied load without permanent deformation or failure.

The key observations from these in **Table 25**, **Table 26**, and **Table 27** are:

- The bottom spar cap experiences the highest Von Mises Stress for each loading level, this could indicate that the load applied to the wing is not evenly distributed across all the wing components, meaning that different parts of the wing support varying proportions of the total load. The bottom spar cap may be designed or positioned in a way that it carries a significant portion of the applied load. however, it is still well below the materials yield strength (441MPa)
- The rib has the lowest Von Mises stress of all five locations for each loading condition. Due to its location, it may be subjected to lower forces and moments compared to the wing's outer regions.
- As the principal stresses and strains, maximum shear stress, and maximum shear strain varies in each location, this means that there is non-uniform deformation and stress distribution within the PC-9 wing structure.

The experimental method may have possible error sources, such as inaccurate raw data measurements from the strain gauge rosettes, this could be due to possible incorrect calibration of the in the equipment and instruments used in the experiment. Further to this, human errors in measuring the physical displacement of the wingtip after each loading level can interfere with the experimental analysis results.

It is crucial to consider possible error sources can interfere with the authenticity of the data, especially as these experimental results are primarily utilised to validate the FEA model.

CHAPTER 4: FINITE ELEMENT MODELLING

4.1 Introduction

Finite Element Analysis (FEA) stands as a fundamental pillar in the realm of aerospace structural design and evaluation. It empowers engineers to virtually model and simulate intricate aerospace components subjected to diverse operational conditions. Through this powerful analytical tool, we gain a deep understanding of structural behaviour, stress distribution, and potential failure mechanisms. FEA enables comprehensive assessments of aeroelastic effects, aiding in the design of wings, control surfaces, and other critical components.

By leveraging FEA, engineers can meticulously optimize aerospace structures, striking the delicate balance between weight, strength, and aerodynamic efficiency. This section delves into the critical role FEA plays in shaping aerospace innovations, ensuring the highest standards of safety, performance, and compliance with industry regulations.

The specific objectives driving the utilization of Finite Element (FE) analysis within this project encompass several key elements. First, it aims to construct a precise FE model of the existing metallic PC9 wing using the Abaqus platform. Subsequently, the FE model's accuracy and reliability will be affirmed through a validation process using experimental data collected.

The primary focus then shifts to a comprehensive analysis of the PC9 wing's performance under conditions of maximum loading. The insights garnered from these simulations will serve as a crucial benchmark for evaluating the efficiency and potential enhancements offered by the proposed composite wing. The application of FE as a powerful numerical simulation and optimization tool in aircraft design is fundamental, offering invaluable guidance and practical advantages.

These advantages include elevating product quality, enhancing performance, streamlining production processes, reducing associated costs, and ultimately expediting the design cycle. Consequently, establishing a precise, well-structured FE model holds paramount importance, forming the foundation for accurate numerical analysis and optimization efforts.

4.2 Numerical Methodology

The process of the FEA or finite element analysis of the PC-9 wing is started by the CAD modelling of the wing. For our group, two CAD models were designed, and various FEA software’s were used to analyse the CAD wing model. For the finite element analysis, the material aluminium 2124 T851 was used for the modelling analysis, and it assumed homogenous throughout the whole assembly and the properties of aluminium 2124 T851 can be found in the appendices.

4.2.1 Initial CAD Model: First model

The first wing model was designed in SolidWorks and the assembly is comprised of ribs with extruded holes, the main spar, and the skin. The FEA software used primarily for the initial CAD analysation is Abaqus as recommended. **Figure 18** shows the model in SolidWorks. However, the model failed to mesh in Abaqus using the default mesh settings but using SolidWorks internal finite element analysis software, the predicted results do not reflect the values in the experimental investigation.

After numerous attempts, we resorted to the use of ANSYS Mechanical to perform the finite element analysis but that was proven not successful as well. The wing model failed to mesh due to invalid geometry as can be seen in **Figure 19**.

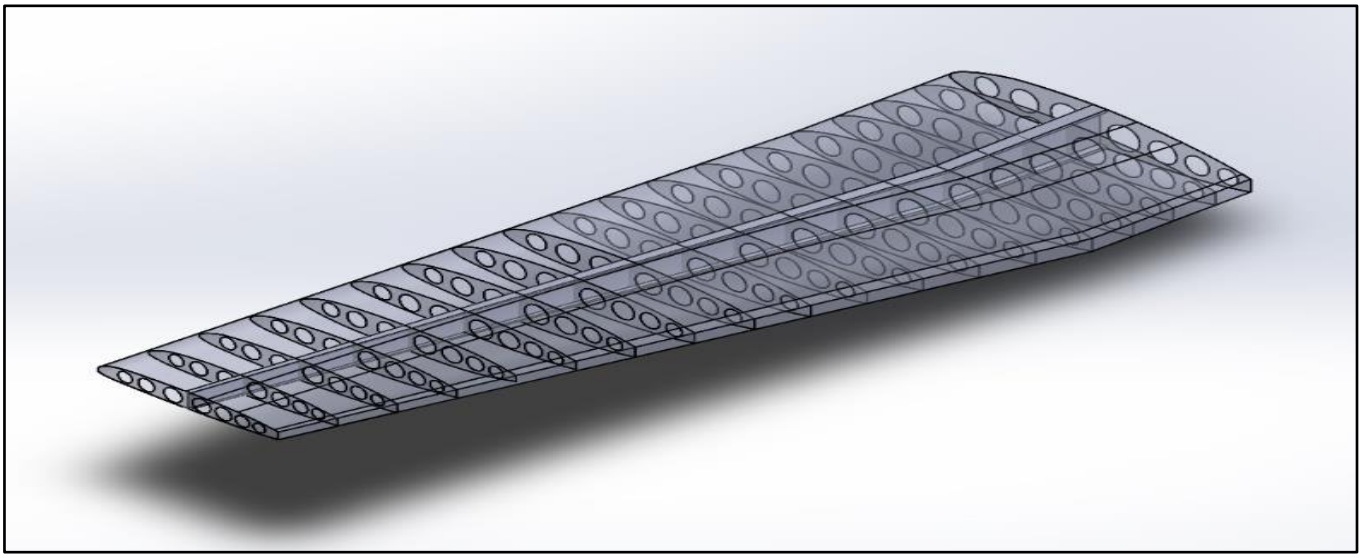

Figure 18 Initial CAD model using SolidWorks.

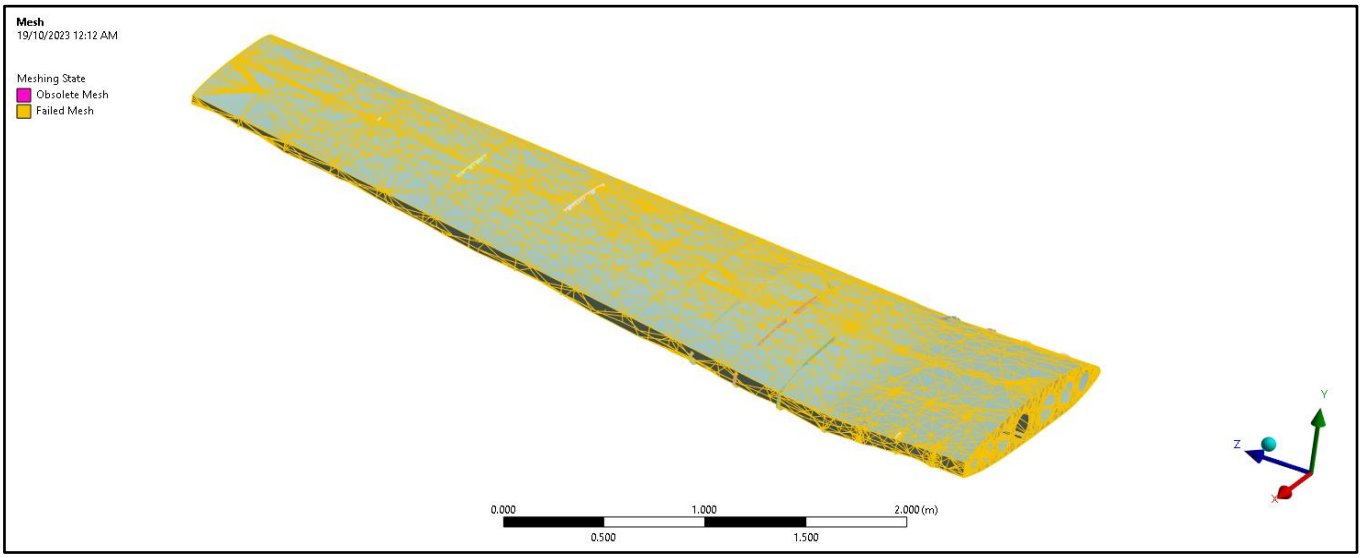

Figure 19 Failed meshing of the initial CAD model.

4.2.2 Initial CAD Model: Second model

The second model of the wing incorporates stringers and rear spar to aid with the geometry issues encountered in the first model. The stringers and rear spar will provide more contact surfaces and better merge quality of the assembly of the wing model as can be seen in **Figure 20**.

The issue with this model is that the total nodes were at an astonishing value of 740000 and element number of 450000. The ANSYS student license is limited to 128000 nodes and elements combined. Therefore, increasing the element size of the mesh will decrease the number of nodes but will decrease the accuracy of the FEA. The wing is modelled as a shell which will provide better accuracy at lower node count.

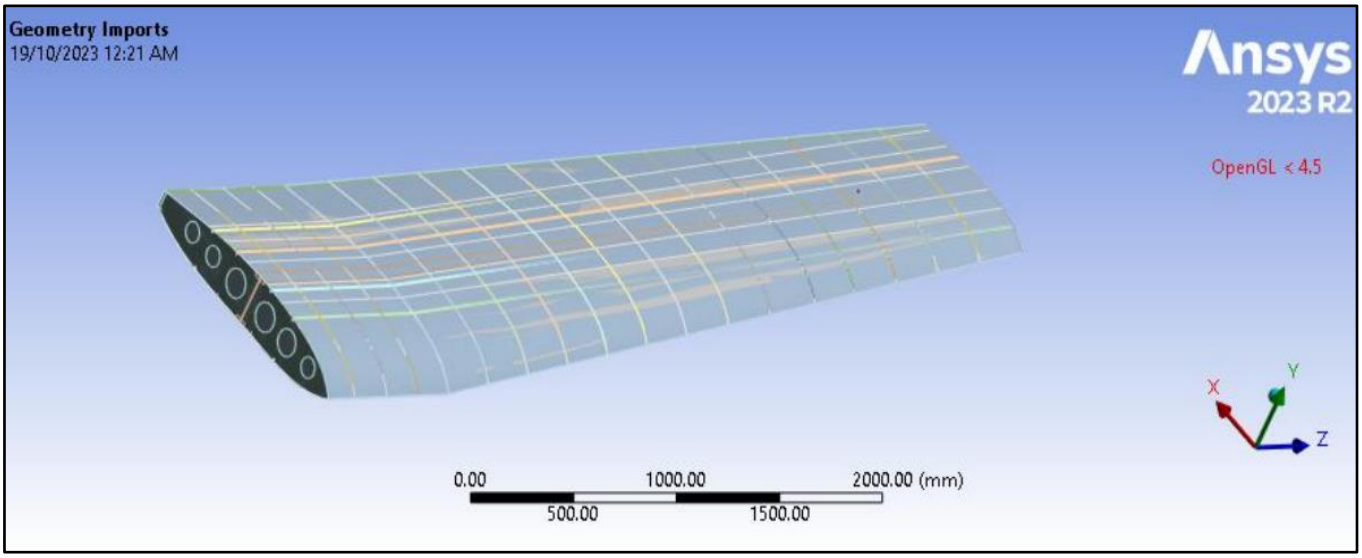

Figure 20 The second model design of the PC-9

4.3 Current FEA Model: Simplifications

Appendix A and Appendix B illustrates the geometry of the PC-9 wing in full details, which will be put through simplification process to decrease the degree of complexity in the Finite Element Analysis, without severely affecting the wing's characteristics against the loading conditions. This simplification process is associated with the lessons learned from above failed model to determine the optimised geometry that satisfies the requirements and objectives.

Outside of core components such as main, rear spars, ribs, and stringers, as well as fastener connections (bolts and rivets), wing structure include numerous additional components that's support the tailored objectives, both on ground and in-flight. An example of those structures is included in Figure 3, consist of a system of supporting struts, as well as actuator brackets where these components account as a secondary structure component. Another structure system could be included such as a few notched geometries that whether placing the fastener connections or assisting fuel systems. The inclusion of those holes at different practical shape, from circle to elliptical, will increase the complexity of the FE model, which potentially leads to inaccuracy of local stress measurement. On the other hand, the inclusion of support struts/brackets or fastener connections without thoughtfully understanding the characteristics, such as materials, rated support force or fastener's torque value will lead to severe faults on the load transmission and connections.

In the purpose of simplify the FEA, model utilized will only consists of core components, including wing skin, main, rear spars, ribs, and stringers. The characteristics of the wing's geometry are preserved, including 7^{o} dihedral, 0.5 taper ratio, 1^{0} of twisting and 2^{0} angle of incidents as those are critical in analysing load and stress components in both local and global coordinate systems. Those constrains, combined with the root and tip chord lengths will construct the overall wing skin, which is displayed in **Figure** 21 below:

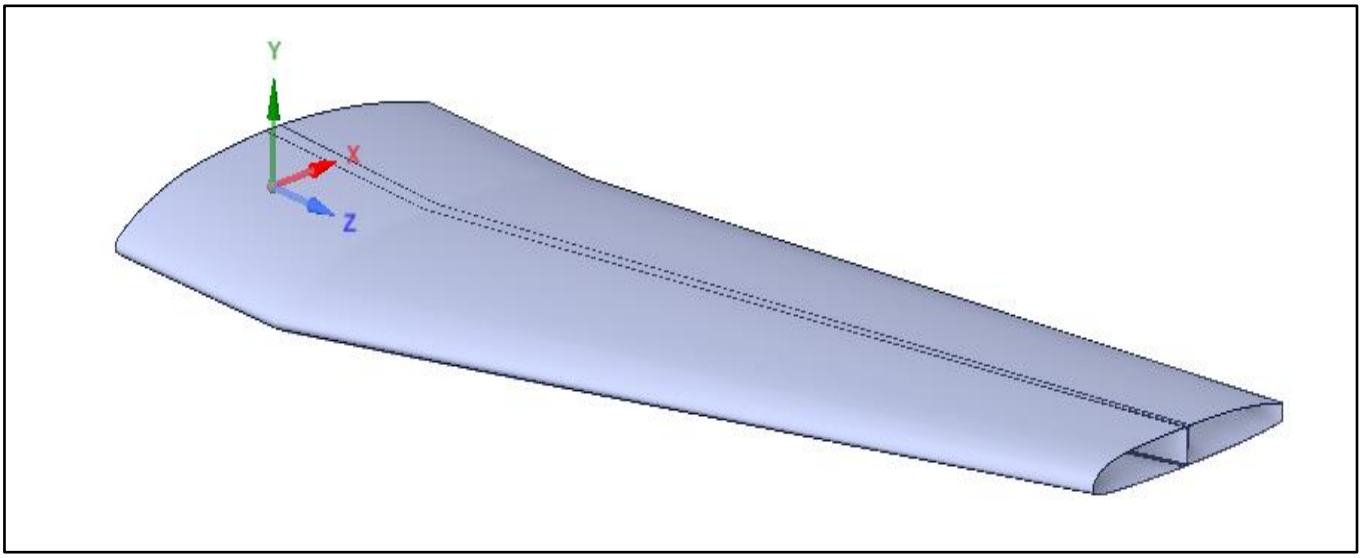

Figure 21 Constraints of the root and tip chord of the overall wing skin

Also, on **Figure 22**, wing's main spar and rear spar are also displayed (with the line on the wing indicated rendering instead of overlapped regions). Cross-section of the main spar and rear spar in root and tip follow the dimensions from Appendix, and also went through the structure modification in term of characteristics (dihedral and taper ratio). Twisting and Angle of Incidence are neglected, as beams in practical applications do not apply those characteristics due to concern in residual stresses from material stiffness, and also thanks to the tolerance allowance for geometry with this length.

Air foil cross-sections are slightly modified to compensate for the distance overlapped between the skin and the rib. Modifications on air foil cross-sections will lead to severe effects on CFD analysis due to the degree of sensitivity, however on FEA it is considered negligible due to the preservation of load transfer from wing skin. The distance between the main spar and rear spar with the wing skin, consecutively, are 1.2 and 1.5mm, which will allow the merged or share topology to be used effectively, and those spaces being filled with the same material. Instead of fasteners utilized in the practical implications, spars and wing skin are considered bonded together, and load transfer is perfect, therefore, this differs from actual situations, where those gaps are existed and included in the experimental procedure.

Like wing skin, ribs and stringers are also inserted into the geometry with the absence of bolts or fasteners, utilizing merge topology to further simplify the geometry, without severe effect on the geometry's characteristics. The completion of internal and merged structure is illustrated in **Figure 22** and **Figure 23**.

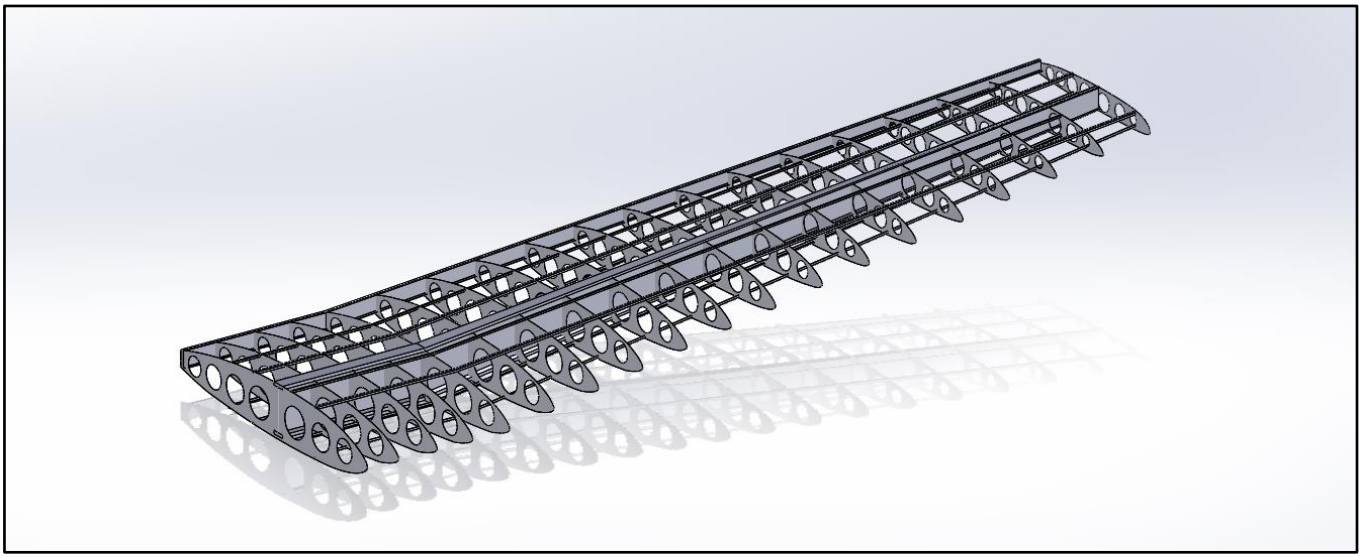

Figure 22 Merged current wing model

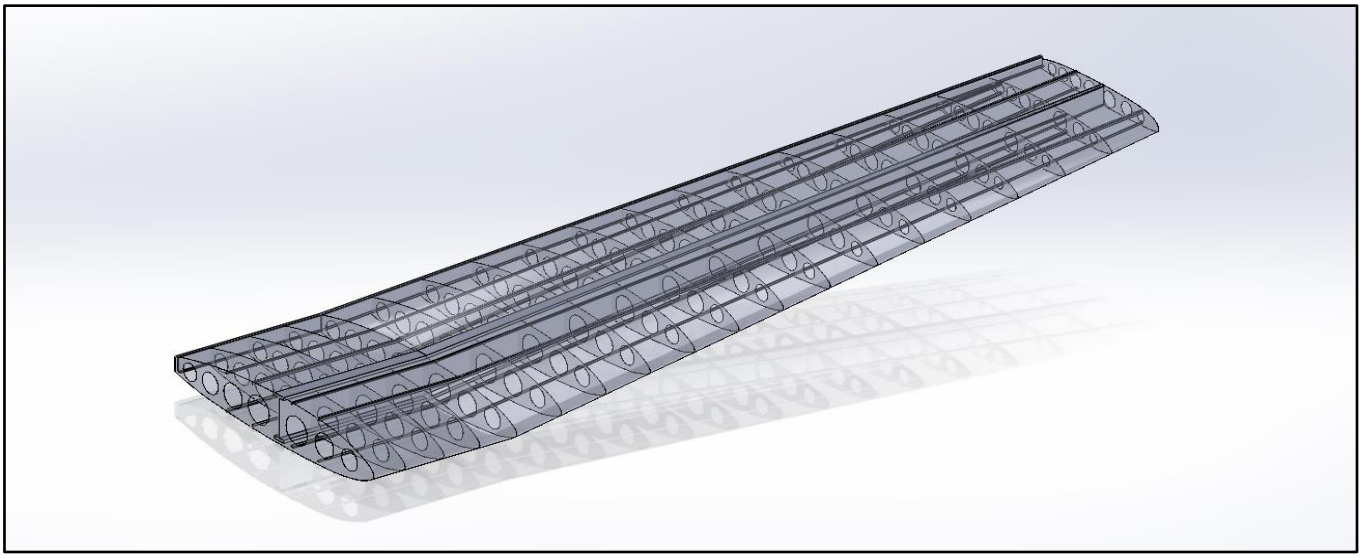

Figure 23 Merged current wing model

4.3.1 Computational Utilisations

The Finite Element Method analysis is operated on ANSYS Mechanical via Ansys Workbench: Static Structural, with base model imported from SolidWorks and processed in ANSYS Space Claim. SolidWorks satisfies the accuracy demand from the connection between parts such as wing skin and main spar, while Static Structural from ANSYS allow the export of desired parameters, including Stress components in x, y, and z-direction, as well as Displacement, Principal Stress/Strain, Maximum Shear Stress/Strain and Von Mises Stress.

Derived from the model mentioned in objectives of FEA utilisations are to investigate the behaviours of PC–9 Wing under different load conditions, including cruise, to develop an alternative material – composite laminate, for the existing aluminium structure. Another purpose is for comparison between FEA and experimental investigations to determine the credibility, as well as accuracy of the model developed.

4.3.2 Boundary Conditions and Load Applied

The boundary conditions used are a fixed support at the root of the wing to simulate the fixed wooden block chop during the experimental investigation, and pressure loads are applied at the skin panel between the ribs 17 and 18 to simulate the hydraulic actuators during the experimental investigation as well. Load is then derived into components in x and y-direction, in order to satisfy the requirements of pressure direction, following the follow example:

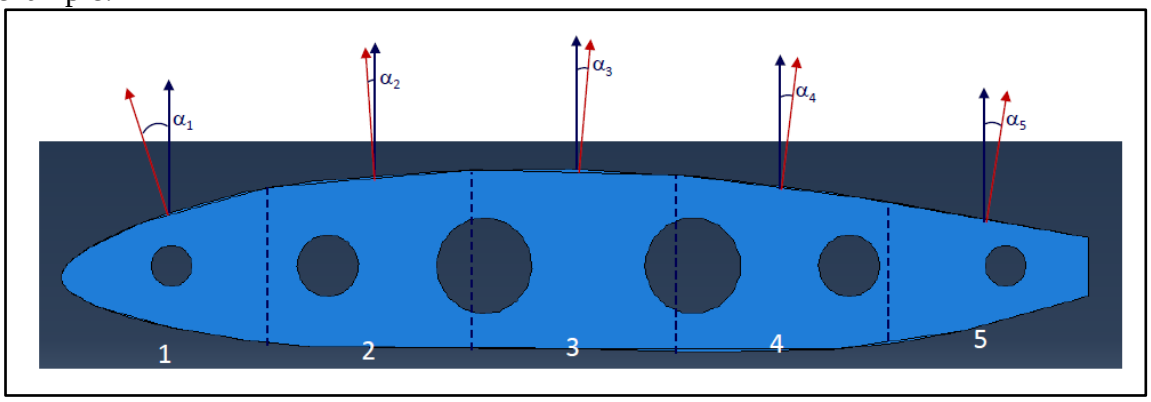

Figure 24: Pressure components on a panel (Source: CANVAS – Aerospace Structure Studio)

A same procedure is applied in the FE model for the Design Ultimate Load, where elliptical load distribution at each rib is then transferred into the panel between 2 ribs and derived into x and y-component to become pressure applied.

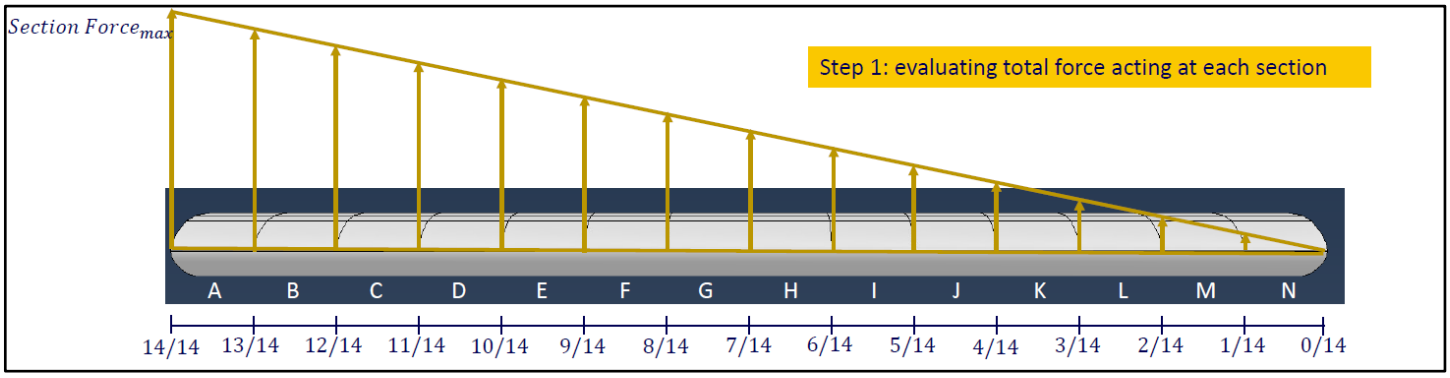

Figure 25: Example of Load components on a wing (Source: CANVAS – Aerospace Structure Studio)

Table 28: Individual Load components at each rib for DUL Analysis.

Rib	MPa	Pa
5 (Root)	0.920351	920350.9
6	0.955712	955712.2
8	0.992432	992432.2
9	1.030563	1030563
11	1.070159	1070159
12	1.111276	1111276
13	1.153973	1153973
14	1.198311	1198311
15	1.244352	1244352
16	1.292162	1292162
17	1.341809	1341809
18	1.393363	1393363
19	1.446898	1446898
20	1.50249	1502490
21	1.560218	1560218
22	1.620165	1620165
23	1.682414	1682414
24	1.747055	1747055
25 (Tip)	1.81418	1814180

Table 29 Loading 1,2 and 3 Loads applied

Over Surface Between Ribs 17 - 18	Loading 1	Loading 2	Loading 3
MPa	0.004803	0.006919	0.01049
Pa	4803.211	6919.43	10490.08
Total Area	527355.6	mm^2	

4.3.3 Mesh Independence

Mesh size, type and other parameters are crucial to determine the credibility and accuracy of the obtained results, acting as the reflection of solver embedded in the computational domain. Falsely chosen mesh characteristics will lead to inaccuracy, inconsistent solver, and lack of converge in the result obtained. Mesh independence refers to the mesh characteristics that balance between result's accuracy and computational time, where decreasing mesh size from this threshold will increase the computational time without better result. On the other hand, increasing mesh height will lead to the saving of computational time and resources, but with the compensation of precision.

In this PC-9 Finite Element Analysis, Deformation will be chosen to as the parameter to examine the mesh sensitivity, and later determining the mesh independence. Deformation is determined based on the sectioned geometry, as the result of the load transfer between components to determine the displacement of the whole wing structure, with the lack of concentration at a particular region once the design is tested to be efficiently.

Other parameters, such as stress, are strongly dependent on the sizing of each component, as well as the point of applied load, therefore considered inefficient parameters for the mesh independence. Furthermore, displacements difference is measured with the first loading condition from the experimental conditions, at the wing tip, where 2533 N is applied between Rib 18 and Rib 19.

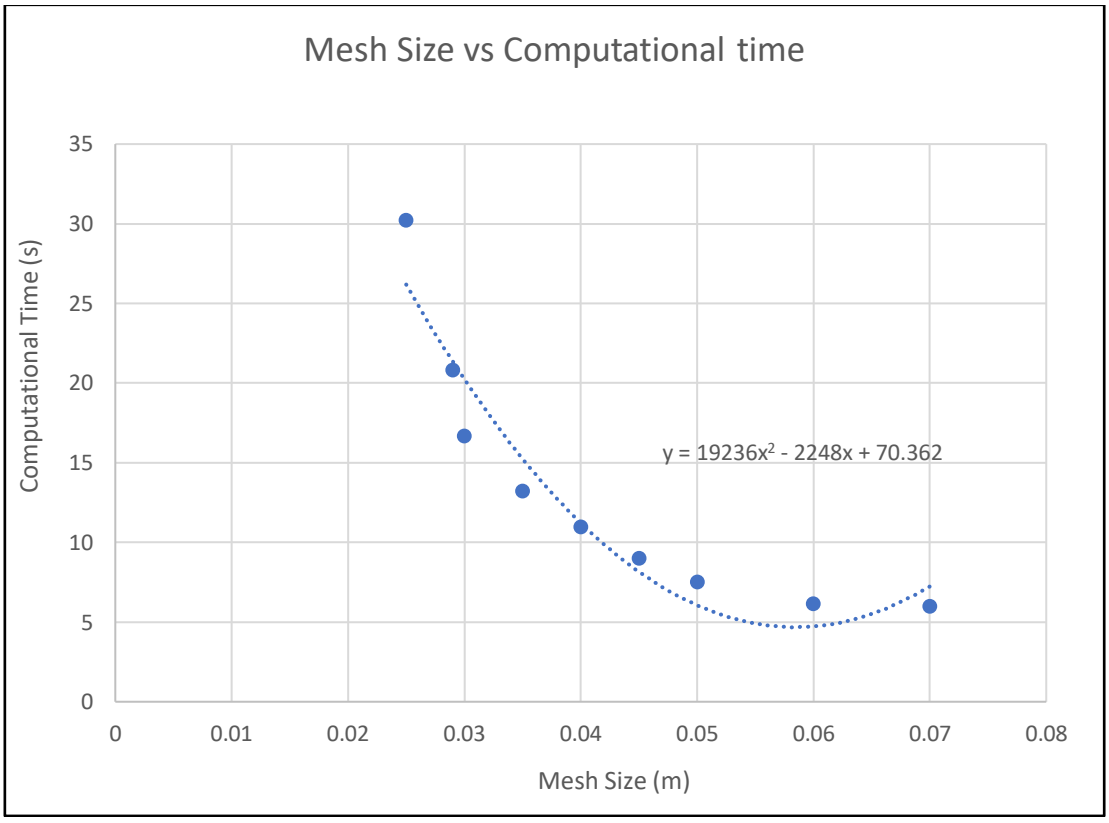

Figure 26 ***Mesh size vs computational time graph***

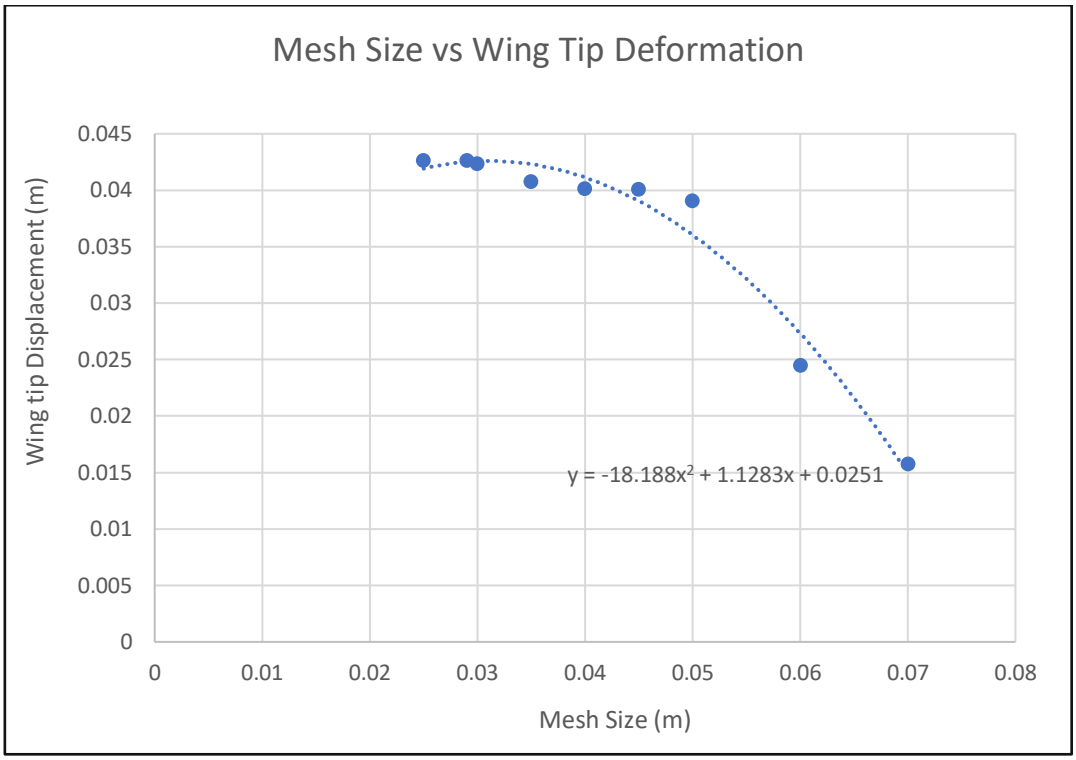

Figure 27: Mesh Size vs Wing Tip Deformation

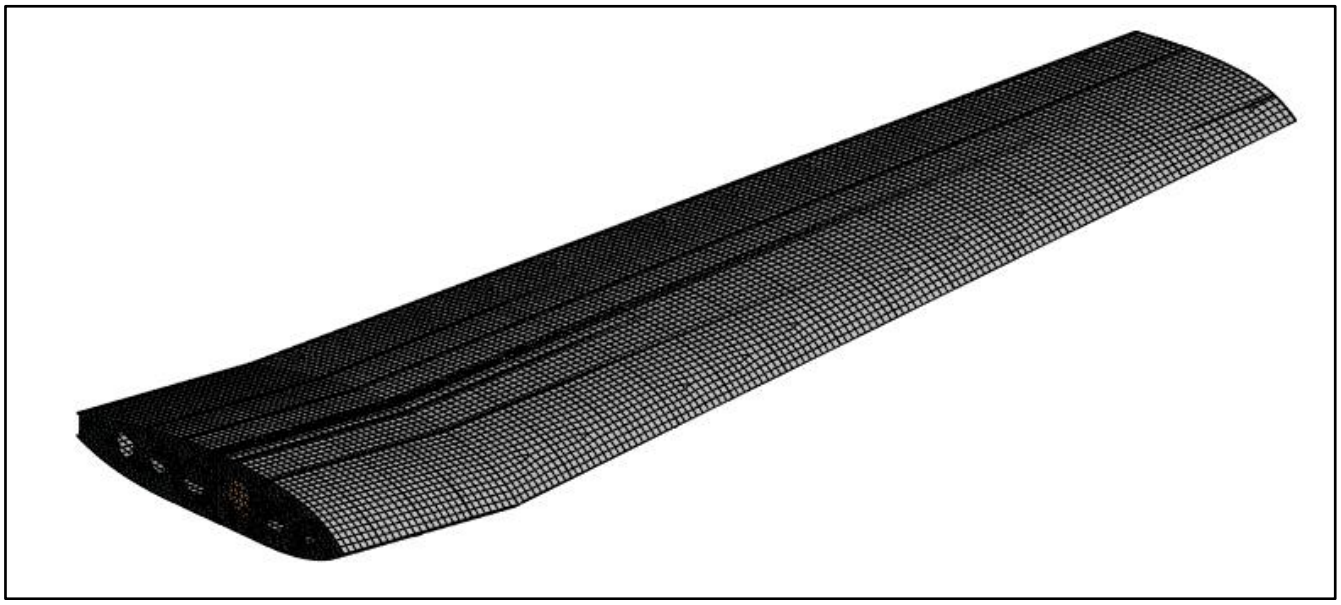

Figure** 28 **Mesh of the current FEA wing model

Bulk mesh size elements are set to be 0.03mm, or 30mm, with adjustments on components with lower width/thickness. This setting was selected based on the balance between the computational time and the accuracy of the results. Further increase of mesh density will cause the computational time to significantly increase, following a quadratic equation trendline.

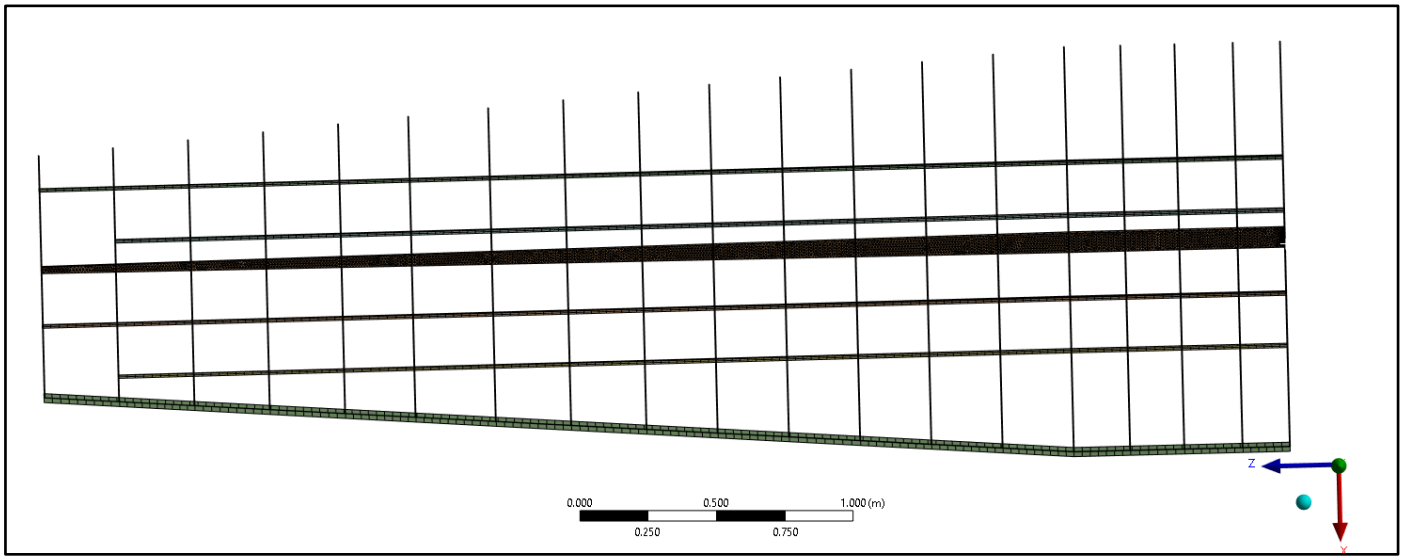

Figure 29 Top view of the wing model without skin

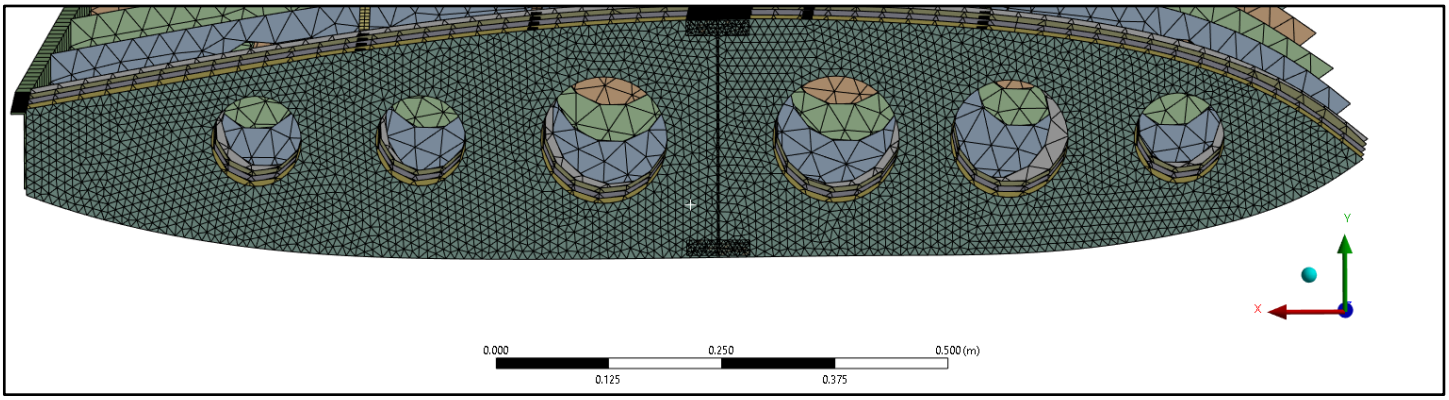

Figure 30 Mesh quality of the ribs of the wing model

4.4 Validation of the FE Model

Validating the FEA model of the PC-9 wing structure involves comparing the predictions from FEA with the experimental results under each loading condition. The parameters for validation are the load displacement at the point of application and the wingtip, and the Von Mises stress at five locations: Top Spar Cap, Bottom Spar Cap, Spar Web, Rib, and Skin. To ensure the accuracy of the FEA predictions, it is crucial to replicate the conditions used in the experiment, dimensions of the wing, and the material properties. This involves mesh generation, applying boundary conditions, and applying pressure loads on the correct locations of the wing.

By comparing the FEA results to the experimental data, this allows us to ensure that it simulates the real-world behaviour of the wing during the experiment. Further to this, having successful validation of the model allows valuable insight for the composite design of the wing.

4.4.1 Comparison between Experimental Investigation and FEA

Table 30 Wingtip displacement comparison

Loading Level	Average Load (N)	Experimental Wingtip Displacement (mm)	FEA Wingtip Displacement (mm)
1	2533.775961	47	42.3
2	3649.37284	69	60.9
3	5532.280164	105	92.4

Table 31 Point of application displacement comparison

Loading Level	Average Load (N)	Experimental Point of Application Displacement (mm)	FEA Point of Application Displacement (mm)
1	2533.775961	27.602	25.512
2	3649.37284	40.738	36.624
3	5532.280164	62.196	57.258

Table 32 Von Mises comparison

Loading Level	Von Mises	Top Spar Cap	Bottom Spar Cap	Spar Web	Rib	Skin
1	Experimental Von Mises σeq (MPa)	14.0645	15.8849	11.0674	1.5196	6.5630
	FEA Von Mises (MPa)	17.412	18.594	15.243	1.557	5.3672
2	Experimental Von mises σeq (MPa)	20.3294	23.6670	16.8233	1.9483	8.1748
	FEA Von Mises (MPa)	25.084	26.786	21.959	2.0045	7.6037
3	Experimental Von mises σeq (MPa)	34.0619	34.8939	26.6420	2.6139	13.3170
	FEA Von Mises (MPa)	40.609	38.028	33.29	2.9736	12.655

4.5 Results

The contour plots of the Von Mises Stress, and wing deflection results are displayed below for each of the experimental loading levels and the Design Ultimate Load (DUL). Contour plots provide insight into the structural behaviour and integrity of the PC-9 wing, further to this, it offers a visual representation of how the PC-9 wing responds to varying loads. By applying the DUL, we can assess the behaviour of the wing during the cruise condition, where the lift load during this phase was identified as 22366.8N in the Progress Report completed previously. The calculation is shown in Appendix M, where this load must be applied as a distributed pressure along the length of wing. Further to this, maximum principal stress and strain contour plots are shown in Appendix N through to Q.

4.5.1 Ansys Results from Experimental Loading Levels

4.5.1.1 Loading Level 1 - 2533.775961N

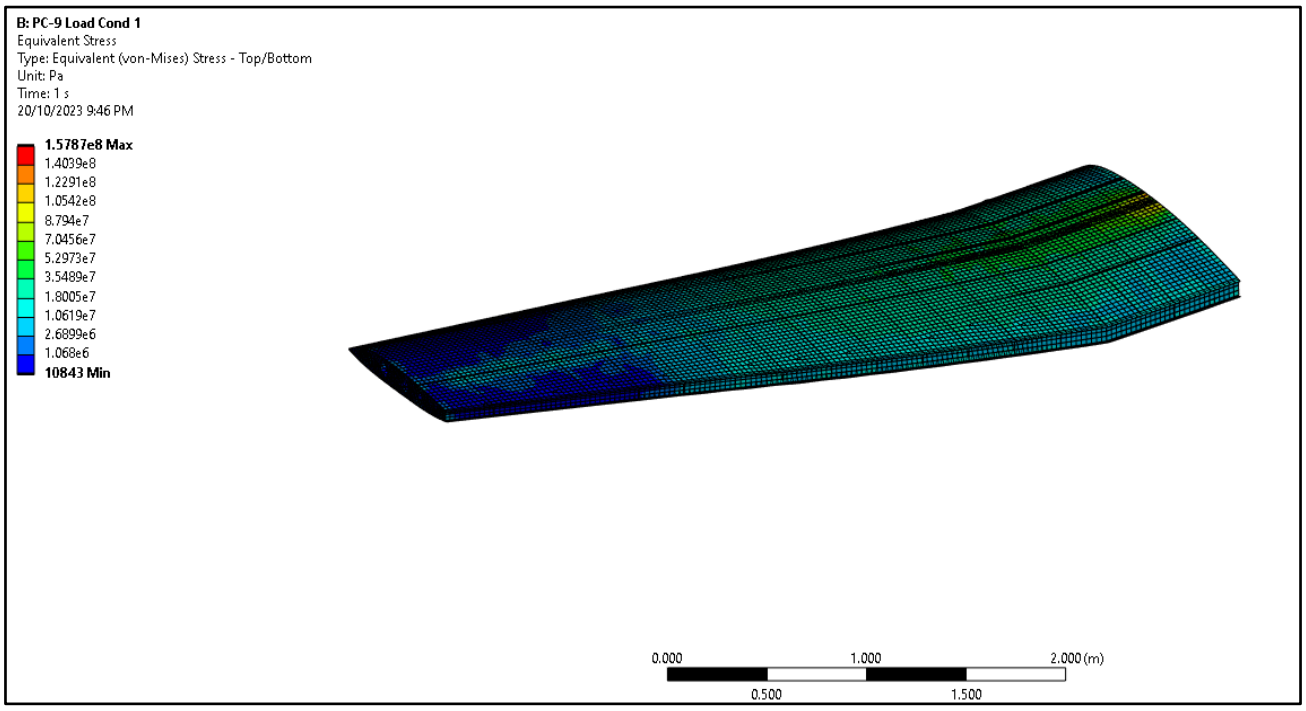

Figure 31: Von-Mises Stress at Loading Condition 1

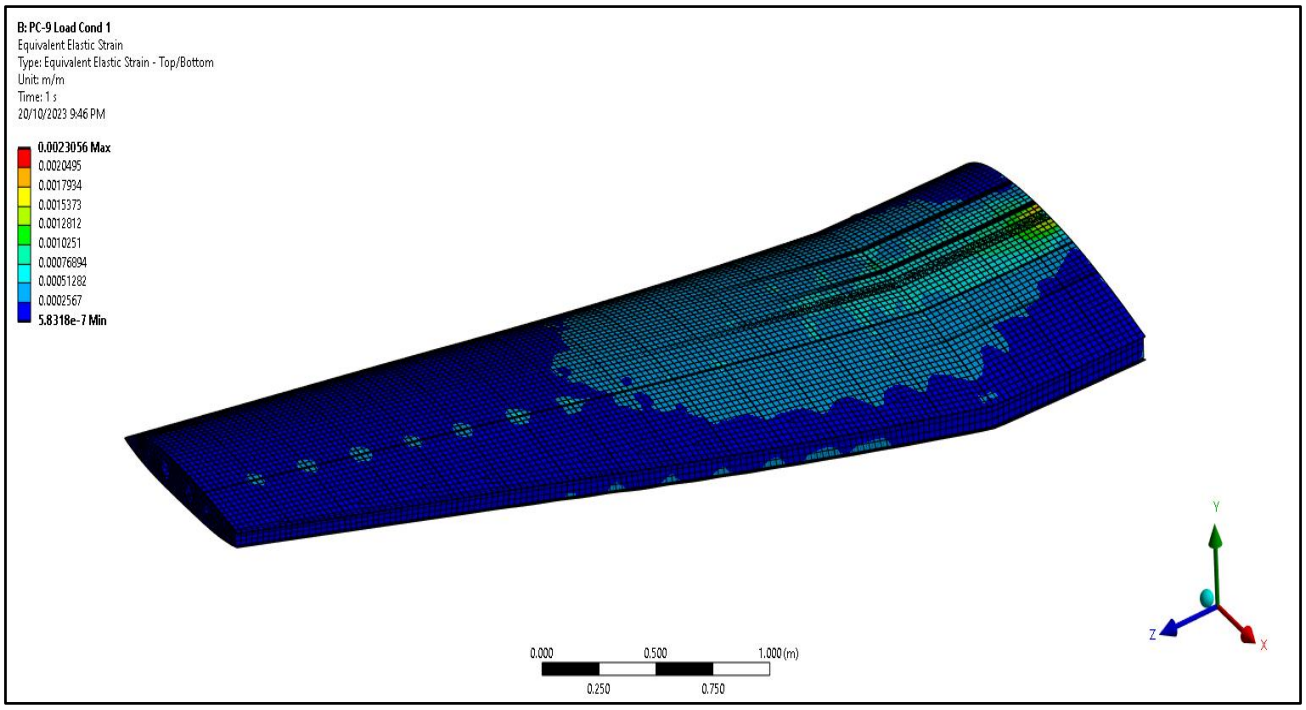

Figure 32 Strain Load

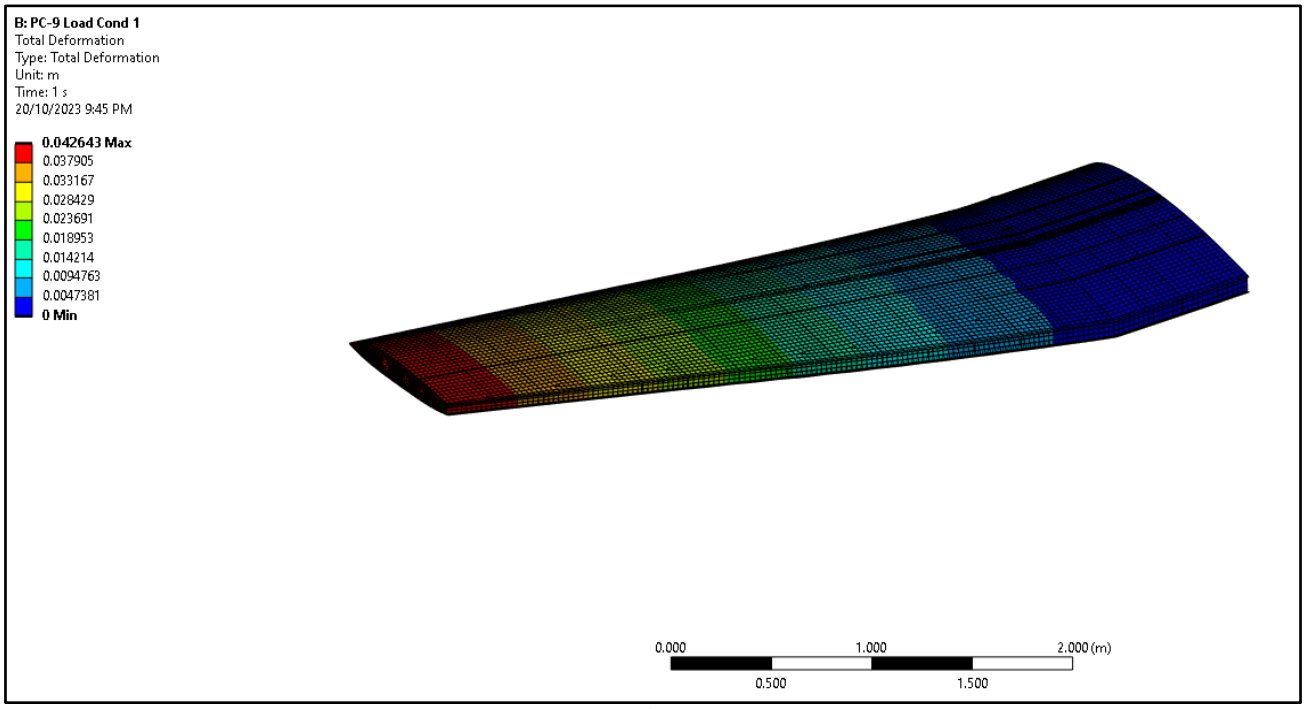

Figure 33 Deformation Load

4.5.1.2 Loading Level 2 - 3649.37284N

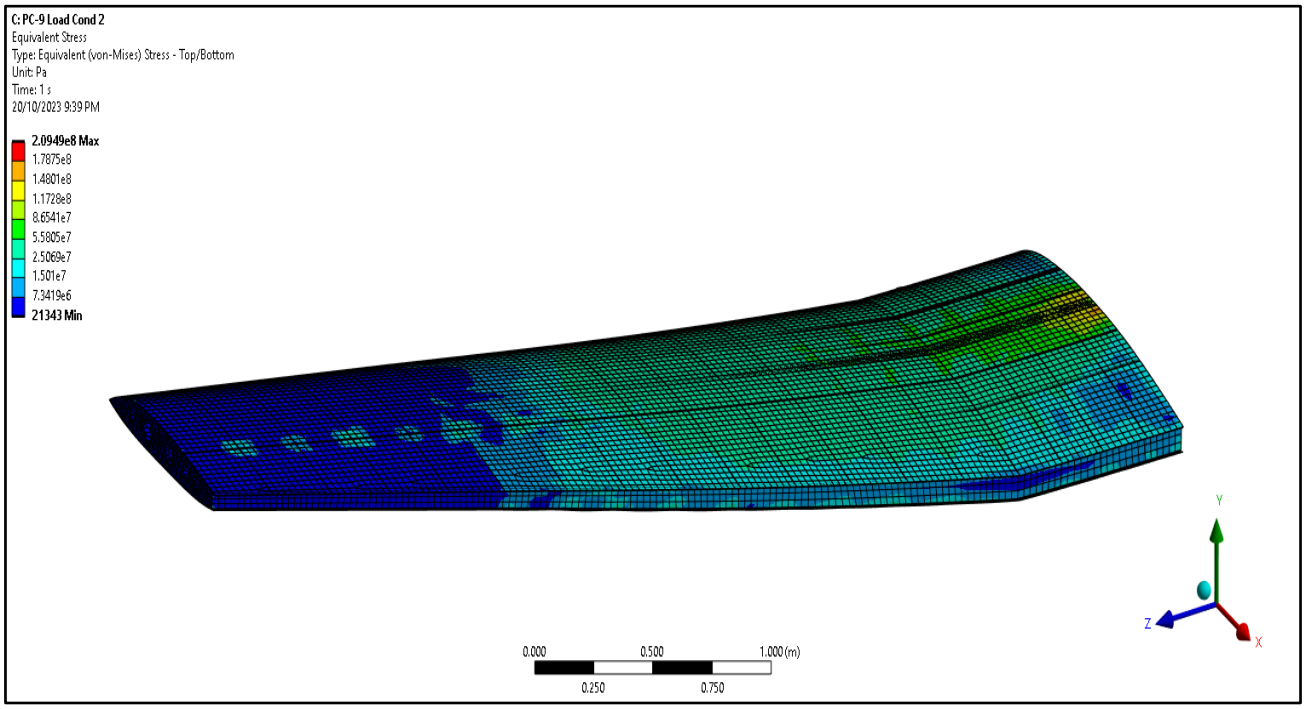

Figure 34 Load Von Mises

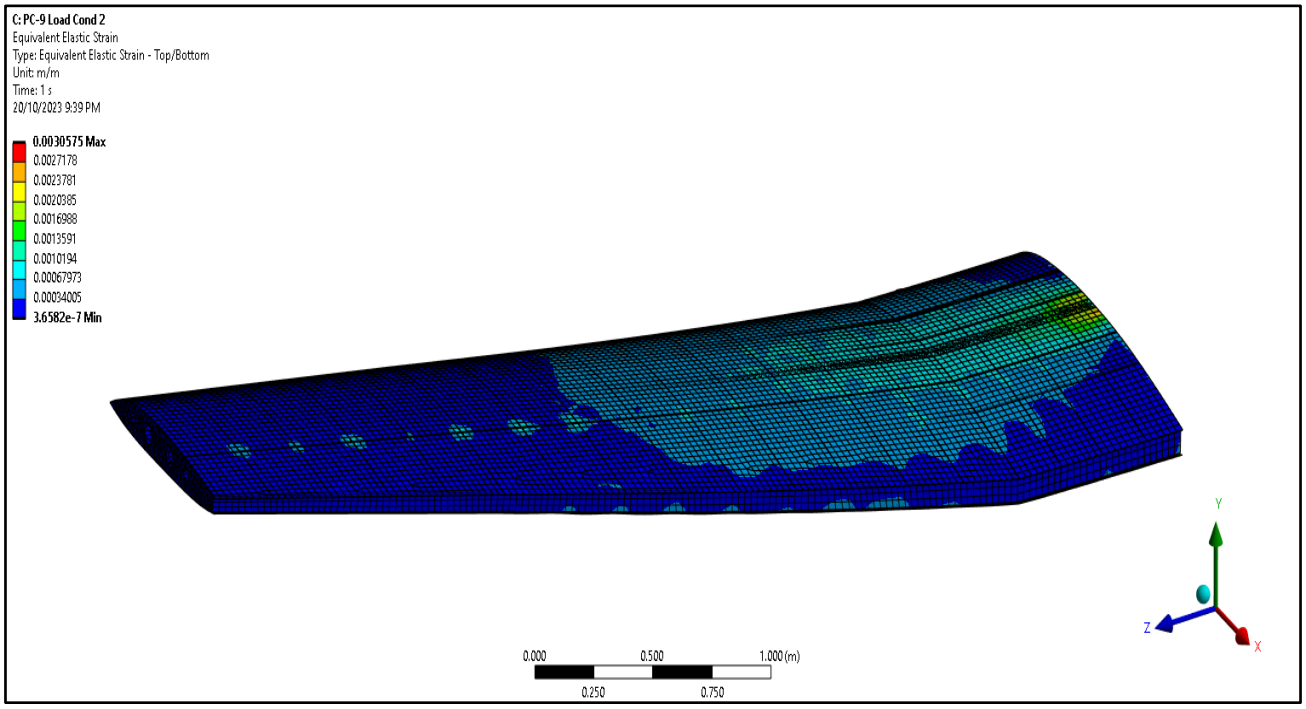

Figure 35 Elastic strain Laad

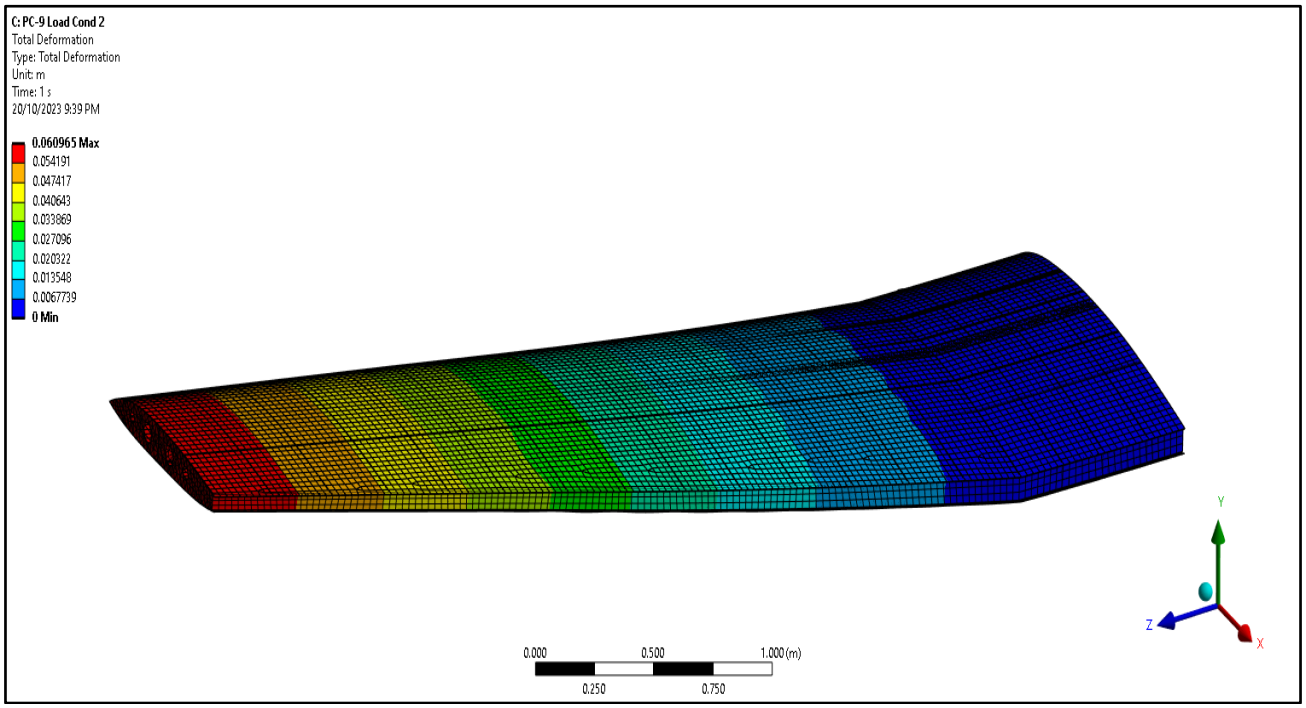

Figure 36 load deformation

4.5.1.2 Loading Level 3 - 5532.280164N

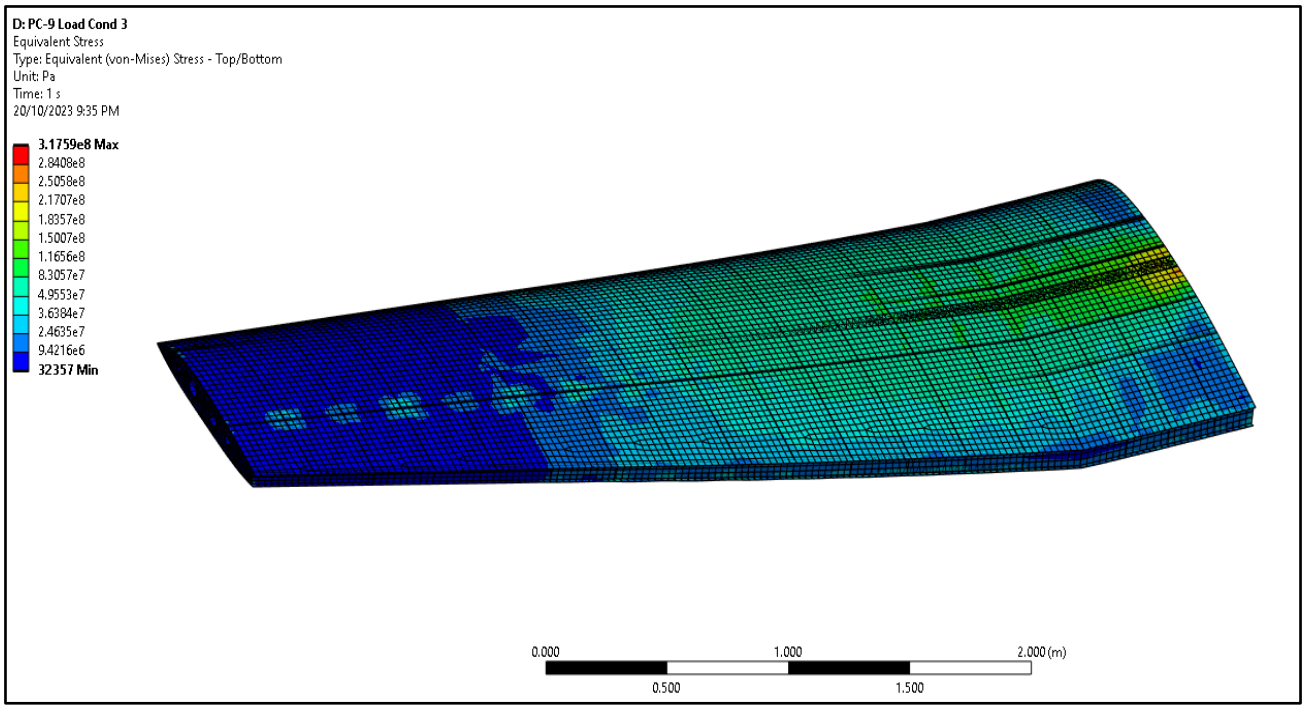

Figure 37 Load 3 von Mises

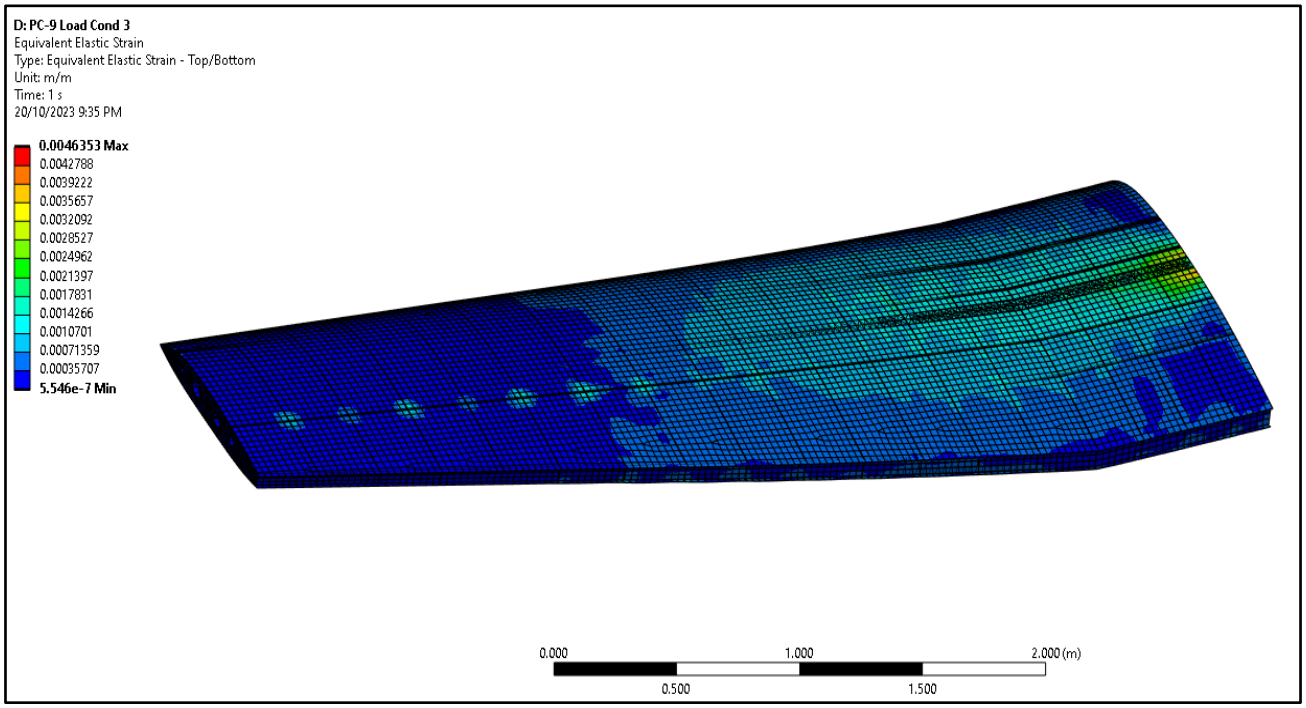

Figure 38: Loading Condition 3 - Equivalent Elastic Strain

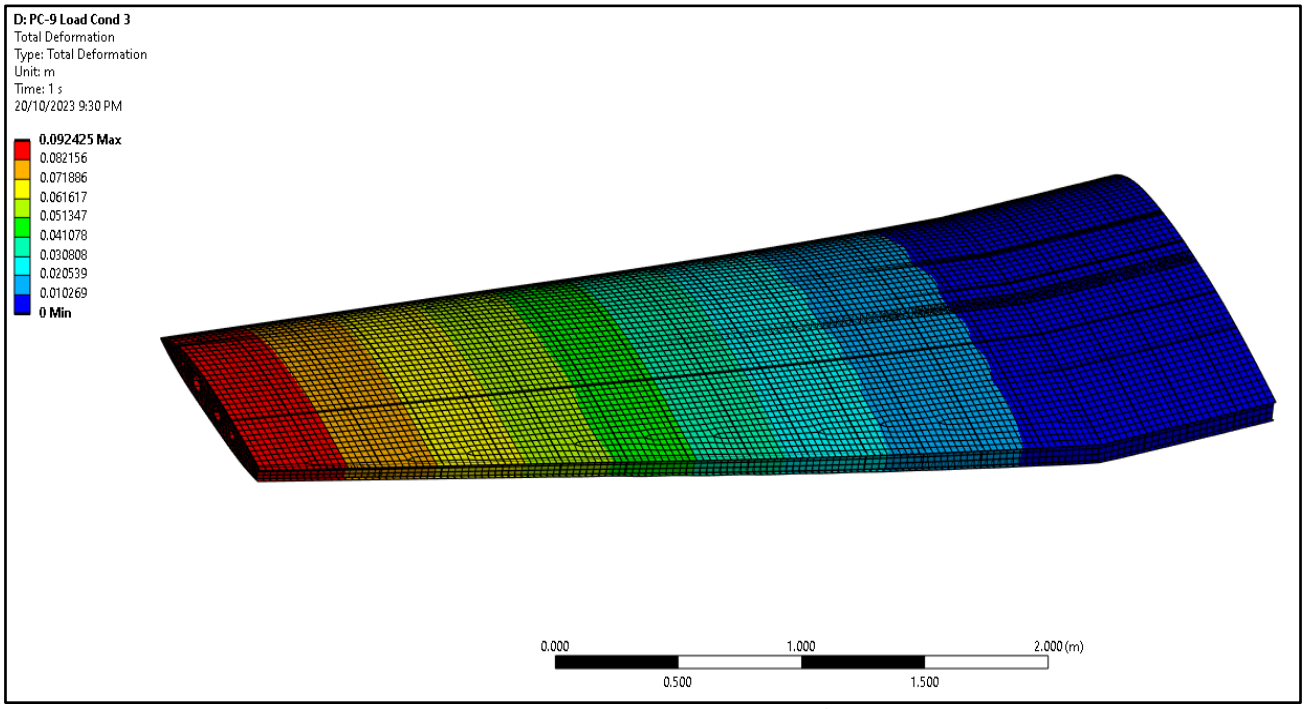

Figure 39: Loading Condition 3 – Wing Deformation

4.5.2 Ansys Results from Design Ultimate Load at Cruise

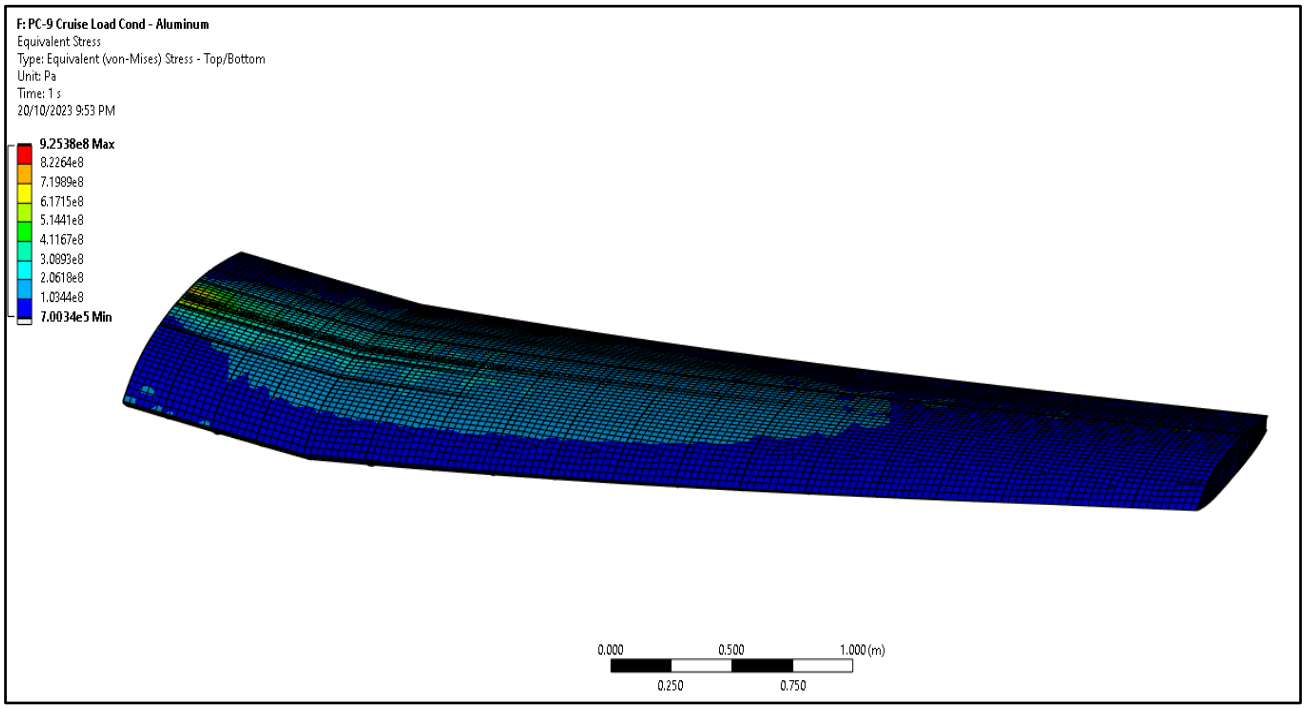

Figure 40: DUL Condition – Von Mises Stress on Wing

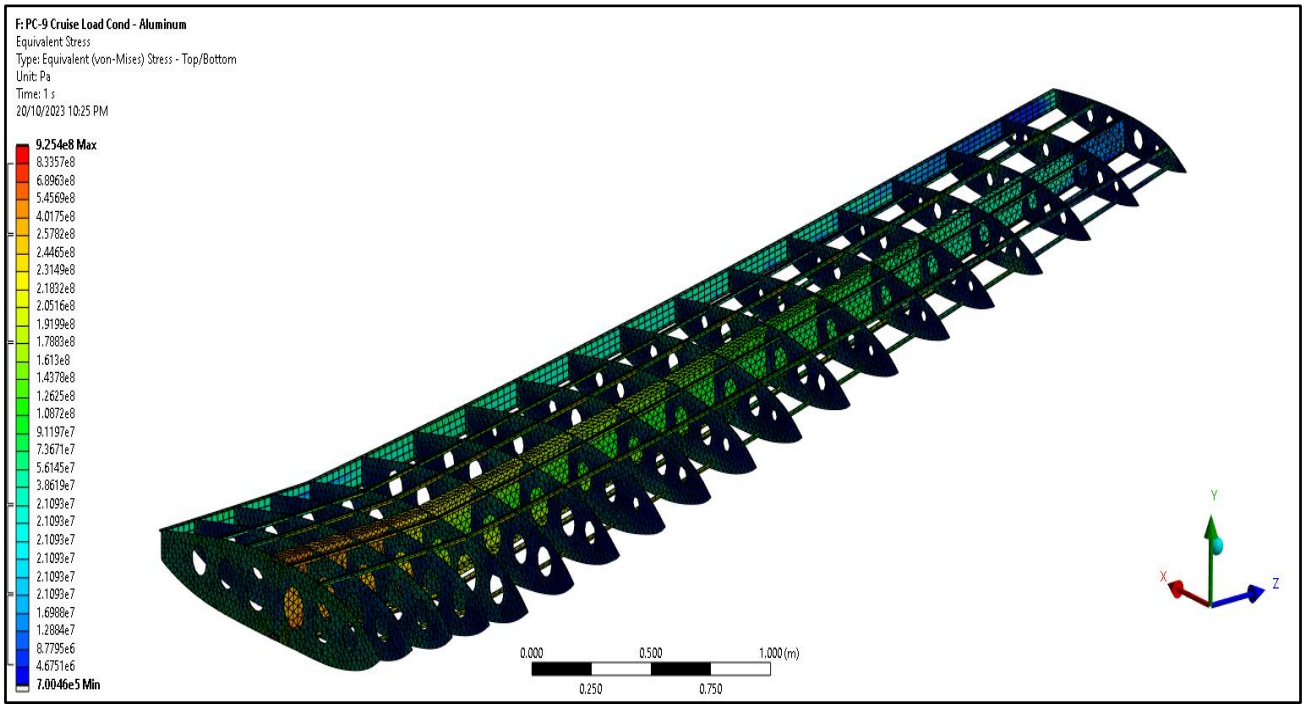

Figure 41: DUL Condition – Von Mises Stress on Ribs

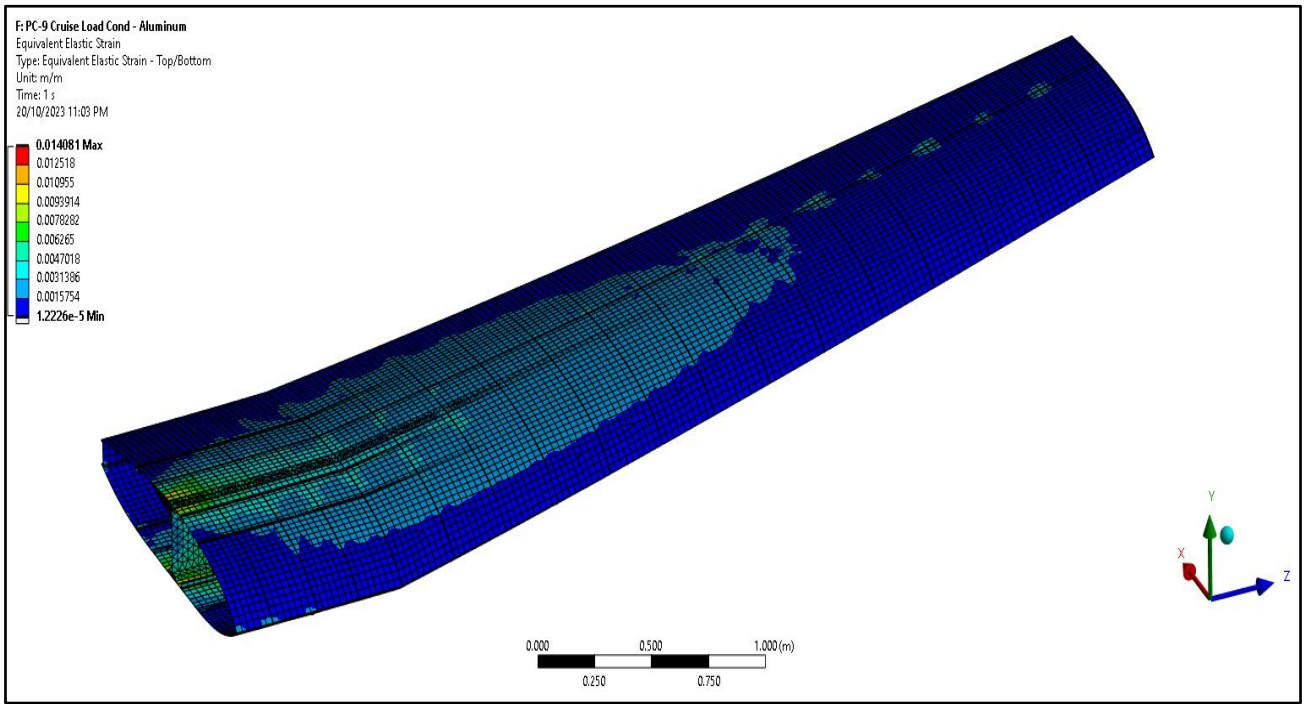

Figure 42: DUL Condition – Equivalent Elastic Strain at Wing

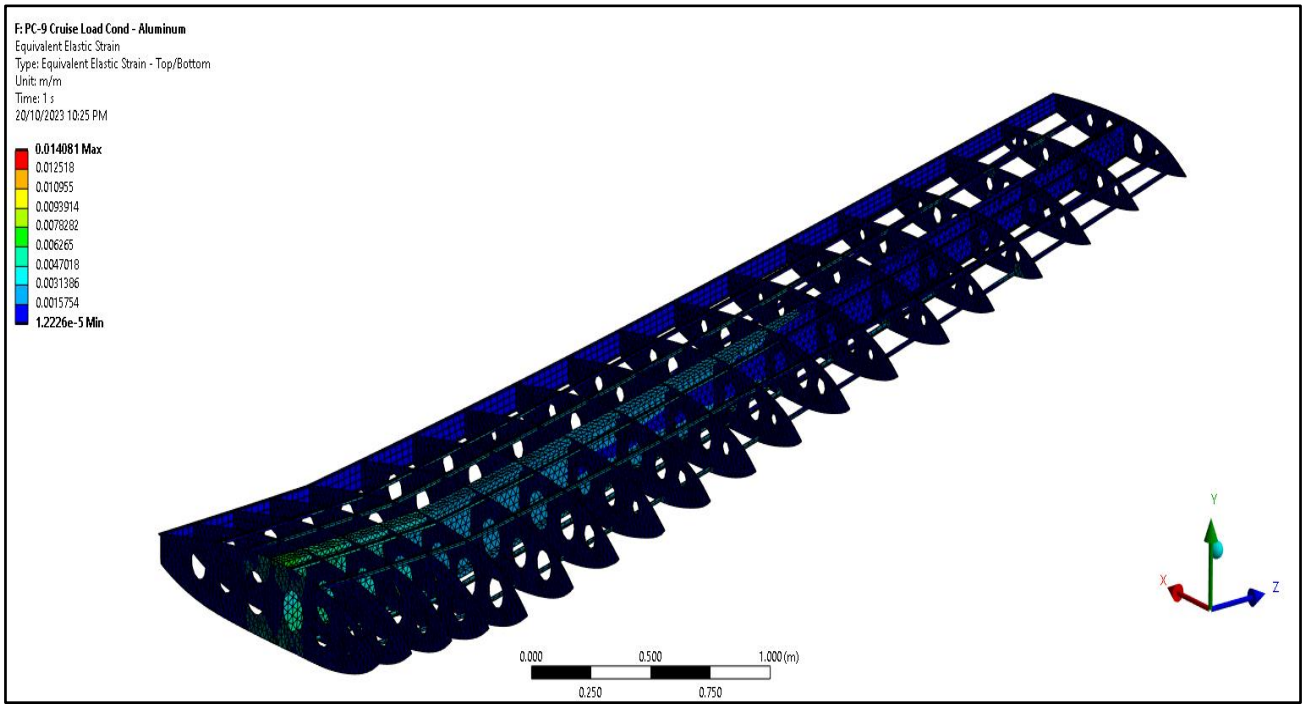

Figure 43: DUL Condition – Equivalent Elastic Strain - Rib

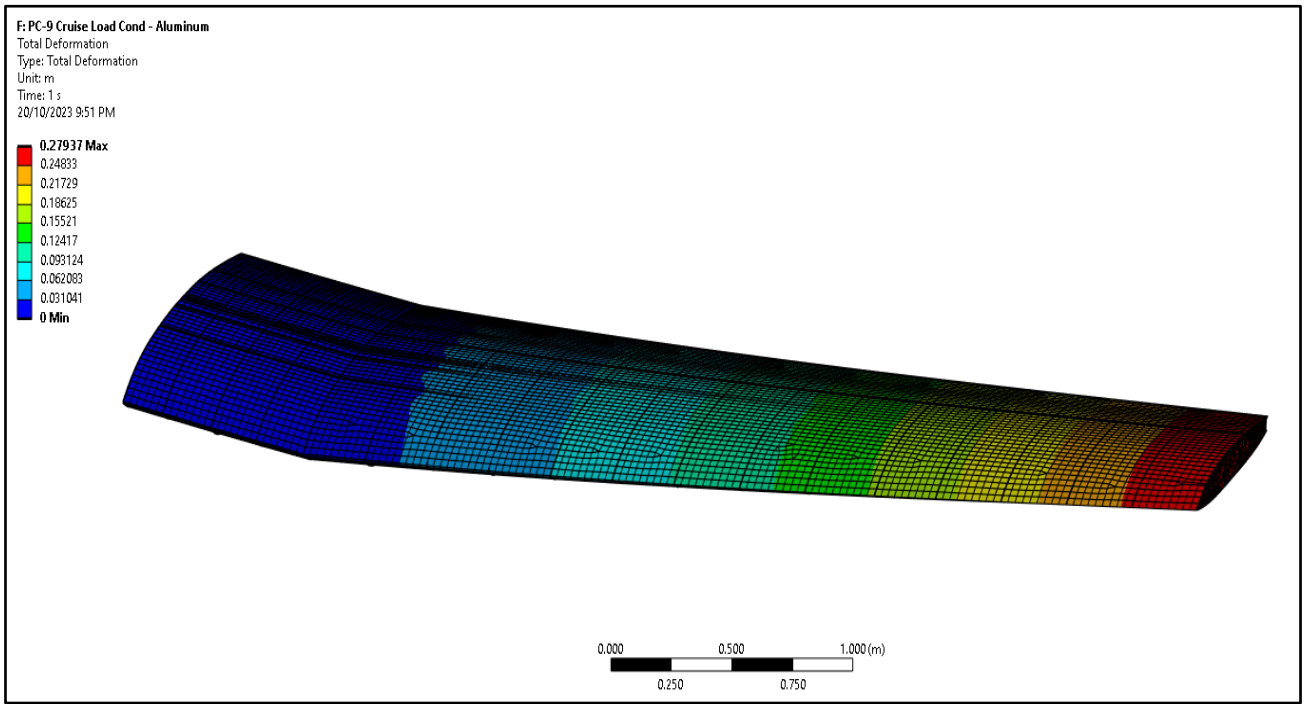

Figure 44: DUL Condition – Wing Deformation

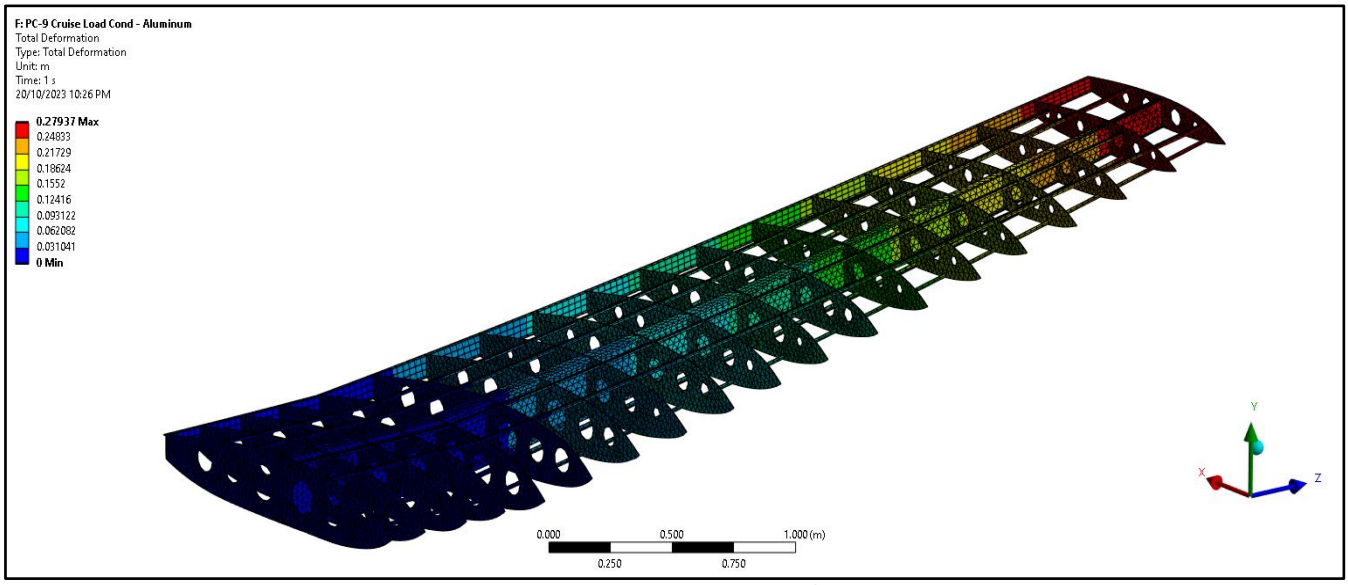

Figure 45: DUL Condition – Ribs deformation

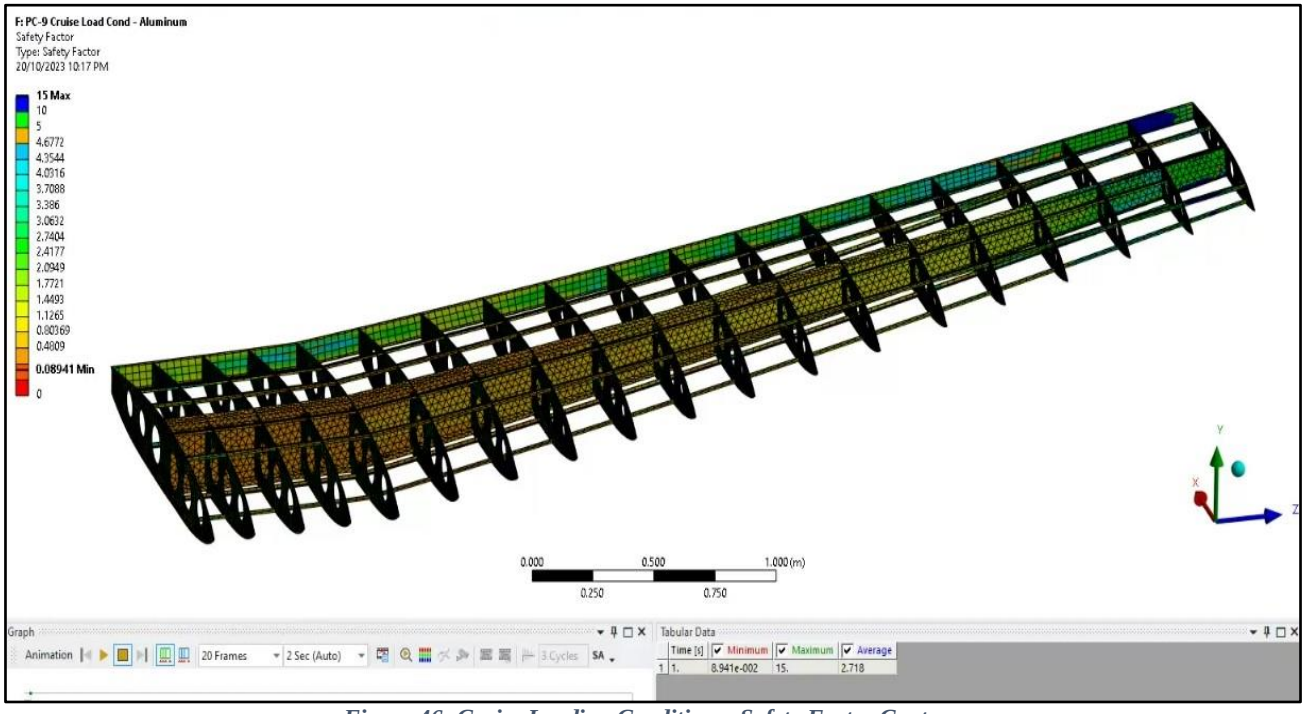

Figure 46: Cruise Loading Condition – Safety Factor Contour

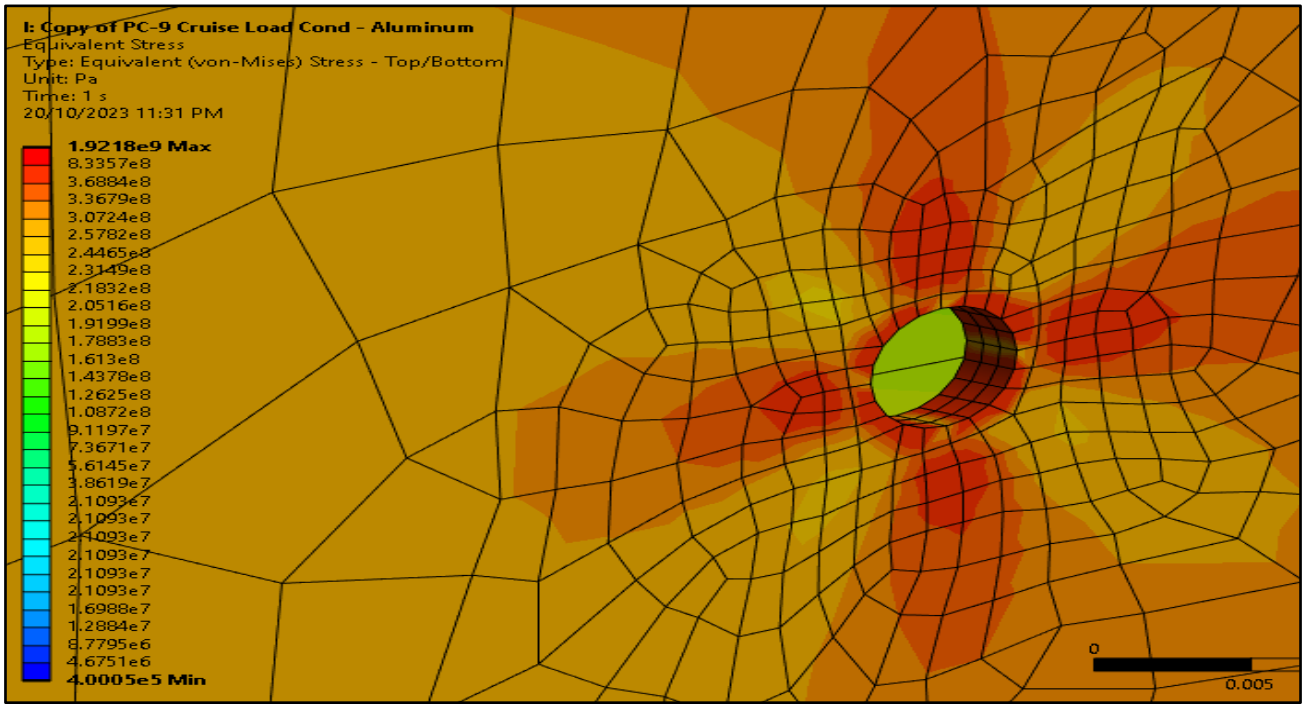

Figure 47: Spar Web Hole Stress Concentration

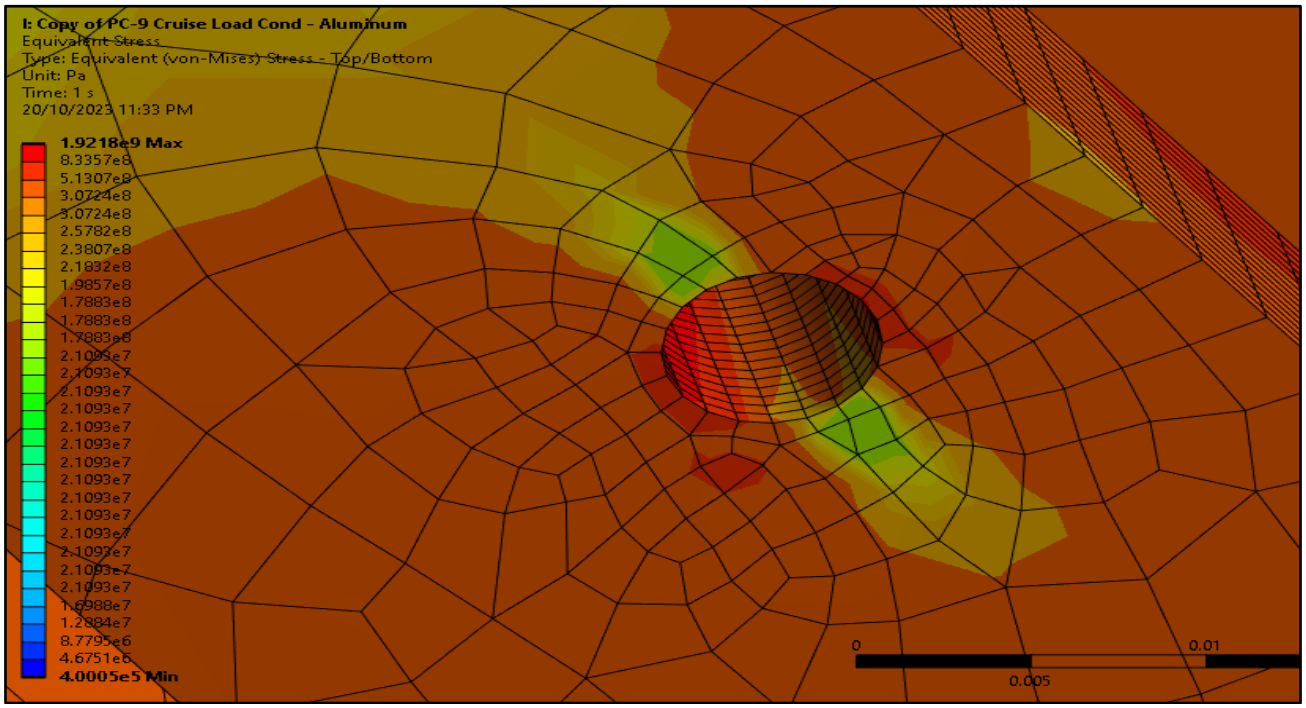

Figure 48: Flanges Hole Stress Concentration

4.6 Discussion

The finite element analysis plays a pivotal role in the development of a composite replacement for the PC9 wing. It enables the computational assessment of the wing's strength and weight characteristics, facilitating a comparative evaluation between an aluminium model and a carbon fibre epoxy composite. The primary goal of this project is to leverage the FEA model to predict the necessary strength for the PC wing and, consequently, determine the optimal composite laminate construction. Subsequently, we will analyse the effectiveness of this composite in maintaining strength while reducing overall weight.

The FEA model in use necessitates numerous simplifications to ensure computational efficiency and achieve numerical convergence. Notably, during the modelling of the wing geometry, the decision was made to exclude the stringers due to their minimal effects on various aspects of the model. These effects included an increase in the number of connections, heightened model complexity, and issues with achieving the necessary convergence for obtaining FEA results. The rationale behind excluding the stringers lies in the project's primary focus on assessing the stress experienced by the PC9 wing's main spar. A potential drawback of this is the FEA model's reduced ability to accurately compute the transfer of loads between the skin, ribs, and main spar, which could be one contributing factor to the finding of the skin carrying a higher stress load than anticipated. Simplifying connections with bonded joints is adequate when you weigh it against the flexibility offered by rivets or welds.

The FEA validation of our model is considered a success as the Von Mises stresses and wingtip displacement values are within 10 percent tolerance with the experimental investigation values calculated. This is accompanied by using the correct boundary conditions, the correct placement of pressure loads, and mesh quality. The mesh quality of the model is shown in Figure [ ] and the type of mesh element used in meshing in Figure [ ]. The model shows no failed mesh and it made primarily of tetrahedron, quadrilateral, and hexagonal predominantly which is the preferred element type for better results accuracy.

ANSYS Mechanical is a more friendly user software compared to Abaqus, but both have nodes limitations where for ANSYS is 128k nodes and Abaqus is 250000 nodes for student license. To reduce the number of nodes, increasing the element size of the mesh to some extent would fail the mesh and therefore have less accurate results. In our case, using 0.03mm element size provides us excellent Von Mises stress and displacement results as well as the weight of the wing model is 89.3kg. The nodes 41070 and the element is 49922.

The average safety factor is 2.7 and the margin of safety is 1.7 which shows our model is just above our theoretical safety factor of 1.5 which is also above the typical aerospace standard of 1.5 and therefore the wing will not fail under the cruise load. Furthermore, measured Von mises stresses of loadings level 1, level 2, level 3, and under design ultimate load at cruise did not exceed the yield strength of the aluminium material used. This confirms that the outcomes from this model meet the criteria for comparing the strength and weight of aluminium with that of a composite material.

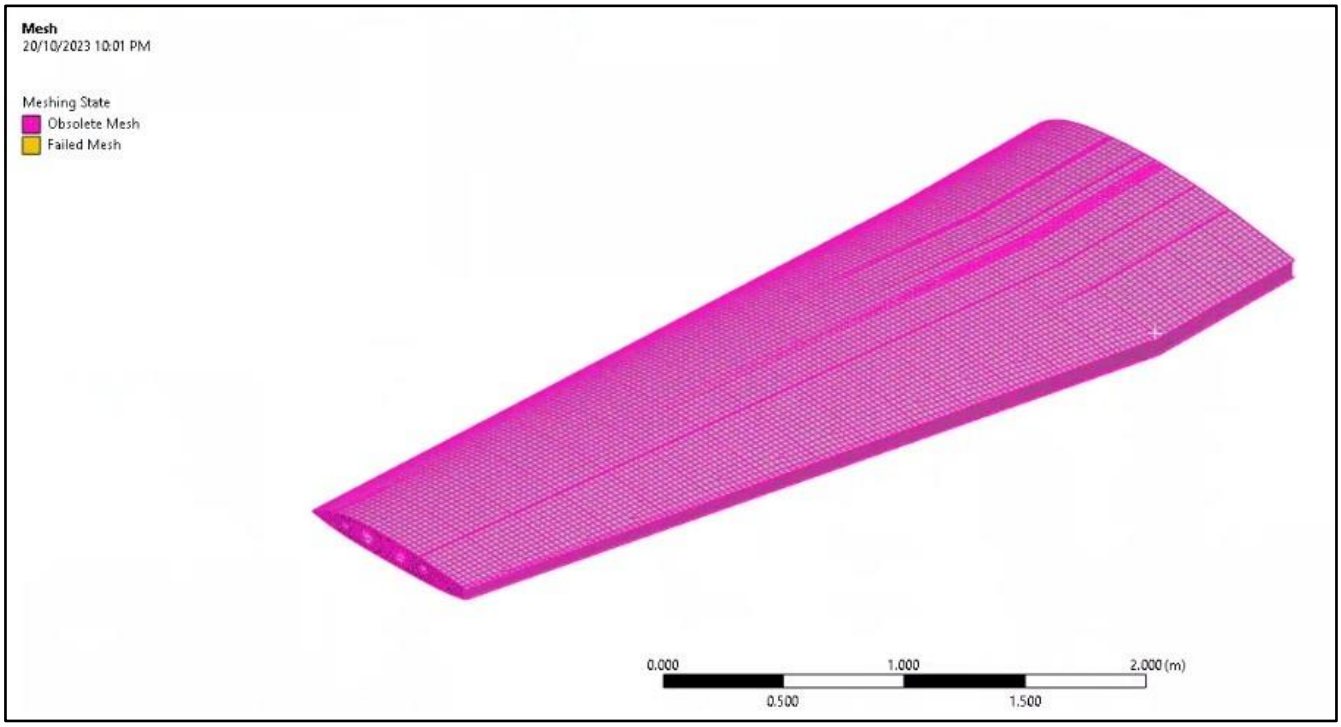

Figure 49 Mesh quality of the CAD model

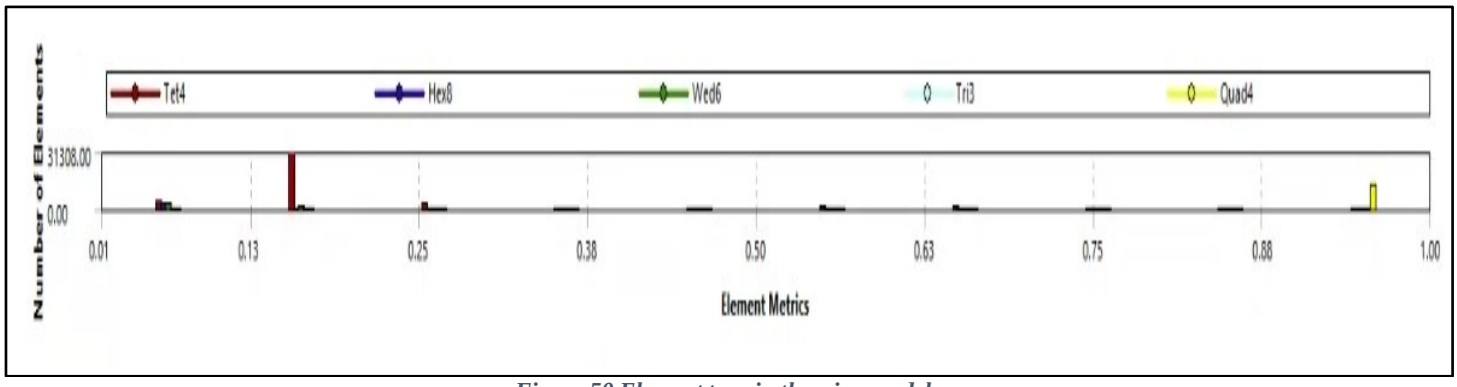

Figure 50 Element type in the wing model

CHAPTER 5: COMPOSITE DESIGN OF THE WING

5.1 Introduction

Composite materials have become integral in contemporary aerospace, reshaping aircraft structure design profoundly. Notably, materials like carbon-fibre-reinforced polymers showcase an exceptional strength-to-weight ratio, leading to a significant reduction in overall weight and thereby enhancing fuel efficiency—an indispensable consideration in wing design, where striking the right balance between weight reduction and structural robustness is paramount. Additionally, composites offer an unmatched level of design flexibility, facilitating the creation of aerodynamically optimized shapes that augment lift-to-drag ratios, ultimately enhancing aerodynamic efficiency. Moreover, their inherent attributes, such as resistance to corrosion, high fatigue tolerance, and superior vibration damping, position composite materials as pivotal components in achieving durable, efficient wing structures. This section ventures into the intricate art and science of composite design, shedding light on the nuanced interplay of materials and engineering principles that underpin the development of high-performance wing sections. In exploring the forefront of composite laminate utilization, we delve into the innovative methods and advanced technologies that are propelling the design and construction of modern, efficient wing sections, setting the stage for the next era of aerospace advancement.

5.2 Laminate Preliminary Design

Material: IM7/997 carbon/epoxy composite material
When it comes to selecting materials for redesigning an aircraft wing, such, as the PC9 trainer wing there are factors to consider. These include strength, weight, durability, cost, and aerodynamic performance. One promising option for the redesign of the PC9 trainer wing is the use of carbon/epoxy material. This high-performance composite offers a range of benefits.

- Optimal Strength to Weight Ratio. The IM7/997 carbon/epoxy composite has a strength to weight ratio. It combines strength with characteristics, which's crucial, for an aircraft wing. By improving integrity while keeping weight low this material contributes to enhanced fuel efficiency and manoeuvrability.
- Stiffness and rigidity: Carbon composites offer a level of stiffness and rigidity ensuring the wing maintains its shape and stability during flight. This is particularly important, for trainer aircraft like the PC9 as it enhances performance and improves handling.
- Fatigue resistance: Moreover, carbon composites have fatigue resistance enabling the wings to withstand repeated stress without compromising their integrity. This is crucial for aircraft that experience stress during take-off, flight and landing.
- Resistance to corrosion: Additionally, carbon composites exhibit resistance to corrosion and various chemicals making them well suited for use, in conditions. This quality extends the lifespan of the wings. Reduces maintenance requirements.
- Design Flexibility: Carbon composites provide a range of design options enabling the creation of aerodynamically efficient wing structures. This flexibility allows for optimized lift, drag and enhanced flight performance.
- Reduced component Count: Because of their moulding capabilities, composite materials can frequently allow for component consolidation, lowering the number of joints and fasteners. This can improve overall structural integrity while simplifying production and assembly operations.
- Environmental Concerns: Carbon composites are regarded more ecologically benign than conventional materials such as aluminium. Because of their modest weight, they can contribute to lower fuel consumption and emissions over the aircraft's service life.
- Technology that is both modern and proven: In the aerospace sector, IM7/997 is a well-established and proven composite material with a track record of effective application in aircraft components. Its qualities and performance have been thoroughly researched and confirmed. (‘STRONGER AND LIGHTER-Composites make their mark - ProQuest’ 2023, *Proquest.com*, viewed 17 October 2023, <https://www.proquest.com/docview/217187560?accountid=13552>.

Laminate Configuration for the Wing skin:

Table 33 Skin dimensions

	Dimensions	
Wing Skin Thickness	0.8	mm

The carefully chosen dimensions of the PC9 wing skin, including its thinness, contribute to weight reduction, enhanced fuel efficiency, improved manoeuvrability, and aerodynamic efficiency while maintaining structural integrity, ensuring the wing's stability and overall performance of the aircraft.

Table 34 Forces applied based on FEA at DUL Loading

Forces	*Values*	*Units*	*Description*
Max Stress X	382	MPa	Applied Stress X
Max Stress Y	142	MPa	Applied Stress Y
S Max In-Plane	147	MPa	Shear Force
Nx	305.6	N/mm	Force Intensity X
Ny	113.6	N/mm	Force Intensity Y
Nxy	117.6	N/mm	Force Intensity Shear

These stress values and force intensities are vital for assessing the structural robustness and safety of the PC9 wing. They help in ensuring that the wing can handle the applied forces and stresses within permissible limits without compromising structural integrity.

Table: 35 Knockdown Factors for Material Strength Reduction

Consideration	*Tension*	*Compression*
Impact	1	0.36
Weather	1	0.84
Notches	1	1
Fatigue	0.57	0.38
Total	0.3477	0.07699104

The redesign of the PC9 wing with IM7/997 carbon/epoxy composite material involves several knockdown factors that need to be considered. These factors contribute to the overall performance and durability of the structure.

Impact: The tension and compression values for impact are 1 and 0.36 respectively. This is due to damage from impact assuming fatigue loading afterward. The impact factor is crucial as it determines how well the wing can withstand sudden forces or shocks without sustaining damage. A high-tension value of 1 indicates that the wing can effectively resist tensile forces during an impact. However, the lower compression value of 0.36 suggests that the wing may be more susceptible to damage under compressive forces following an impact.

Weather: The tension and compression values for weather are 1 and 0.84 respectively. This is due to hot/wet conditions. Weather conditions can significantly affect the performance and lifespan of the wing material. The carbon/epoxy composite material must be able to withstand various weather conditions, including high temperatures and humidity. A high compression value of 0.84 suggests that the material can maintain its structural integrity under compressive forces in hot/wet conditions.

Notches: The tension and compression values for notches are 1. This could be affected by rivets or similar passthrough requirements. In the case of our problem the wing would be bonded without the use of rivets which is typical in these sorts of applications.

Fatigue: The tension and compression values for fatigue are 0.57 and 0.38 respectively. This is due to fatigue with Barely Visible Impact Damage (BVID). Fatigue is a critical factor in aircraft design as repeated stress cycles can lead to material degradation over time, especially when there's barely visible impact damage.

The total knockdown factors for tension and compression are calculated as 0.3477 and 0.07699104 respectively, indicating the overall effect of these factors on the wing's performance.

Table 36 Material properties - IM7/997 carbon/epoxy composite material

Material Property	*Value*
Youngs Modulus Longitudinal	164000 MPa
Youngs Modulus Transverse	9860 MPa
Poisson's Ratio	0.33
Shear Modulus	4950 MPa
Ply Thickness	0.13 mm
Density	1615 kg/m^3
Unnotched Strain Failure Tension	0.015 mm/mm
Unnotched Strain Failure Compression	0.008 mm/mm
Shear Strength In-Plane	110 MPa

The material properties we've selected work together like an advanced system. Each property contributes uniquely to make the PC9 wing strong, stable, and lightweight. It's a well-coordinated system, where each property plays a crucial role, ensuring the wing performs at its best, efficiently, and safely.

Table 37 Material Properties and Strength Coefficients for Different Fibre Orientations in the PC9 Wing Redesign Project

Strength Coefficients			
X0(T)	1402.2	MPa	Longitudinal Tensile Strength
X45(T)	140.22	MPa	Longitudinal Tensile Strength
X90(T)	84.303	MPa	Longitudinal Tensile Strength
X0(C)	150.764544	MPa	Longitudinal Compression Strength
X45(C)	15.0764544	MPa	Longitudinal Compression Strength
X90(C)	9.06425856	MPa	Longitudinal Compression Strength
Y0(T)	84.303	MPa	Transverse Tensile Strength
Y45(T)	140.22	MPa	Transverse Tensile Strength
Y90(T)	1402.2	MPa	Transverse Tensile Strength
Y0(C)	9.06425856	MPa	Transverse Compression Strength

Y45(C)	15.0764544	MPa	Transverse Compression Strength
Y90(C)	150.764544	MPa	Transverse Compression Strength

The laminate configuration aligns with the material's specific strengths in different orientations, strategically utilizing these properties to enhance the overall structural integrity and performance of the PC9 wing in various stress and loading scenarios. The high tensile strength in the longitudinal direction (X0(T)) is leveraged to withstand tensile forces along the wing's length, while the high tensile strength in the transverse direction (Y90(T)) contributes to resisting forces perpendicular to the wing's surface. The compression strength in the longitudinal direction (X0(C)) is crucial for withstanding compressive forces along the wing's length, and the compression strength in the transverse direction (Y90(C)) is important for resisting compressive forces perpendicular to the wing's surface. Shear strength values (X45(T), Y45(T), X45(C), Y45(C)) are critical for the wing's ability to withstand shear stresses during flight manoeuvres. The laminate configuration with most layers oriented at 45° takes advantage of the highest tensile strength (X45(T)) and transverse tensile strength (Y45(T)), and the balance of compression strength in both longitudinal (X45(C)) and transverse (Y45(C)) directions contributes to structural integrity. The orientation at 0° (N0) aligns with the highest longitudinal tensile strength (X0(T)), enhancing resistance to tension along the wing's length, while the dominant orientation at 45° (N45) aligns with optimized tensile and compression strength, making it a strategic choice for most of the layers. The orientation at 90° (N90) aligns with the highest transverse tensile strength (Y90(T)), providing reinforcement against forces perpendicular to the wing's surface. In conclusion, the laminate configuration strategically aligns with the material's specific strengths in different orientations, ensuring that it is optimized to withstand the specific forces and stresses experienced during flight, contributing to the success of the PC9 wing redesign project.

Table 38 Wing Skin laminate Configuration

Layers	Number of Layers	Percentage Contribution
0	2	16.67
45	8	66.67
90	2	16.67
Total	12	
Composite Thickness	1.65 mm	

Final Configuration is:

[45, -45, 45, -45, 90, 0]$^{\text{Symmetrical-Even}}$

The laminate configuration offered in the context of a PC9 wing redesign project reveals the layer orientations and distribution of composite materials inside the wing structure. The arrangement implies a composite construction made up of many layers, each oriented at different angles (0°, 45°, and 90°) relative to the wing's longitudinal axis. This configuration's major orientation is 0° (parallel to the longitudinal axis), which accounts for roughly 68.42% of the layers. This orientation gives great strength and stiffness over the length of the wing, which is critical for load-bearing components and structural integrity during flight. The 45° orientation, which

accounts for approximately 21.05% of the layers, provides a good mix of strength and flexibility. Placing fibres at 45° aids in load distribution, especially in off-axis or shear loading circumstances. This is especially important in the context of the wing because various sections are subjected to differing stress patterns during flight. The 90° orientation, which accounts for approximately 10.53% of the layers, gives strong transverse strength. This orientation is required to counteract forces operating perpendicular to the wing's longitudinal axis, hence improving torsional stiffness and stability. The presented design suggests a symmetrical layout, with the layers mirrored on both sides of the wing's midline. In aeronautical applications, symmetry is crucial because it guarantees a balanced and predictable reaction during flight. The specified value of 2.47 mm for composite thickness represents the total thickness of all layers in the laminate. This thickness is an important design element since it affects the total weight, strength, and aerodynamic properties of the wing. In summary, this laminate structure is designed to optimise the strength, stiffness, and weight of the PC9 wing. The use of 0°, 45°, and 90° orientations, as well as symmetrical stacking, illustrates a deliberate approach to

Table 39 Material Properties for final skin laminate, values obtained via eLaminate

	eLaminate Material Properties
Ex (MPa)	50182
Ey (MPa)	50182
Vxy (mm/mm)	0.447
Gxy (MPa)	29726
Exb (MPa)	21092
Eyb (MPa)	22997

We can use eLaminate to get the final material properties for the new skin structure. These can be validated with FEA to confirm the layup performs as expected.

Laminate Configuration for the Spar:

Table 40 Spar Dimensions, for both flange and web. Including variations for composite where relevant.

Parameter	***Flanges***	***Web***	***Units***
b	65.8682635	214.9269461	mm
t	15.6502994	2.3	mm
t Composite	13.3375	2.3375	mm
A	1030.85804	494.331976	mm^2
I	13722656	1902914.141	mm^4
A Composite	878.517964	502.3917365	mm^2
I Composite	11456742.6	1933939.915	mm^4

Table 41 Material Properties of IM7/997 Composite

Material Properties IM7/997 Composite	**Value**	**Units**	**Description**
E_1	164000	MPa	Youngs Modulus Longitudinal

E_2	9860	MPa	Youngs Modulus Transverse
v_12	0.33		Poissons Ratio
G_12	4950	MPa	Shear Modulus
t_ply	0.1375	mm	Ply Thickness
Rho	1615	kg/m^3	Density
Ult_Strain_T	0.015	mm/mm	Unnotched Strain Failure Tension
Ult_Strain_C	0.008	mm/mm	Unnotched Strain Failure Compression
S45	110	MPa	Shear Strength In-Plane

Table 42 Material Properties of 2124-T851 Aluminium

Material Properties 2124-T851 Aluminium	Value	Units
Rho	2780	kg/m^3
E	73100	MPa
Poissons Ratio	0.33	
Yield strength	441	MPa
Ultimate tensile strength	483	MPa

The dimensions for the spar are outlined above. The original dimensions are based on the geometry of the spar. Further values are calculated dynamically for the composite, this is done based on the number of layers used for each member. This is required to preserve the accuracy of the results given the changing geometry.

Table 43 Number of layers needed to match the geometry of the main spar

	Flange	Web
Layers to match geometry	113.82	16.73

The number of layers needed for each member to maintain the dimensions of the original spar are calculated. This is based on the ply thickness and member thickness values. Notably, eLaminate has support for a maximum of 100 layers, which means we had to consider some options:

- Add a core material to maintain the overall geometry size.
- Use a tool other than eLaminate that has support for more layers
- Attempt to match the relevant properties with a reduced geometry

We choose to take the last approach as from our testing we found the laminate could closely match the stiffness values with just under 100 layers. We only altered the flange sizes preserving the geometry of the original web.

The final laminate layouts are defined below:

- Flange - $[\ 45_5, -45_5, 0_{28}, 90_{21}, 0_{11}\ ]^{\text{Symmetrical-Odd}}$
- Web - $[\ -45_2, 45_3, 0_1, 90_1, -45_1, 0_1\ ]^{\text{Symmetrical-Odd}}$

Both laminates are symmetrical and odd. The 45-degree layers are interwoven with alternating positive and negative angles where possible and both laminates contain at least 10% of each fibre orientation. This is summarised in the table below.

Table 44 Number of fibres for each member and their percentage contribution

Fiber	Flange Layers	Percentage	Web Layers	Percentage
+45	10	10.31	6	35.29
-45	10	10.31	6	35.29

0	56	57.73	3	17.65
90	21	21.65	2	11.76
Total	97	100	17	100

The surface of the spar is designed with layers of fibres oriented at both plus and minus 45 degrees, facilitating the even distribution of forces between its components. These 45-degree fibres primarily make up the web, where shear stress is most prevalent. On the other hand, the flange primarily consists of fibres aligned at 0 degrees to optimize axial and bending strength, which are the primary types of loads it encounters. Additional fibres are interlaced throughout to provide resistance against other forms of stress.

Calculating the stiffness values based on the data provided by eLaminate show that these configurations closely match the stiffness of the aluminium spar.

Table 45 Laminate values for the different layups

eLaminate Values			
Member	***Em (x)***	***Eb (x)***	***Units***
1	105525	91,099	MPa
2	50477	26076	MPa
3	105525	91,099	MPa

Table 46 Stiffness values for both composite and Aluminium including the difference

Member and Stiffness	***Composite***	***Aluminium***	***Units***
EA Member 1	92705608.16	75355723.04	N*mm
EA Member 2	25359227.68	36135667.45	N*mm
EA Member 3	92705608.16	75355723.04	N*mm
EI Member 1	1.0437E+12	1.00313E+12	N*mm^2
EI Member 2	50429417231	1.39103E+11	N*mm^2
EI Member 3	1.0437E+12	1.00313E+12	N*mm^2
EA Total	210770444	186847113.5	N*mm
EI Total	2.13783E+12	2.14536E+12	N*mm^2
EA Difference	12.80369282	%	Composite 12% Greater
EI Difference	-0.35100628	%	Composite 0.34% Less

This configuration offers a good theoretical equivalence with the aluminium. Even gaining a 12.8% increase in axial stiffness.

Given the variation in the geometry between the composite spar and aluminium calculating the weight savings would not be a simple comparison of the material density. Instead, we took the cross-sectional areas for each spar and used that as a normalised volume (depth of 1m). The density values could then be applied to that volume to get a mass value useful for comparison.

Table 47 Mass comparison for the calculation of weight savings

Parameter	*Value*	*Unit*
Composite Cross-sectional Area	0.002259428	m^2

Aluminium Cross-sectional Area	0.002556048	m^2	
Normalised Volume of Composite	0.002259428	m^3	
Normalised Volume of Aluminium	0.002556048	m^3	
Mass Comp (Norm)	3.648975678	kg	
Mass Alum (Norm)	7.10581362	kg	
Weight Savings	48.65	%	of the original main spar mass

This constitutes significant weight savings compared to the original design of the spar.

To account for the taper in the spar we decided to recommend a redesign that maintains the same cross-section along the span. The reason for this is that to taper the spar would have two disadvantages on the material strength.

- The spar would need to be sectioned to determine an appropriate layup for the laminate. The issue of bonding those sections together would then create stress points at their junctions and limit the spars overall effectiveness as the fibres do not run continuously along the span
- If the same layup is kept while removing outside layers the spar will continue to lose some of the advantages of the original layup potentially creating further unexpected problems in the material

Overall, this theoretical re-design should provide weight savings of 48.65% for the spar while maintaining the same load carrying capabilities.

5.3 FE Analysis on the Composite Wing

We applied the theoretical laminate configurations to the FEA model. These were applied as orthotropic materials, which allowed us to outline the different properties along the 3 major axes. Evaluating the new structure under the same DUL loading condition used for the aluminium yielded the following results, which we provide for comparison and validation.

Table 48 Comparison of Von Misses stress at the same points for the two material models

DUL Loading	Composite	Aluminium	Units
Skin	44.8	43	MPa
Top Spar	180	243	MPa
Spar Web	172	216	MPa
Bottom Spar	179	239	MPa

We have outlined the Von misses' stresses at the same points on the model for both the composite and aluminium wing. The overall results show that we achieved a better performance in most places with the skin showing the closest stress.

The Tip Deflection was found to be 29 mm compared to 27 mm for the aluminium wing. This is also comparable.

Table 49 Weight difference between Wing Models

Model	*Composite*	*Aluminium*	*Units*
Weight	67.1	89.3	kg

This constitutes a weight reduction of 24.9%. This reduction does not include the ribs or stringers which remained aluminium.

5.4 Discussion

The complete numerical study of the PC-9 wing design demonstrates the enormous benefits of switching from standard aluminium materials to advanced composites. This transition is a significant step towards improving aircraft performance and reducing weight. The use of composite materials in the skin design of the wing provides a significant weight savings. With its varied angles and layers, the laminate pattern allows for optimal material consumption, weight reduction, and structural efficiency. The decreased density of the composite material adds greatly to total weight reduction, which is an important consideration in aircraft design. Furthermore, the composite's superior strength-to-weight ratio strengthens the wing's integrity, which is critical in improving overall performance. The numbers linked with the laminate composition illustrate the composite material's excellent mechanical capabilities, notably the remarkable E1 values for Members 1 and 3. These numbers represent a significant improvement in material performance, positioning the design to fulfil the stringent requirements of the aerospace sector. The increased axial and flexural rigidity is an essential aspect of the design revolution. The comparison of composite and aluminium materials demonstrates that composites are clearly superior in several areas. The enhanced axial stiffness for Members 1 and 3 emphasises the material's capacity to bear increasing structural stresses while maintaining wing integrity. The maintained flexural stiffness (EI) in Member 1 emphasises the composite's suitability for the PC-9 wing spar. This material successfully resists bending and torsional pressures, resulting in greater stability and performance. Furthermore, the increase in axial stiffness (EI Total) highlights the composite's excellent performance, particularly in terms of weight savings.

Overall, when modelled the composite handles the same loading condition admirably exceeding or matching the conditions in almost every case while providing a significant weight reduction of nearly 25%.

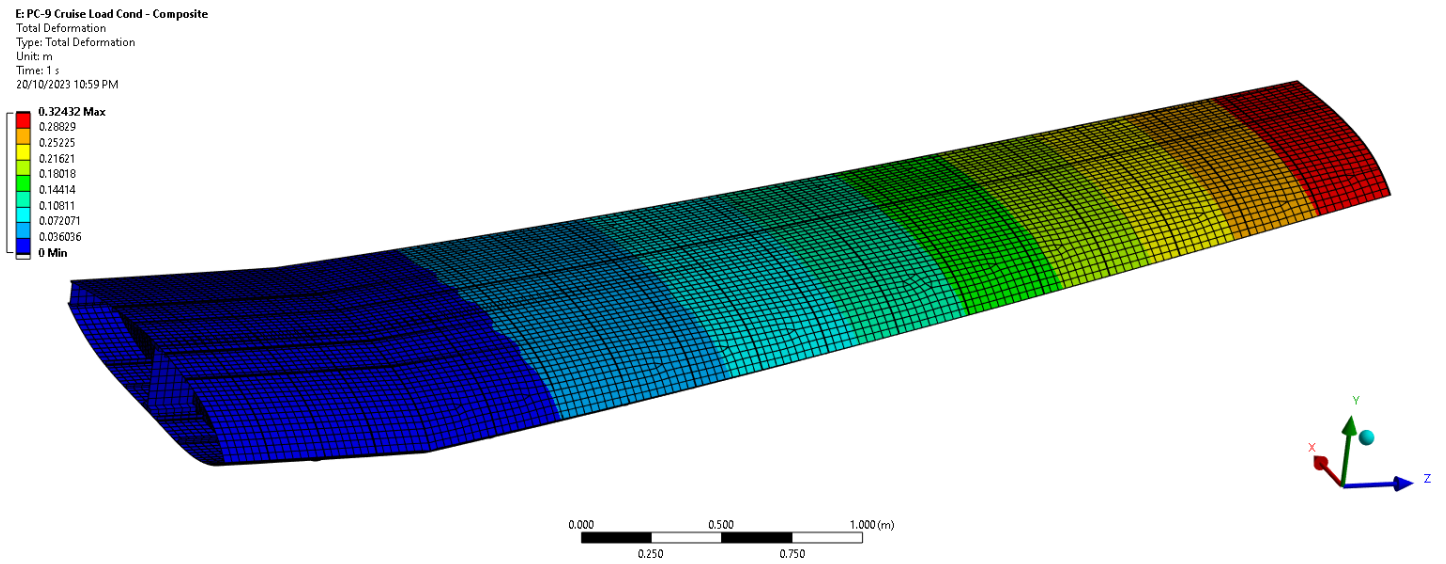

Figure 51 Deformation Contour Composite under DUL Loading

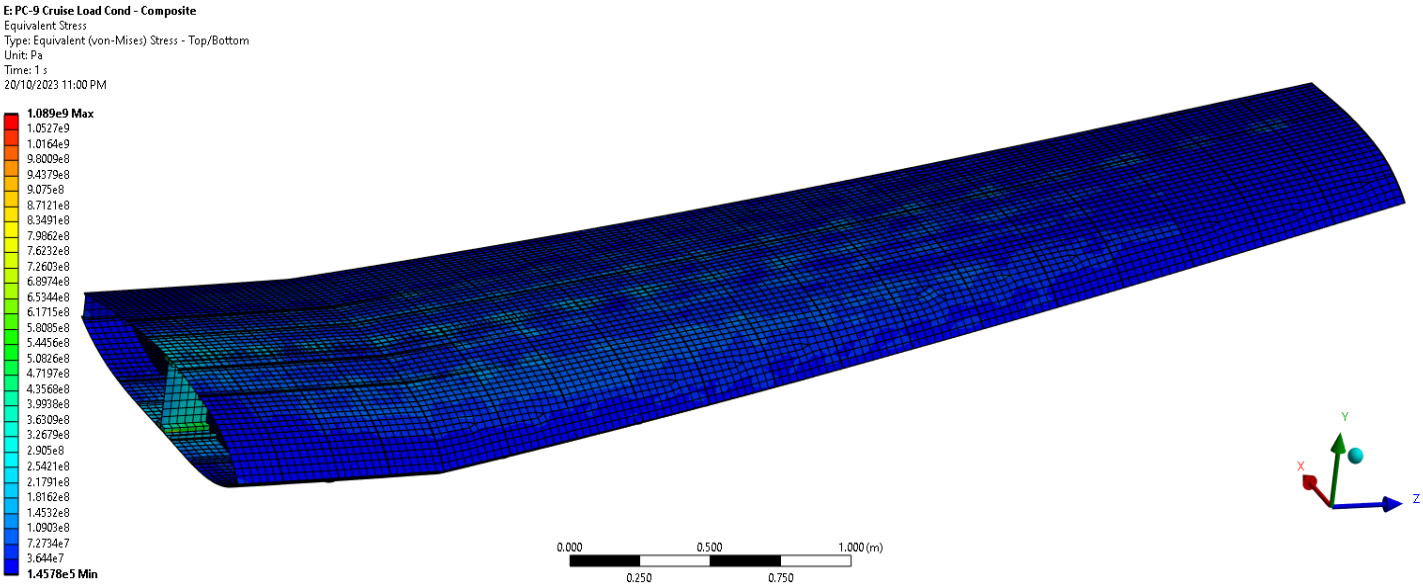

Figure 52 Stress Contour Composite under DUL Loading

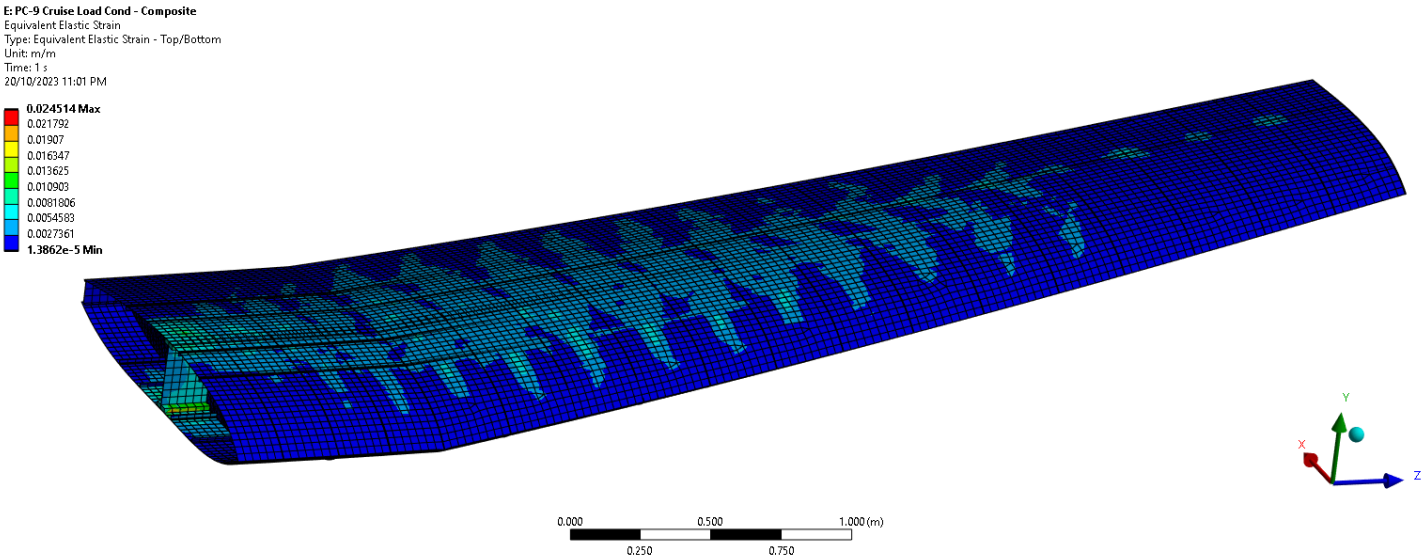

Figure 53 Elastic Strain Contour Composite under DUL Loading

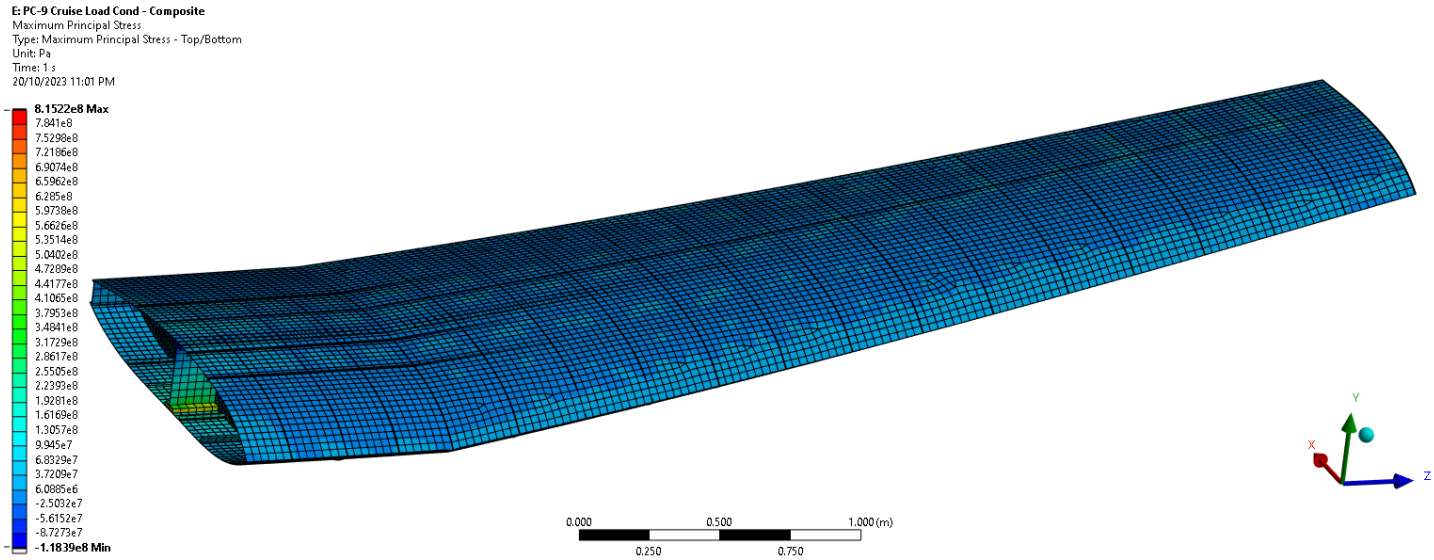

Figure 54 Max Principal stress Contour Composite under DUL Loading

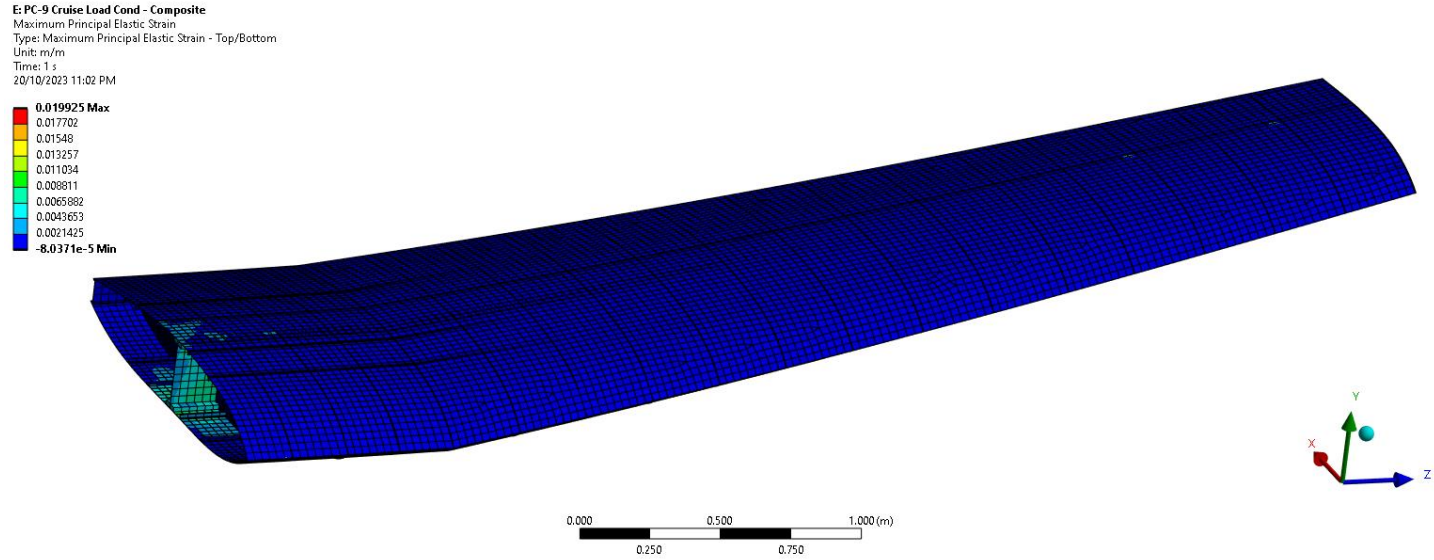

Figure 55 Maximum Principal Elastic Strain Contour Composite under DUL Loading

CONCLUSION

The progress report discusses the enhancements in the wing design of the PC9 aircraft for environmentally friendly aviation. It encompasses static and dynamic analysis outcomes, incorporating methodology, assumptions, theoretical models, and analysis results such as unnotched and notched strength, fracture analysis, safe-life, fail-safe, and damage tolerant design approaches. The report establishes the viability of advancing the PC9 wing design for greener aviation. It emphasizes the significance of integrating both static and dynamic analyses, while acknowledging project limitations and challenges. The report's findings serve as a foundation for forthcoming project phases, focusing on wing design optimization and assessing the ecological implications of these improvements. This progress report offers a robust basis for future research and development in the realm of eco-friendly aviation. The anticipation is that these results will contribute to the evolution of sustainable and ecologically conscious aircraft designs in the times ahead. In our analyses, we assessed both the static and dynamic performance of aircraft components. The static analysis revealed that stress levels for an unnotched spar remain well below the material's yield stress, indicating a low risk of permanent deformation under the given loading conditions, however the notched analysis did show plastic deformation due to the high local maximum stresses at the notched regions.

Fracture analysis identified critical crack lengths that would lead to failure:

- **Cracks Emanating from Flange Notches:**
  - Brittle Fracture: 5.58 mm
  - Plastic Collapse: 8.86 mm
- **Single Edge Cracks in Flange:**
  - Brittle Fracture: 1.70 mm
  - Plastic Collapse: 9.27 mm
- **Web Crack:**
  - Brittle Fracture: 20.58 mm
  - Plastic Collapse: 82.55 mm

Our dynamic analysis estimates that the main spar should endure approximately 200,000 flights before succumbing to fatigue failure. As for pre-existing defects, cracks measuring as small as 1.5 mm in the notches, flanges, or webs are generally low risk, requiring minimal inspections. Specifically, notch defects should be inspected every 1,379 flights, and single edge cracks in the flange should be inspected every 14,265 flights. Importantly, the centre crack in the web was determined to be a non-issue within the expected lifespan of the aircraft. Several key findings emerge from this FEM discussion: First, the significance of careful model simplifications, which strike a balance between computational efficiency and convergence. Excluding stringers, for instance, was a strategic choice to focus on assessing the stress on the PC9 wing's main spar while simplifying connections with bonded joints. This approach proved to be sufficient for assessing load transfer and maintaining model flexibility.

Second, the successful validation of the FEA model against experimental results demonstrated its credibility. The Von Mises stresses and wingtip displacement values were within a 10 percent tolerance range, affirming the model's capability to simulate real-world wing behaviour during experiments. These validation efforts were bolstered by appropriate boundary conditions, accurate placement of pressure loads, and mesh quality. Moreover, the FEA model aided in verifying the PC-9 wing's structural integrity. With an average safety factor of 2.7 and a margin of safety at 1.7, the model surpasses the theoretical safety factor of 1.5, which is above the typical aerospace standard. This assurance that the wing will not fail under cruise load is complemented by stress levels that remained below the yield strength of the aluminium material used, affirming the viability of comparing the strength and weight of aluminium with that of a composite material.

In essence, this discussion underscores the multifaceted benefits of employing FEA in aerospace engineering, showcasing its crucial role in the PC-9 wing redesign project. Through a judicious approach to modelling and a rigorous validation process, FEA serves as a guiding light, offering a path toward optimal material selection, structural integrity, and weight reduction, contributing significantly to the overall enhancement of the PC-9 wing's performance and safety.

In Conclusion, the incorporation of the Composite material into the PC-9 wing design constitutes a critical step towards greener aviation practises. The lightweight features of this new material led to lower fuel consumption and emissions, harmonising with the industry's eco-friendly goals. Its improved durability and fatigue resistance offer prolonged operating life, lowering the environmental effect of wing replacements and production. Furthermore, the material's corrosion resistance reduces maintenance requirements, reducing environmental footprints even further. Finally, the use of this new material not only improves the performance of the PC-9 wing, but also highlights its commitment to a more sustainable and ecologically responsible aviation sector.

REFERENCES

[1] "*Aviation's impact on the environment*", Aviation Benefits Beyond Borders, viewed 18th July 2023.

https://aviationbenefits.org/environmental-efficiency/aviations-impact-on-the-environment/#:~:text=Aviation's%20carbon%20footprint&text=Aviation%2C%20producing%202%25%20of%20all,greenhouse%20gas%20emitted%20by%20aircraft.

[2] Candelaria Bergero, Greer Gosnell, Dolf Gielen, Seungwoo Kang, Morgan Bazilian & Steven J. Davis. (2022), Pathways to net-zero emissions from aviation. Nature Sustainability, 6, pp123-135.

https://www.nature.com/articles/s41893-022-01046-9

[3] Smith, J. (2015). Future Directions of Fuel Efficiency in the Aviation Industry. ResearchGate. Available at:

https://www.researchgate.net/publication/273927130_Future_directions_of_fuel_efficiency_in_aviation_industry

[4] Runze Huang, Matthew Riddle, Diane Graziano, Joshua Warren, Sujit Das, Sachin Nimbalkar, Joe Cresko, and Eric Masanet (2020), Energy and Emissions Saving Potential of Additive Manufacturing: The Case of Lightweight Aircraft Components. Available at:

https://iopscience.iop.org/article/10.1088/1755-1315/889/1/012068/pdf

[5] Ric Abbott (December 2000), Composites in General Aviation. Comprehensive Composite Materials (pp.165-180). Available at:

https://www.researchgate.net/publication/300294351_Composites_in_General_Aviation

[6] Bisma Parveez, M.I.Kittur, Irfan Anjum Badruddin, Sarfaraz Kamangar, Mohammed Hussien, M.A.Umarfarooq. (2022). Scientific Advancements in Composite Materials for Aircraft Applications: A Review, 14(22), 5007. Available at:

https://www.mdpi.com/2073-4360/14/22/5007

[7] Yongxiang Yang, Rob Boo, Brijan Irion, Derk-Jan van Heerden, Pieter Kuiper, Hans de Wit. (2011). Recycling of composite materials. Chemical Engineering and Processing: Process Intensification. Volume 51, January 2012, Pages 53-68 Available at:

https://www.sciencedirect.com/science/article/abs/pii/S0255270111002029

[8] Rui Barreira-Pinto, Rodrigo Carneiro, Mário Miranda, and Rui Miranda Guedes (2023). Polymer-Matrix Composites: Characterising the Impact of Environmental Factors on Their Lifetime. Materials 2023, 16(11), 3913. Available at:

https://www.mdpi.com/1996-1944/16/11/3913

[9] Dhanenthiran Mohan, Balamurugan Chinnasamy, Senthil Kumar Naganathan, Nagaprasad Nagaraj, LetaTesfaye Jule, Bayissa Badassa, Krishnaraj Ramaswamy, Parthiban Kathirvel, Gunasekaran Murali and Nikolai Ivanovich Vatin. Experimental Investigation and Comparative Analysis of Aluminium Hybrid Metal Matrix Composites Reinforced with Silicon Nitride, Eggshell and Magnesium (2022). Materials (Basel). 2022 Sep; 15(17): 6098. Available at:

https://www.ncbi.nlm.nih.gov/pmc/articles/PMC9458176/

[10] Gregory Szuladzinski. (2017). Performance of Composites Versus Metals Under Extreme Loading. ResearchGate. International Journal of Protective Structures 8(1):86-108. Available at:

https://www.researchgate.net/publication/315876008_Performance_of_composites_versus_metals_under_extreme_loading

[11] Tariq, U. and Mazhar, F. (2021) 'Static structural analysis of fighter aircraft's wing spars', ***2021 International Bhurban Conference on Applied Sciences and Technologies (IBCAST)*** **[Preprint]. doi:10.1109/ibcast51254.2021.9393241.]**

https://www.researchgate.net/publication/350936709_Static_Structural_Analysis_of_Fighter_Aircraft's_Wing_Spars

[12] Standard Specification for Design and Performance of a Light Sport Airplane 2023, Astm.org, viewed 29 August 2023,

https://www.astm.org/f2245-20.html

[13] Salu Kumar Das & Roy, S 2018, 'Finite element analysis of aircraft wing using carbon fiber reinforced polymer and glass fiber reinforced polymer.', IOP conference series, vol. 402, pp. 012077–012077, viewed 29 August 2023,

https://www.proquest.com/docview/2557066139?accountid=13552&parentSessionId=U2hqDsX1fTubH%2Bx8bpSuKQuziwB%2BG5BalJ9hCGNHk10%3D&pq-origsite=primo

[14] A ground and operational vibration assessment of the RAAF PC-9/A airframe 2015, Informit, viewed 29 August 2023,

https://search-informit-org.ezproxy.lib.rmit.edu.au/doi/10.3316/informit.253542970326058

[15] Harijono Djojodihardjo 2015, 'Green Aircraft Technology Imperatives for Environmental Sustainability', Applied Mechanics and Materials, Trans Tech Publications, viewed 30 August 2023,

https://www.proquest.com/docview/1903436336?accountid=13552&parentSessionId=x7XpQy5kdQ6YOBGeEZLqgnIPBqcc7LTQ7SlFPnOP59A%3D&pq-origsite=primo

[16] "Pilatus PC-9 Twin-Seat, Single-Engine Basic Trainer Aircraft [1984]", Military Factory, viewed 29th August 2023.

https://www.militaryfactory.com/aircraft/detail.php?aircraft_id=1840

[17] "*Flying the Pilatus PC-9 / A*", Carla Kopp, Air Power Australia, December 1991, viewed 29th August 2023.

https://www.ausairpower.net/APA-PC-9-Report.html

[18] Dowling, N.E., Kampe, S.L. and Kral, M.V. (2020) *Mechanical behavior of materials: Engineering methods for deformation, fracture, and fatigue*. Harlow, England: Pearson.

[19] n.d. *ASM material data sheet*. (Accessed: 01 September 2023). Available at:

https://asm.matweb.com/search/SpecificMaterial.asp?bassnum=MA2124T851

[20] Marc Meyers & Krishan Chawla, "*Mechanical Behaviour of Materials*", Cambridge University Press, 2009, viewed 1st September 2023,

https://ceimusb.files.wordpress.com/2015/04/mechanicalbehaviormeyers.pdf

[21] Stress-strain curve Ramberg-Osgood equations and calculator, Engineers Edge - Engineering, Design and Manufacturing Solutions. (Accessed: 01 September 2023). Available at:

https://www.engineersedge.com/calculators/stressstrain_curve_15438.htm

[22] Efatigue + EFatigue: Fatigue analysis on the web n.d. https://www.efatigue.com/, viewed 1st September 2023 Available at:

https://efatigue.com/training/Chapter_7.pdf,

[23] Gates, N. and Fatemi, A. (2014) 'Notched fatigue behavior and stress analysis under multiaxial states of stress', *International Journal of Fatigue*, 67, pp. 2–14. doi:10.1016/j.ijfatigue.2014.01.014.

https://www.researchgate.net/publication/263737167_Notched_fatigue_behavior_and_stress_analysis_under_multiaxial_states_of_stress

[24] Tutluoglu, L. and Keles, C. (2011) 'Mode I fracture toughness determination with straight notched disk bending method', *International Journal of Rock Mechanics and Mining Sciences*, 48(8), pp. 1248–1261. doi:10.1016/j.ijrmms.2011.09.019.

https://www.researchgate.net/publication/251670847_Mode_I_fracture_toughness_determination_with_straight_notched_disk_bending_method

[25] Adams, D. (2023) *Compact tension fracture toughness testing*, *CompositesWorld*. Available at: https://www.compositesworld.com/articles/compact-tension-fracture-toughness-testing (Accessed: 20 October 2023).

https://www.compositesworld.com/articles/compact-tension-fracture-toughness-testing

APPENDICES

***APPENDIX* A – The Pilatus PC-9 aircraft wing's outer auxiliary structure (Source: RMIT Canvas)**

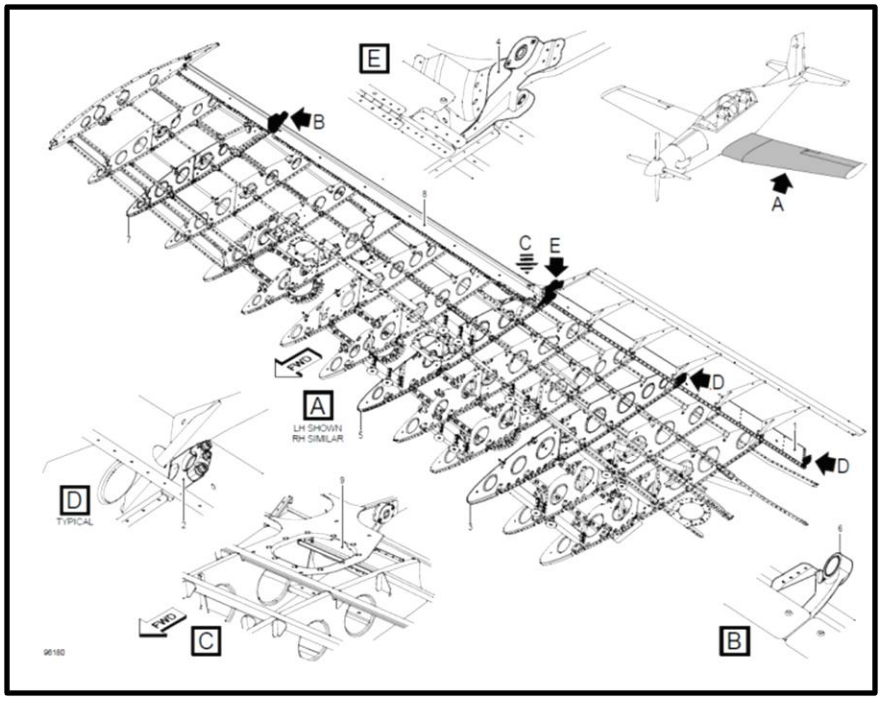

***APPENDIX* B – The Pilatus PC-9 aircraft main spar and front outer auxiliary structure (Source: RMIT Canvas)**

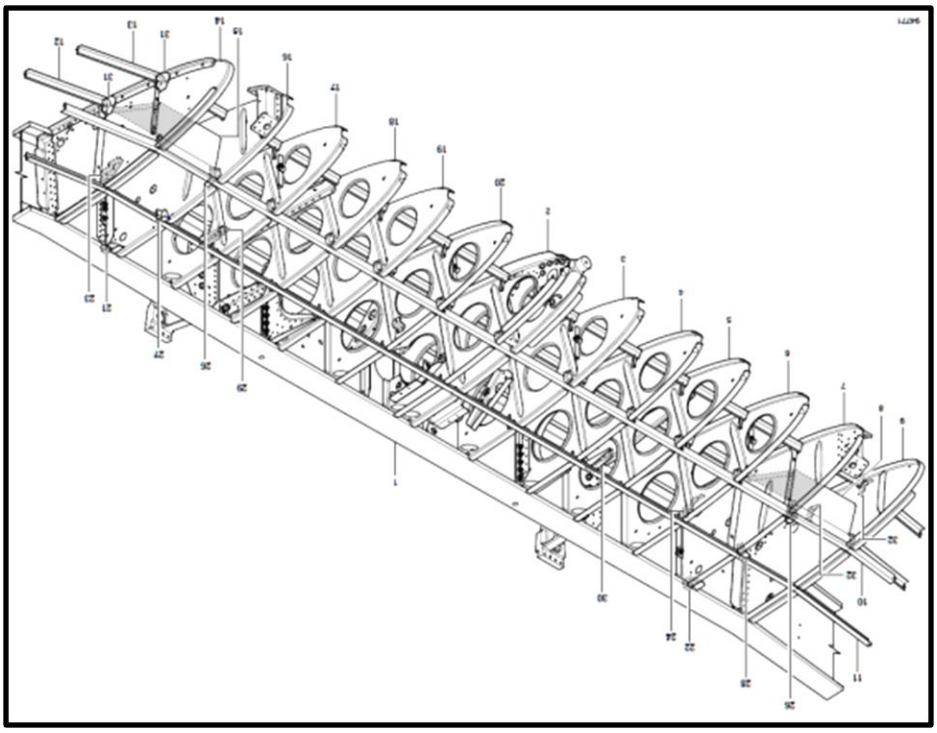

***APPENDIX C – Location of wing, ribs*, stringers, aileron, and flap ribs (Source: RMIT Canvas)**

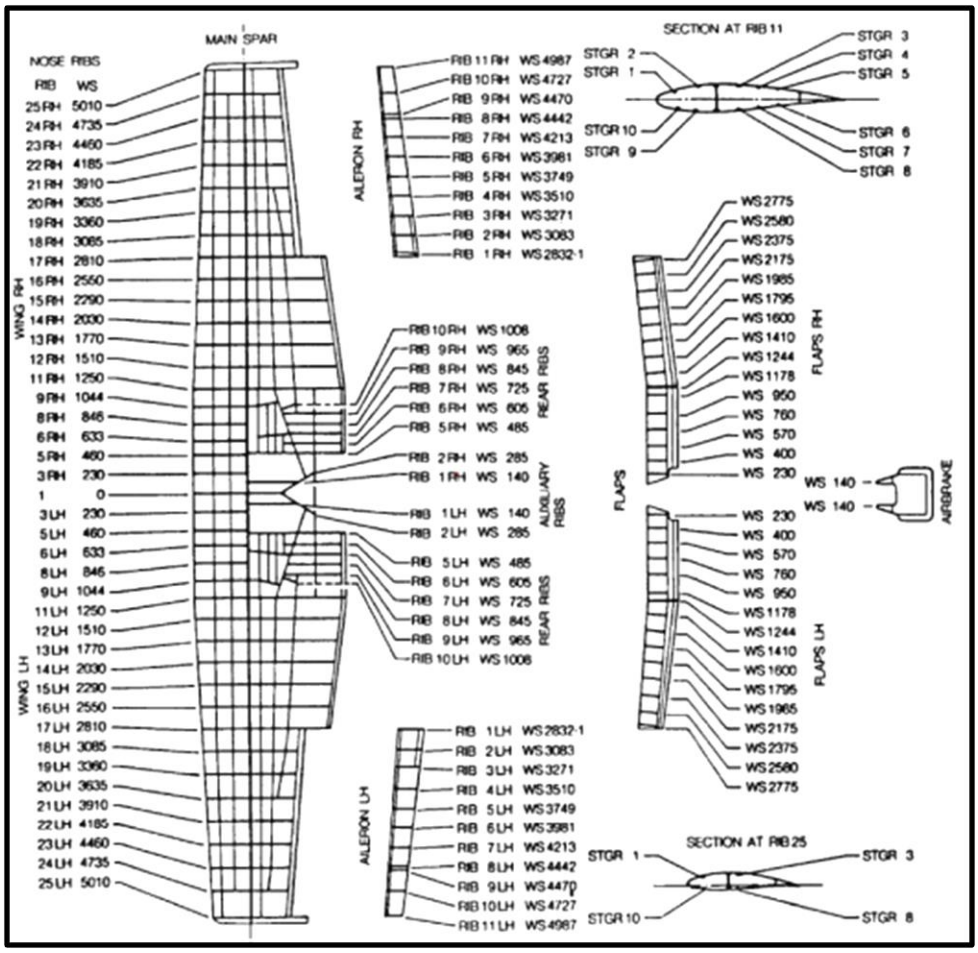

***APPENDIX D* – Technical specification of PC9 aircraft (Source: RMIT Canvas)**

Crew	2
Propulsion	1 Turboprop Engine
Engine Model	Pratt & Whitney Canada PT6A-62
Engine Power	858 kW
Speed	556 km/h
Service Ceiling	11,582 m
Range	1643 km
Empty Weight	1620 kg
Max. Take-off Weight	3200 kg
Wingspan	10.124 m
Wing Area	16.29 m^2
Length	10.05 m
Height	3,26 m
First Flight	7/05/1984
Wing root aerofoil	PIL15M825
Wingtip aerofoil	PIL12M850

***APPENDIX E – Material* properties of aluminium 2124-T851 (Source: RMIT Canvas)**

Parameter	Value
Density (kg/m^3)	2780
Young's Modulus (GPa)	73.1
Poisson's ratio	0.33
Yield Strength (MPa)	441
Ultimate Tensile Strength (MPa)	483

APPENDIX F – Internal structure of PC9 wing (Source: RMIT Canvas)

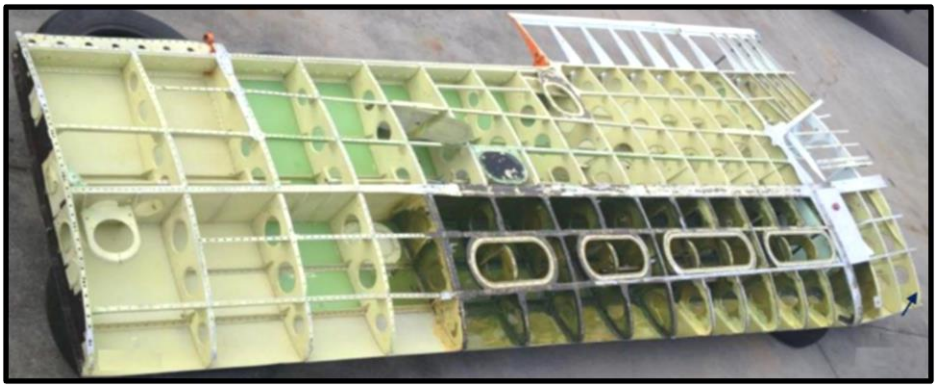

***APPENDIX G – Thickness of skin and* ribs (Source: RMIT Canvas)**

Component	Thickness (mm)
Skin	0.8 ± 0.08
Ribs	0.8 ± 0.08

***APPENDIX* H – Ribs coordinates at wing root and wing tip (Source: RMIT Canvas)**

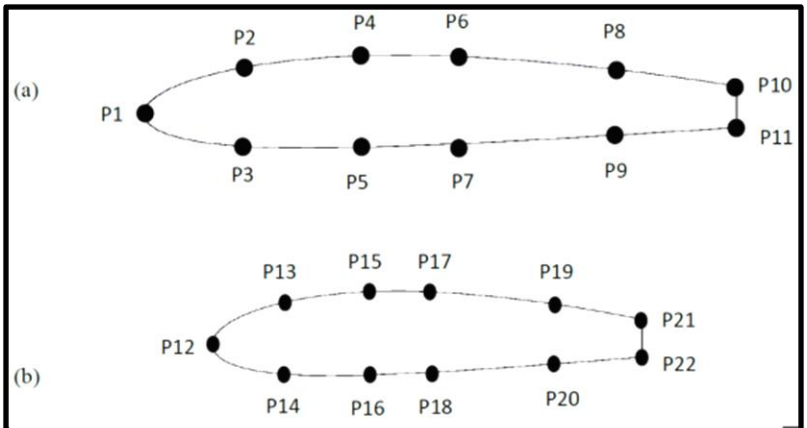

Point	x (mm)	y (mm)
P1	-750	0
P2	-510	120
P3	-510	-85
P4	-350	145
P5	-350	-100
P6	-80	160
P7	-80	-100
P8	520	102
P9	520	-85
P10	750	60
P11	750	-25

Point	x (mm)	y (mm)
P12	-450	462
P13	-250	537
P14	-250	434
P15	-50	550
P16	-50	430
P17	150	542
P18	150	432
P19	350	522
P20	350	444
P21	450	512
P22	450	462

***APPENDIX* I – Spar and stringers dimensions (Source: RMIT Canvas)**

		H (mm)	W (mm)	T_f (mm)	T_w (mm)
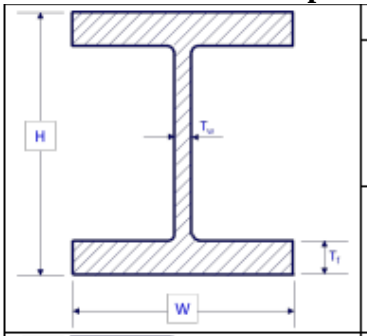	Main Spar (root)	260	70	17	2.3
	Main Spar (tip)	110	25	2.3	2.3
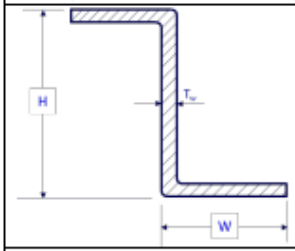	Rear Spar (root)	85	17	-	2.3
	Rear Spar (tip)	50	17	-	2.3
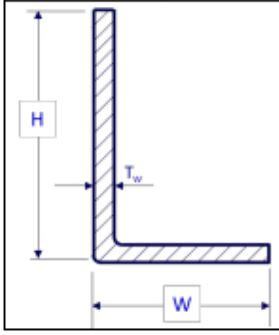	Stringers	14	11	-	2.3

APPENDIX J – Fatigue equations (Source: RMIT Canvas)

cyclic stress range	$\Delta\sigma = \sigma_{max} - \sigma_{min'}$
cyclic stress amplitude	$\sigma_a = (\sigma_{max} - \sigma_{min})/2,$
mean stress	$\sigma_m = (\sigma_{max} + \sigma_{min})/2,$
stress ratio	$R = \sigma_{min}\sigma_{max},$

Appendix K1 – Average Strain Recorded at Each Location during Loading Level 1 in the Experiment

LEVEL 1				
SKIN RED	RIB RED	TOP CAP SPAR RED	SHEAR WEB RED	BOTTOM CAP SPAR RED
µm/m	µm/m	µm/m	µm/m	µm/m
-35.88849894	8.35449836	-115.8348462	-116.1866187	92.30591491
SKIN BLUE	RIB BLUE	TOP CAP SPAR BLUE	SHEAR WEB BLUE	BOTTOM CAP SPAR BLUE
µm/m	µm/m	µm/m	µm/m	µm/m
-91.26040048	-7.589421676	-184.6292431	-30.49526901	215.9608536
SKIN YELLOW	RIB YELLOW	TOP CAP SPAR YELLOW	SHEAR WEB YELLOW	BOTTOM CAP SPAR YELLOW
µm/m	µm/m	µm/m	µm/m	µm/m
-36.54249805	-20.30372063	-22.02670407	109.7228832	53.20358031

Appendix K2 - Average Strain Recorded at Each Location during Loading Level 2 in the Experiment

LEVEL 2				
SKIN RED	RIB RED	TOP CAP SPAR RED	SHEAR WEB RED	BOTTOM CAP SPAR RED
µm/m	µm/m	µm/m	µm/m	µm/m
-27.96998456	24.70984782	-177.2731043	-163.8038679	139.4563763
SKIN BLUE	RIB BLUE	TOP CAP SPAR BLUE	SHEAR WEB BLUE	BOTTOM CAP SPAR BLUE
µm/m	µm/m	µm/m	µm/m	µm/m
-109.5385124	2.722563882	-253.8739357	-25.29427969	325.7507344
SKIN YELLOW	RIB YELLOW	TOP CAP SPAR YELLOW	SHEAR WEB YELLOW	BOTTOM CAP SPAR YELLOW
µm/m	µm/m	µm/m	µm/m	µm/m
-36.01213255	-13.96355831	0.896023823	182.1974376	97.96467776

Appendix K3 - Average Strain Recorded at Each Location during Loading Level 3 in the Experiment

LEVEL 3				
SKIN RED	RIB RED	TOP CAP SPAR RED	SHEAR WEB RED	BOTTOM CAP SPAR RED

µm/m	µm/m	µm/m	µm/m	µm/m
56.74842502	21.32834488	-324.8723235	-276.6917725	186.6731116
SKIN BLUE	**RIB BLUE**	**TOP CAP SPAR BLUE**	**SHEAR WEB BLUE**	**BOTTOM CAP SPAR BLUE**
µm/m	**µm/m**	**µm/m**	**µm/m**	**µm/m**
183.0873479	9.453888954	-411.6892551	-46.85563766	478.0619148
SKIN YELLOW	**RIB YELLOW**	**TOP CAP SPAR YELLOW**	**SHEAR WEB YELLOW**	**BOTTOM CAP SPAR YELLOW**
µm/m	**µm/m**	**µm/m**	**µm/m**	**µm/m**
72.99656644	31.60940427	22.37359052	275.3506052	142.3568751

Appendix L –Risk Assessment

HSW Activity Risk Assessment Template
HSW-PR09-TM01

RMIT UNIVERSITY

SECTION 3: RISK ASSESSMENT

Activity or Task *List the steps required to perform the activity or task in the sequence they are carried out.*	Hazards & Risks *List the hazards and risks that could cause injury when the activity or task is performed*	Current Risk Controls *Detail the controls currently in place that will reduce the risk. If none exist, please note this*	Current Risk Rating *(with existing controls)* *(Refer to risk score matrix in Section 4)*			Additional Risk Control Measures *List the control measures required to eliminate or further minimise the risk of injury/incident arising* *Identify the hierarchy of controls by using the following:* *El= Elimination, S = Substitution, En = Engineering, A = Administrative, and PPE = Personal Protective Equipment*	Residual Risk Rating *(after additional controls)* *(Refer to risk score matrix in Section 4)*			Responsibility *Name the person responsible to implement the control measure identified*
			Consequence	Likelihood	Risk Rating		Consequence	Likelihood	Risk Rating	
Briefing	Nil	Follow instructor's guide	1	B	Low					
Taking photo evidence	Equipment at head height, confined spaces	Be careful of surroundings	1	C	Low					
Measuring wing dimensions	Crowded and confined spaces, sharp objects	Be careful of surroundings	1	C	Low					

Note: *Add more rows if required.*

Prepared by:
Health, Safety & Wellbeing

Printed copies are considered uncontrolled

Rev: 3.0
Page 3 of 7

Appendix M – Calculation of Design Ultimate Load (DUL) during Cruise

$$W = m \times g$$

$$W = 3200kg \times 9.81\frac{m}{s^2} = 31392N$$

$$L = W \times FoS$$

$$L = 31392 \times 1.5 = 47088\ N$$

$$L_{Both\ Wings} = 0.95 \times 47088 = 44733.6\ N$$

$$L_{Single\ Wing} = \frac{44733.6}{2} = 22366.8N = 22.3668\ kN$$

***Appen**dix N1 – Loading Level 1 - 2533.775961N Maximum Principle Elastic Strain*

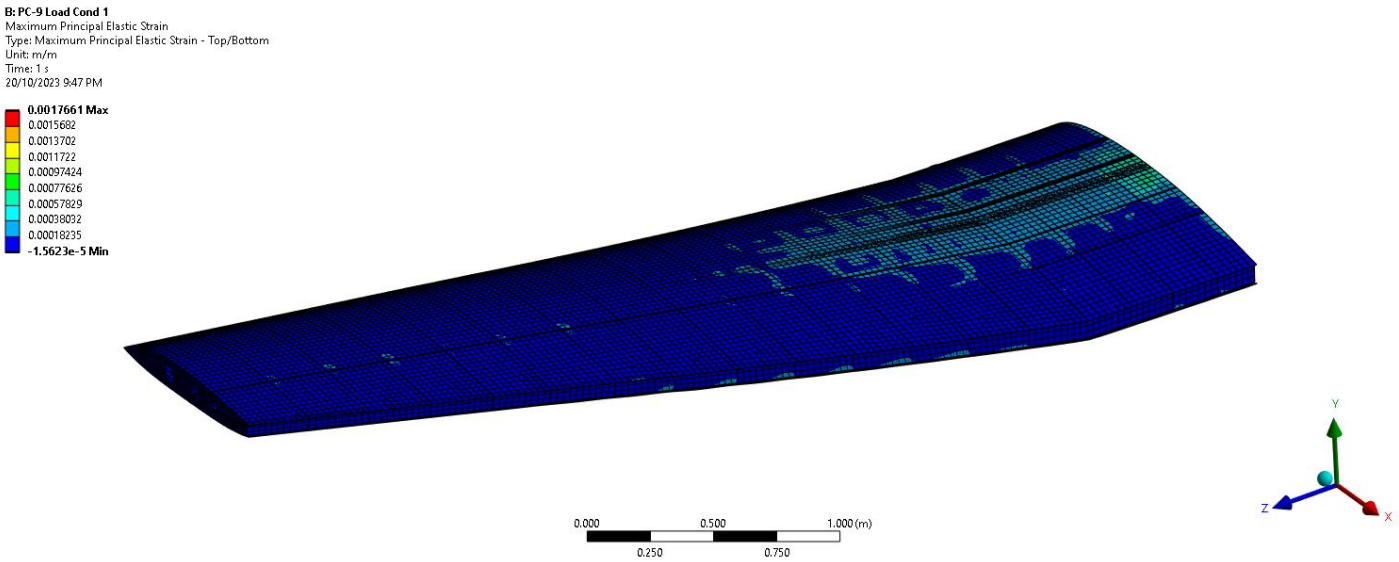

Appendix N2 – Loading Level 1 - 2533.775961N Maximum Principle Stress

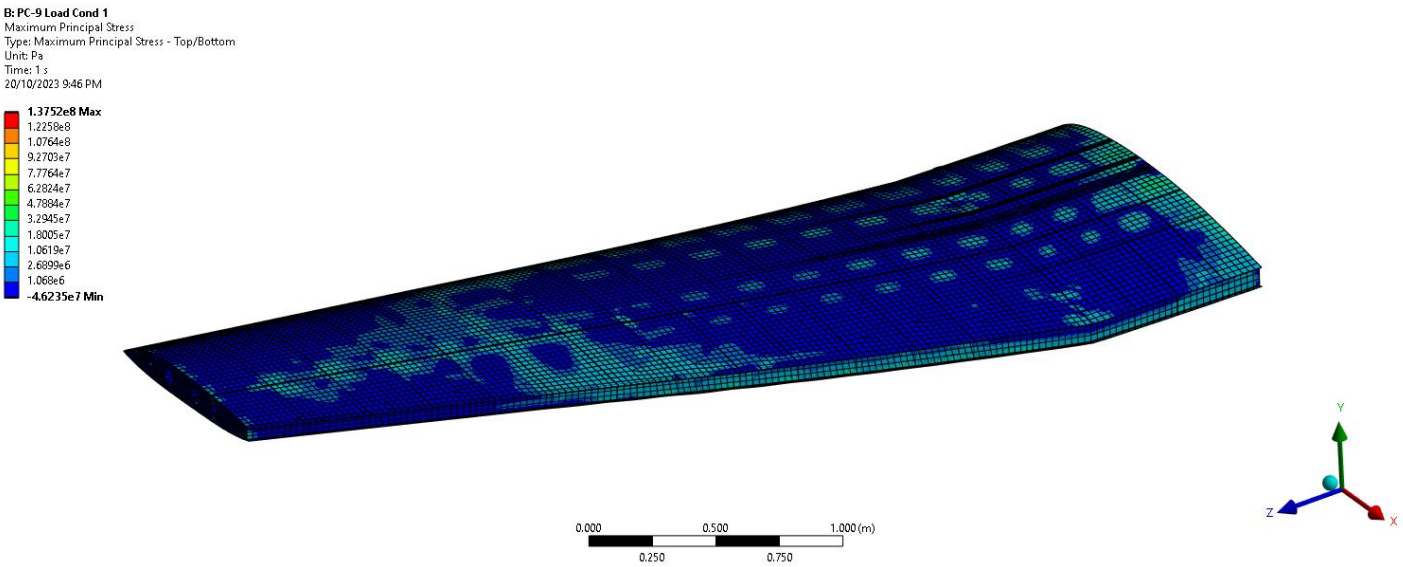

Appendix O1 – Loading Level 2 - 3649.37284N Maximum Principle Elastic Strain

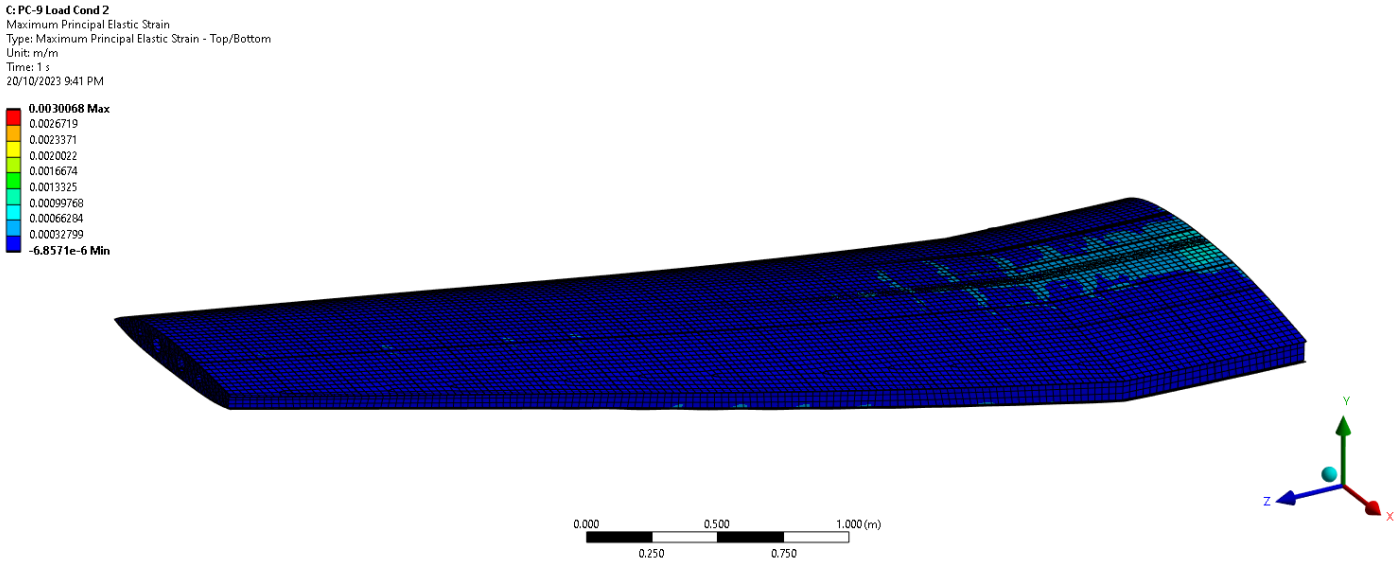

Appendix O2 – Loading Level 2 - 3649.37284N Maximum Principle Stress

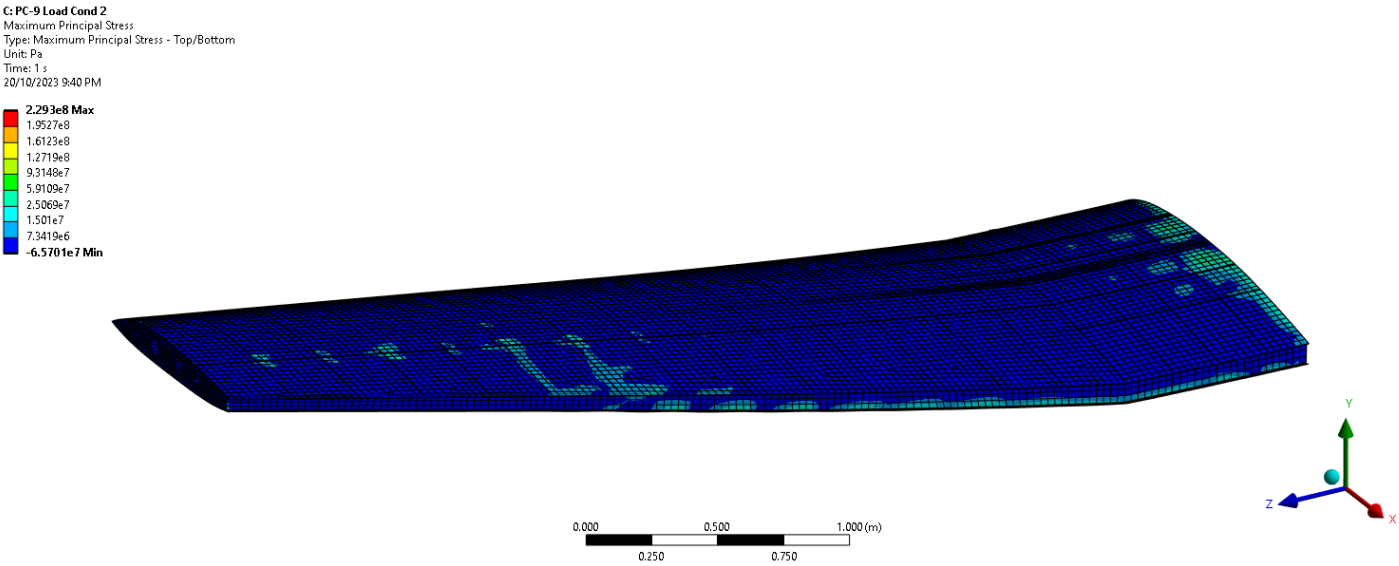

Appendix P1 – Loading Level 3 - 5532.280164N Maximum Principle Elastic Strain

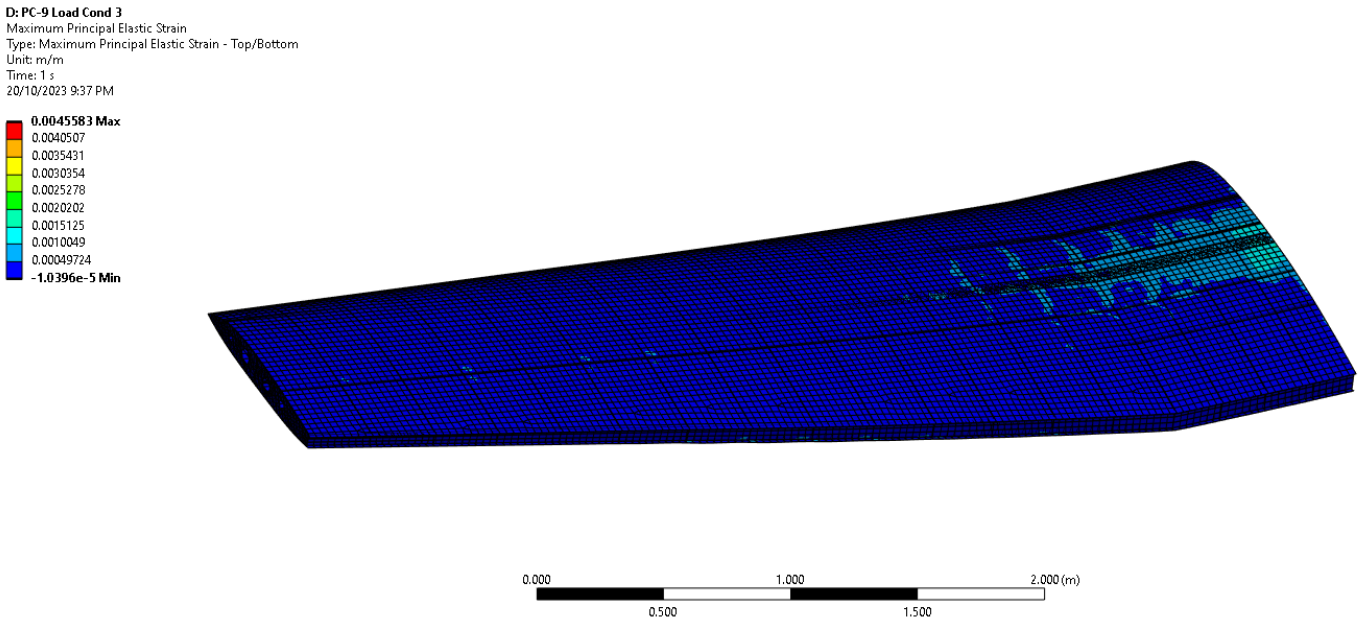

Appendix P1 – Loading Level 3 - 5532.280164N Maximum Principle Stress

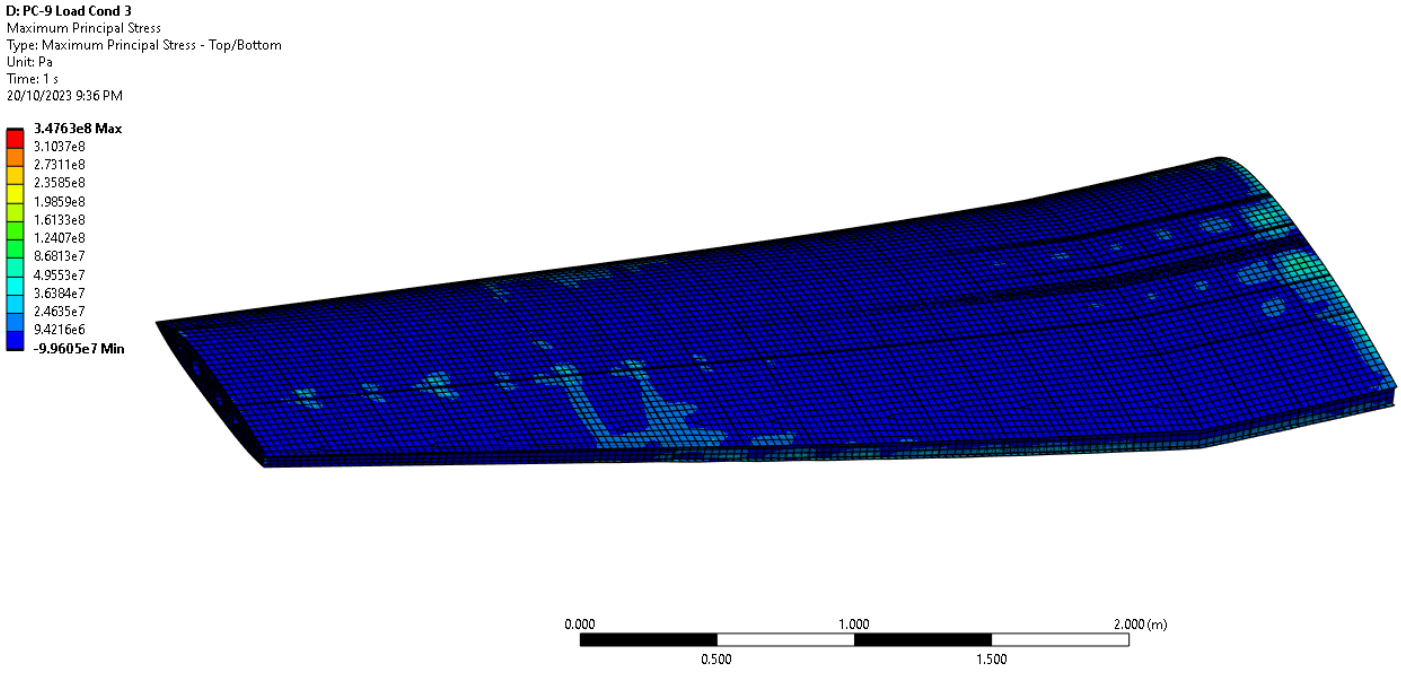

Appendix Q1 – Design Ultimate Load at Cruise Maximum Principle Elastic Strain

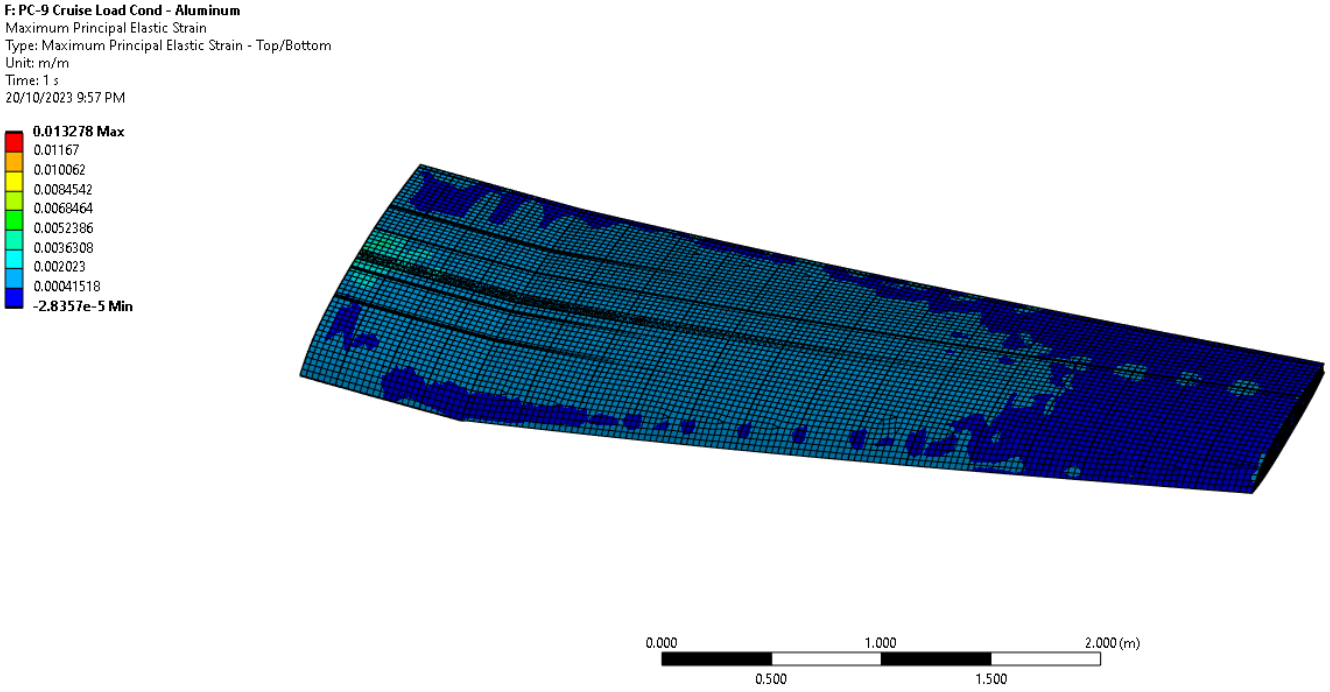

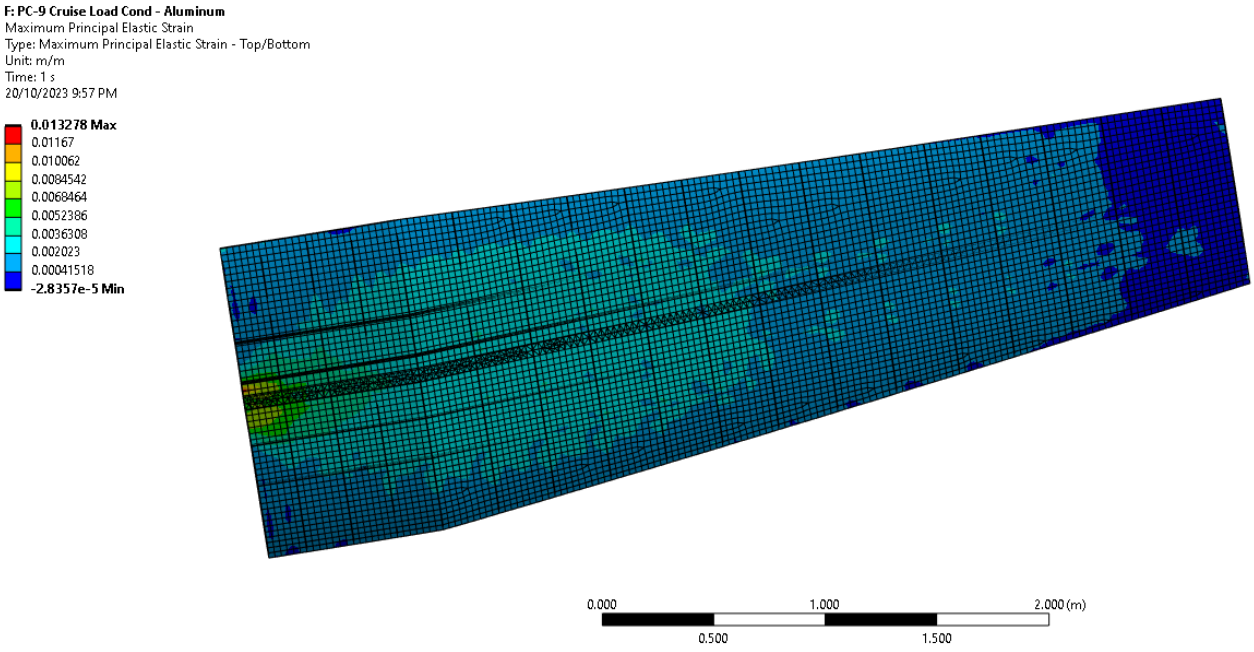

Appendix Q2 – Design Ultimate Load at Cruise Maximum Principal Stress

F: PC-9 Cruise Load Cond - Aluminum
Maximum Principal Stress
Type: Maximum Principal Stress - Top/Bottom
Unit: Pa
Time: 1 s
20/10/2023 9:56 PM

1.0198e9 Max
8.3357e8
6.8963e8
5.4569e8
4.0175e8
2.5782e8
2.4465e8
2.3149e8
2.1832e8
2.0516e8
1.9199e8
1.7883e8
1.6159e8
1.4436e8
1.2712e8
1.0988e8
9.2648e7
7.5412e7
5.8176e7
4.094e7
2.3704e7
7.5145e6
8.916e5
-2.9906e8 Min

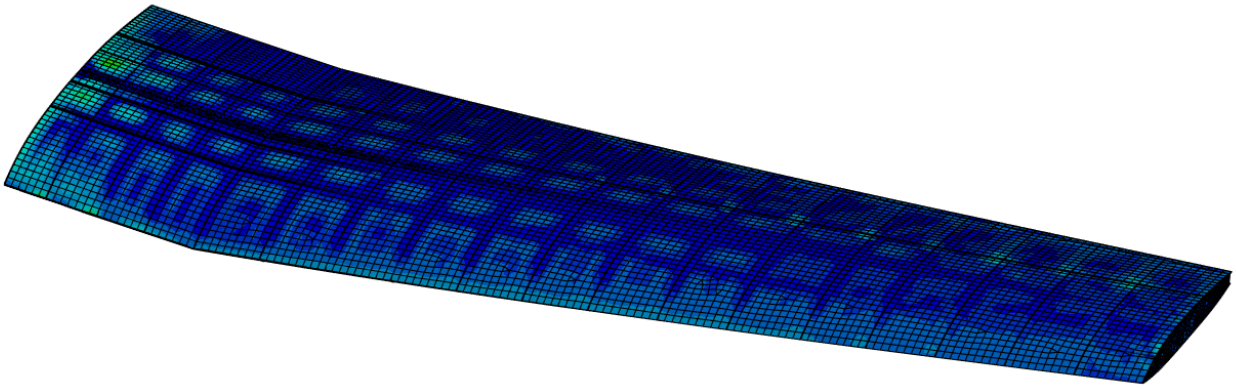

0.000 0.500 1.000 (m)
0.250 0.750

F: PC-9 Cruise Load Cond - Aluminum
Maximum Principal Stress
Type: Maximum Principal Stress - Top/Bottom
Unit: Pa
Time: 1 s
20/10/2023 9:56 PM

1.0198e9 Max
8.3357e8
6.8963e8
5.4569e8
4.0175e8
2.5782e8
2.4465e8
2.3149e8
2.1832e8
2.0516e8
1.9199e8
1.7883e8
1.6159e8
1.4436e8
1.2712e8
1.0988e8
9.2648e7
7.5412e7
5.8176e7
4.094e7
2.3704e7
7.5145e6
8.916e5
-2.9906e8 Min

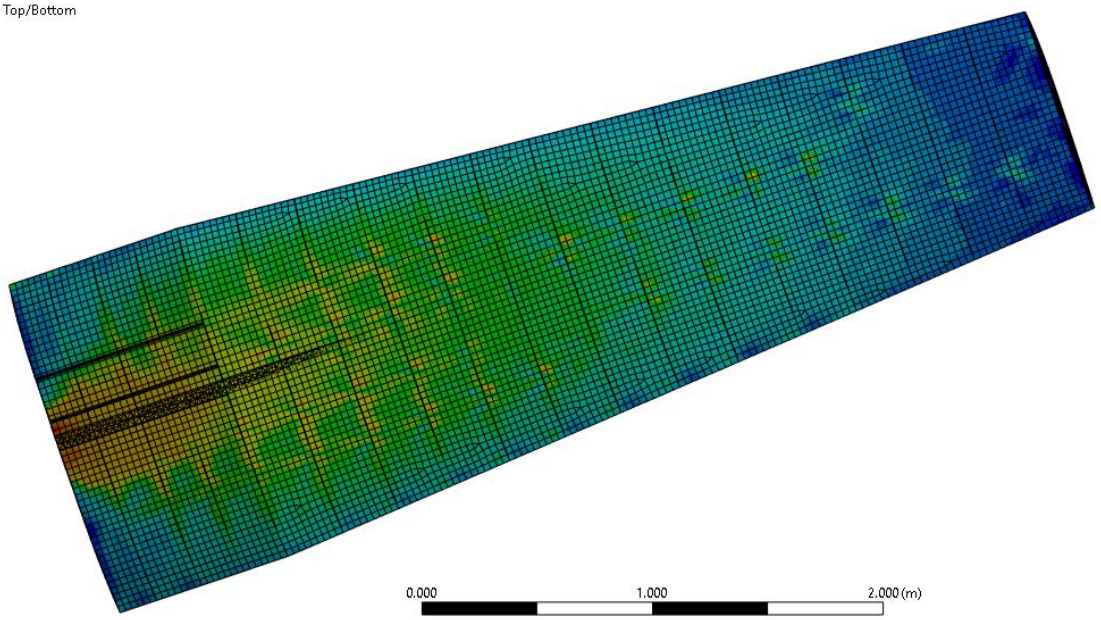

0.000 1.000 2.000 (m)
0.500 1.500

F: PC-9 Cruise Load Cond - Aluminum
Maximum Principal Stress
Type: Maximum Principal Stress - Top/Bottom
Unit: Pa
Time: 1 s
20/10/2023 10:24 PM

1.0198e9 Max
8.3357e8
6.8963e8
5.4569e8
4.0175e8
2.5782e8
2.4465e8
2.3149e8
2.1832e8
2.0516e8
1.9199e8
1.7883e8
1.613e8
1.4378e8
1.2625e8
1.0872e8
9.1197e7
7.3671e7
5.6145e7
3.8619e7
2.1093e7
2.1093e7
2.1093e7
2.1093e7
2.1093e7
2.1093e7
2.1093e7
1.6988e7
1.2884e7
8.7795e6
4.6751e6
-2.9905e8 Min

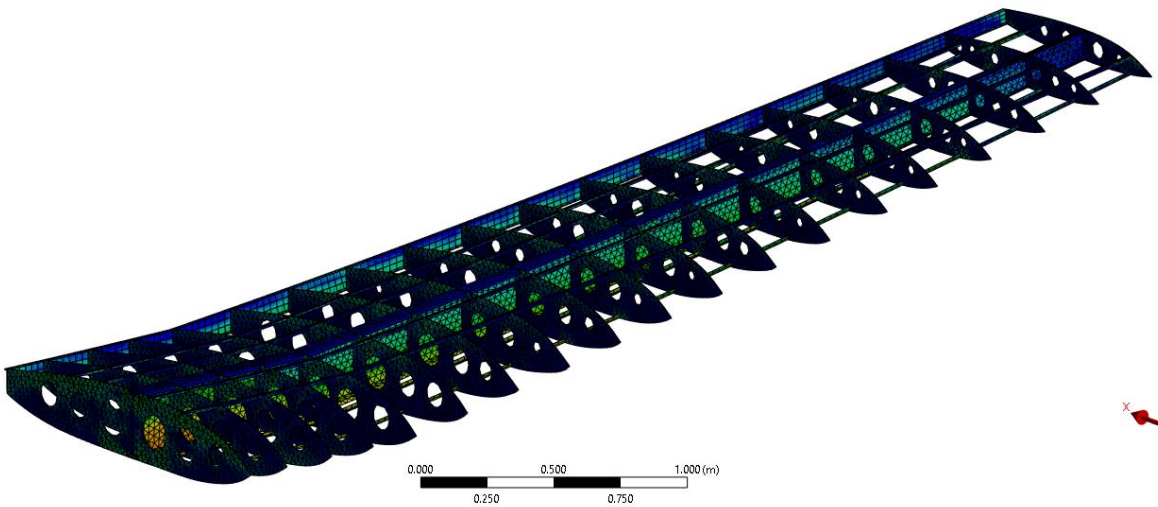

0.000 0.500 1.000 (m)
0.250 0.750

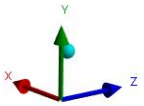

Appendix Q3 – Design Ultimate Load at Cruise Maximum Principal Stress

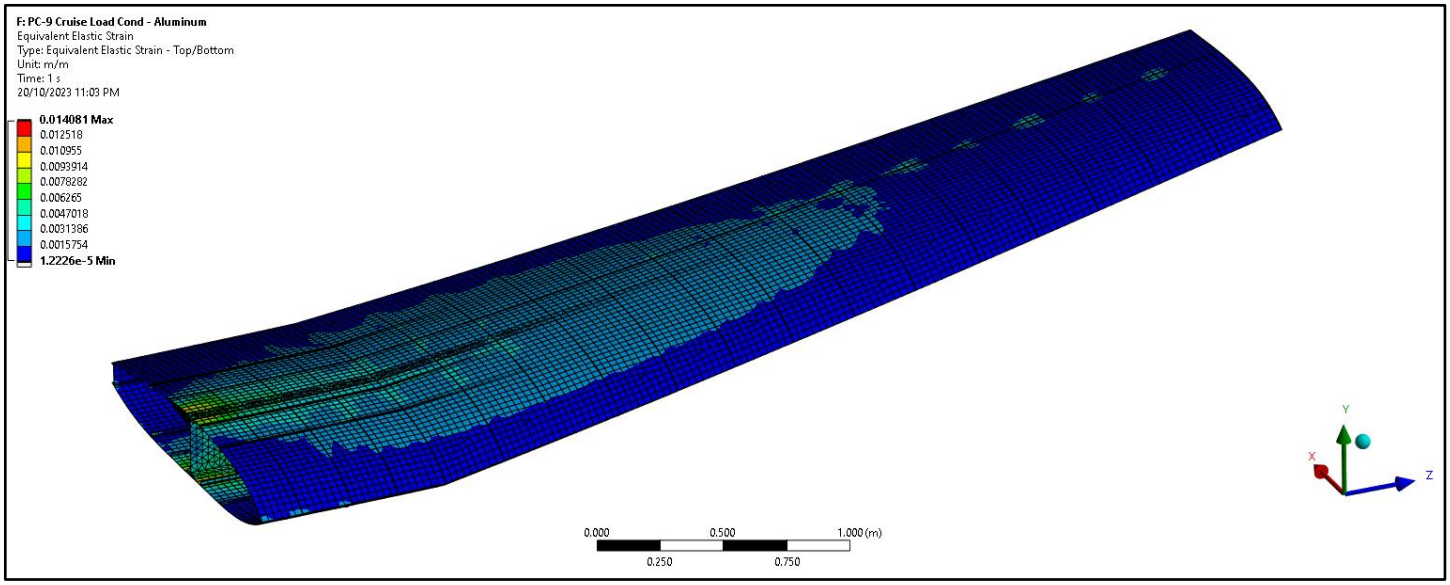

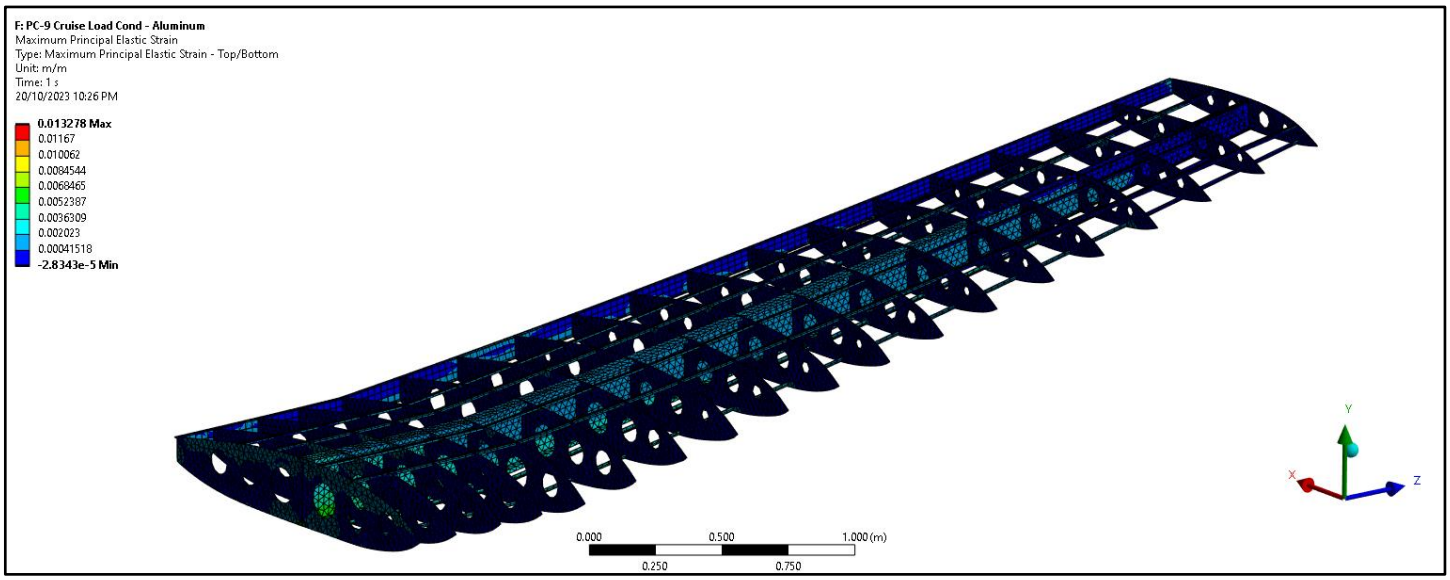

MEMBER CONTRIBUTION TABLE

Criteria	Weight (%)	Faris Roslan	Jay Dickson	Mary Denkha	Olivia Curtis	Khac Son Trinh
Updating Executive summary, Introduction, Static & dynamic analyses, adding new conclusions, formatting the report	20	5	0	5	5	5
Conducting the experiment, analysing the results and writing corresponding sections	20	7.5	0	0	7.5	5
Developing the FE model for aluminium wing, validating, running simulations, and writing corresponding sections	30	7.5	5	0	7.5	10
Designing composite skin and spar, updating the FE model, post-processing and writing corresponding sections	30	0	15	15	0	0
Total (%)	100	20	20	20	20	20

Signature	F.A.R	J.A.D	M.D	O.J.C	K.S.T